SEISMIC STRATIGRAPHY OF THE GEORGES BANK BASIN: IMPLICATIONS FOR CARBON SEQUESTRATION

By

ALEXANDRA CATHREN ADAMS

A thesis submitted to the

School of Graduate Studies

Rutgers, The State University of New Jersey

In partial fulfillment of the requirements

For the degree of

Master of Science

Graduate Program in Earth and Planetary Sciences

Written under the direction of

Kenneth G. Miller

And approved by:

_____

_____

_____

New Brunswick, New Jersey

October 2019

ABSTRACT OF THE THESIS

Seismic Stratigraphy of the Georges Bank Basin:

Implications for Carbon Sequestration

by ALEXANDRA C. ADAMS

THESIS DIRECTOR:

Dr. Kenneth G. Miller

I evaluate Cretaceous sediments in the western part of the Georges Bank Basin (WGBB), offshore Massachusetts, United States, for carbon capture and storage (CCS) potential as part of Mid-Atlantic Offshore Carbon Storage Resource Assessment Program (MAOCSRAP). Previous studies have recognized that Cretaceous sands in the GBB may be viable targets for carbon injection due to the high porosity and permeable nature of the reservoirs, as well as a suitable cap rock confinement, but questioned their suitability due to shallow burial depths. Using the modern techniques of sequence stratigraphy and a modern analysis software tool (Petrel), I evaluate WGBB CCS potential using ~13,800 km of recently released 2D multi-channel (MCS) profiles integrated with 10 previously interpreted geophysical well-logs from the Eastern GBB. By mapping significant seismic horizons, defining internal reflection terminations and seismic geometries correlated with depositional facies, I identify five Cretaceous seismic sequences within four sedimentary units. The Berriasian to Barremian fluvial-deposited sand-prone Missisauga Formation was deposited during a regressive interval with northern-sourced sediment depocenters. A transition to a relatively thin shale-rich depositional sequence, the Naskapi Shale,

represents the beginning of a major marine transgression initiated during the early Aptian. As sedimentation rates increased in the Albian to early Cenomanian, and sequence depocenters subsequently shifted landward, depositional environments transitioned from primarily terrestrial to nearshore/shelf/deltaic coeval with deposition of the thick, sandy Logan Canyon Formation sequences. Slightly irregular, hummocky, low-angle Albian clinoforms occur in the southeastern region. Reflection surfaces become more parallel upsection, coinciding with deeper paleowater depths. Prograding Cenomanian shingled clinoforms associated with toplap and downlap indicate prodelta to nearshore environments. Turonian to Coniacian deposition of the shale Dawson Canyon Formation and a shift in sedimentary depocenters to outer shelf deposits suggest a marine regression following the Aptian to late Cenomanian rise in relative sea-level.

The sand reservoirs are mapped below the depth of supercritical CO_2 storage (~800 m) and have sufficient shale cap rock confinement, therefore supporting the Lower Cretaceous Missisauga sands and mid-Cretaceous Logan Canyon sands in the southeastern subarea as potential viable targets for effective CCS. However, to assure successful sequestration, wells must be drilled locally to provide accurate porosity and permeability values, as well as to reinforce interpretations of the depositional facies and lithostratigraphy.

ACKNOWLEDGEMENTS

First and foremost, I would like to thank my advisor, Dr. Kenneth Miller, for guiding me through my graduate education. Your unwavering enthusiasm for science, and life in general, has inspired me to be a more curious scientist in my future, as well as encouraging me to remind myself to never take life too seriously. My three years as your graduate student have been life-changing, for which I will always be thankful.

My research would not have been possible without the support of my committee: Dr. Gregory Mountain and Dr. Donald Montverde; for who both I would like to thank for their support, patience, and encouragement.

I would also like to thank Dr. James Browning, for your extreme patience, continually reading my thesis, and providing support whenever I was on the verge of a mental breakdown, as well as your immediate direct help on just about anything.

I would like to thank my fellow graduate students for being extraordinary friends, inside and outside of the department, as well as wonderful sources of support. The memories I have made in the past three years will not be forgotten.

TABLE OF CONTENTS

LIST OF FIGURES

INTRODUCTION

Carbon capture and storage (carbon sequestration) is the technical approach of directly capturing anthropogenic emissions of carbon dioxide (CO_2). The CO_2 is then compressed to its supercritical fluid form, transported via pipeline, and ultimately injected into the subsurface for storage (Benson and Surles, 2006). Two storage options for potential CO_2 injection currently exist – deep underground sedimentary basins either on land or under the ocean. The underground storage approach directly captures CO_2 from the industrial source, concentrates it into an almost pure form, and injects it deep into sedimentary basins located in tectonically stable areas (Gunter, et al., 2004). The offshore ocean storage approach captures CO_2 from a stationary emissions source, transports the highly compressed CO_2 via sub-sea pipeline and injects CO_2 into deep (1000-3000 m) saline aquifers where the CO_2 displaces the saline formation water (Hitchon, 1996). Hypothetically, the CO_2 will be trapped in the sedimentary basin for hundreds of thousands of years where it is stored initially as a supercritical fluid but mineralizes on scales of decades to millennia and permanently well isolated from possible return to the atmosphere (Benson and Surles, 2006). Due to controversies and public opposition regarding NUMBY (not under my backyard) and the potential risk of groundwater contamination, offshore storage in deep saline aquifers may now be a better option for carbon capture and storage than onshore options (Krause, 2013; Litynski and Vikara, 2011). Previous studies (Miller et al., 2018; Schmelz et al., 2019) have suggested that the Baltimore Canyon Trough (BCT), offshore Maryland to New Jersey, is a potential target for offshore CO_2 storage due to the presence of laterally continuous, highly permeable and highly porous sand bodies with good shale seals within the basin.

Farther north on the margin, the Georges Bank Basin (GBB), offshore Massachusetts, may also provide an additional target for offshore carbon storage. However, the GBB has not been studied in as much depth as the BCT and the potential for carbon storage and sequestration is not well known.

The elongate, asymmetric GBB, located approximately 150 km SE of Cape Cod, MA (Fig. 1), is the northernmost offshore sedimentary basin along the U.S. Atlantic Margin. It is ~70,000 km^2 in area and has accumulated 6-10 km of Upper Triassic and younger strata that overlie 4-5 km of Paleozoic and older block-faulted crystalline basement (Schlee and Klitgord, 1988). Geographically, the GBB is positioned between the LaHave platform to the northeast, the Long Island Platform to the west, and the Gulf of Maine to the north (Fig. 2). The landward edge of the Gulf of Maine is defined by the basement hinge zone (BHZ), the steepening of basement gradients observed on seismic profiles, where areas of unstretched crust (slow subsidence) become stretched and rates of subsidence increase rapidly seaward (Hutchinson and Klitgord, 1986; Klitgord and Behrendt, 1979; Withjack et al., 2005; Manspeizer and Cousminer, 1988). The seaward edge of the main basin is defined by the East Coast Magnetic Anomaly (ECMA), that has been interpreted as seaward-dipping volcanics near the present-day continent-ocean boundary (Grow & Sheridan, 1988) (Fig. 2). The basin narrows southwesterly, ending where the Atlantis Fracture zone intersects the margin (Klitgord et al., 1988).

Initial basin studies reported the Yarmouth Arch, a Paleozoic-age structural high separated the West Georges Bank Basin (WGBB) and the East Georges Bank Basin (EGBB) (Carswell et al., 1990; Koning, 2011). The Yarmouth Arch was also thought to be the dominant influence on basin sedimentation until the Middle Jurassic resulting in

significantly different structural and stratigraphic evolutions of the WGBB and the EGBB basins. More recent work, however, shows that the Yarmouth Arch separates the Canadian Scotian Basin from the GBB on the United States side (Kidston et al., 2005, Wade and Maclean, 1990) (Fig. 2). At the start of the current study, work on the GBB was to be split into two separate basins, the WGBB and EGBB, based entirely on the location of the Yarmouth Arch. However, once discovering the Yarmouth Arch separates the GBB from the Scotian Basin, for this study, the GBB is split by an arbitrary line based on location of 10 wells drilled in the eastern region. Graham (2018) evaluated these well logs in detail and provided preliminary evaluation of seismic profiles within the EGBB. An extensive amount of seismic data exists in the WGBB, but regionally lacks well control. Therefore, in order to assess the storage potential in the western GBB, I have exported and traced seismic reflectors from the eastern GBB, where well data provides good geological constraints (Graham, 2018).

My research on the western subarea of the Georges Bank Basin is a contribution to the Mid-Atlantic U.S. Offshore Carbon Storage Resource Assessment Project (MAOCSRAP) managed by Battelle under the U.S. Department of Energy's Carbon Storage Program. MAOCSRAP consists of a complete assessment of potential storage resources of offshore Mid-Atlantic regions that have not yet been evaluated for carbon sequestration (Cummings et al., 2017).

Previous Research

Graham (2018) primarily utilized gamma ray logs reinforced with neutron porosity logs, density porosity logs, and previously published permeability and porosity data to correlate ten exploratory wells drilled across the eastern GBB. To determine

general lithologies, trends in gamma log rays were examined for high or low readings, inferred to represent mud/shale-rich or sand-prone units, respectively. This “back to basics” technique of sequence stratigraphy (identifying coarsening- and fining- upward packages and stratal stacking patterns) presented in Miller et al. (2018), was used to identify depositional sequences and ultimately systems tracts. Sequence boundaries (SB) were delineated and three distinct depositional sequences within the Logan Canyon Formation (LC1, LC2, LC3 - youngest to oldest) and three depositional sequences within the Missisauga Formation (MS1, MS2, MS3 - youngest to oldest) were identified. Utilizing observable stacking patterns, individual sequences typically consist of a sandy upper regressive highstand systems tract (HST) at the top, a maximum flooding surface (MFS) below the HST a silty transgressive systems tract (TST, and a sandy/silty lower regressive lowstand systems tract (LST) below the TST. Biostratigraphy, described in previously published Bureau of Ocean Energy Management (BOEM) reports (Amato and Bebout, 1980; Amato and Simonis, 1980; Edson et al., 2000), assisted in chronostratigraphic correlations. The wells were correlated through the basin on two gamma ray log cross sections: 1) four western wells (NE to SW: COST G1, Exxon 133, Mobile 312, and Shell 357); 2) and six eastern wells (NE to SW: Exxon 975, COST G2, Mobil 273, Tenneco 187, Conoco 145, and Shell 410) in the EGBB (Fig. 3A, 3B). Integration of well log and seismic data concluded that the top of the Logan Canyon Formation is generally shallower than the depth of supercritical storage (SCS) in the EGBB. Approximately 55 percent of the EGBB LC sands lies above the depth of SCS (2500 feet below Kelly Bushing (ftbKB), ~760 m) - a depth too shallow for safe and efficient carbon sequestration. Considering unit thickness, depth, permeability, porosity

and possible seals, Graham (2018) concluded that the Missisauga Formation is a more suitable for target for effective CCS in the eastern GBB.

BACKGROUND

Structural Evolution of the Margin

The Mid-Atlantic margin evolved through three major tectonic events composed of compressional, rifting, and subsidence through the Phanerozoic (Klitgord, et al., 1988). Three compressional Paleozoic Appalachian orogenies (Ordovician-Silurian Taconic orogeny, Devonian-Mississippian Acadian orogeny, Mississippian-Permian Alleghanian orogeny) resulted in the creation of supercontinent Pangea (Rast, 1988; Thomas, 2006; Klitgord et al. 1988). The GBB initially formed in response to extensional rifting of the North American and African plates in Late Triassic to earliest Jurassic (~230-198 Ma) (Withjack et al., 1998). The early rifting phase is associated with the development of coastal-plain adjacent asymmetric rift basins bounded by northeast-southwest striking normal faults (Withjack et al., 1998). Rapid stretching of the crust during rifting was accompanied by intense igneous activity, folding, faulting, and deposition of synrift sediments. A later stage of rifting is characterized by uplift and erosion near the basement hinge zone (BHZ) and regional subsidence seaward of the BHZ. The now-buried rift basins formed seaward of the BHZ on stretched and thinned continental crust (Hutchinson and Klitgord, 1986).

The rifting phase is also associated with a widespread, intense, short-lived (<1 million years long) igneous event named the Central Atlantic Magmatic Province (CAMP). CAMP is primarily represented by flood basalts, dikes, and sills. Previous isotopic dating and stratigraphic and structural analysis studies (May, 1971; Withjack et

al., 1998; Withjack et al., 2005; Olsen et al., 2003; Olsen, 1999; Knight et al., 2004) have interpreted CAMP-related igneous activity as occurring in the earliest Jurassic (~201 Ma). Within the GBB, CAMP-related flood basalts are found within the synrift strata, implying CAMP activity during the rifting phase (Withjack et al., 2005).

Rifting ceased with the onset of seafloor spreading, first occurring on the southern portion of the US Atlantic margin around 201 Ma (Withjack et al., 1998; 2005). Seafloor spreading progressed northward in a "zipper"-type movement by 180 Ma. This "zipper" spreading is associated with a diachronous post-rift unconformity (PRU) that marks a significant change in the evolution of the margin. The PRU separates landward dipping, deformed synrift rocks ("rift-stage" deposits) from overlying largely conformable, less deformed post-rift strata ("drift-stage" deposits) (Withjack et al., 1998; Withjack et al., 2005). The oldest post-rift strata occurring in the GBB are early Middle Jurassic age, supporting the initiation of the "drifting-stage" by the Pliensbachian - Toarcian (Klitgord et al., 1988; Withjack et al., 1998, 2005).

Seafloor spreading was followed by passive simple thermoflexural subsidence and sediment loading (Grow and Sheridan, 1988; Steckler and Watts, 1978). Offshore subsidence initiated in the GBB area during the Bathonian - Bajocian. From Late Jurassic to Early Cretaceous, subsidence rates increased as a thermoflexural response to increasing crustal rigidity, leading to subsidence progressively moving onshore (Grow and Sheridan, 1988).

GBB Stratigraphy

The stratigraphic nomenclature used in the GBB was developed for the Nova Scotian shelf by McIver (1972) using offshore exploratory well data. In 1976, several

U.S. petroleum industry companies, along with the USGS, drilled the first two deep offshore wells in the GBB: the Continental Offshore Stratigraphic Test (COST) G-1 (total depth=4899 m) and the COST G-2 (total depth=6667 m). GBB lithostratigraphy was determined by the petroleum companies by using regional well data correlated with regional multichannel seismic (MCS) reflection profiles, geomagnetic, and gravity data.

Mid-Jurassic to Late Cretaceous (175-66 My) stratigraphy is the primary focus of this research. Two Early Jurassic stratal units directly overly the post-rift unconformity, Mid to Late Jurassic post-rift strata comprise one group, divided into four formations. Cretaceous strata also comprise one group, subdivided into four formations (Fig. 4). Early Jurassic interbedded arkosic terrestrial sandstones (Mohican Group) and marine shelf dolomites and evaporates (Iroquois Formation), and volcanics unconformably lie on top of Paleozoic crystalline basement lows, filling basement half-grabens created during rifting. The Iroquois Formation accumulated on the most seaward regions of the basin, building a seaward prograding carbonate platform. The Mohican Formation eventually prograded onto the carbonate platform. Four formations make up the Jurassic Western Bank Group: the Abenaki, the Verrill Canyon, the Mohawk, and the Mic-Mac. The carbonate-rich Abenaki Formation contributed to the building of a prograding carbonate platform in the Middle Jurassic. The Verill Canyon Formation, a carbonaceous, splintery shale unit found on the Nova Scotian shelf, is not present in the GBB. The siliciclastic-rich, heterolithic Mohawk and Mic-Mac Formations interfinger with the Jurassic carbonate platform below.

Four formations – from oldest to youngest: the Mississauga, the Naskapi Shale, the Logan Canyon, and the Dawson Canyon (Fig. 4, Table 1) - comprise the lowermost

Early Cretaceous (Berriasian) to lower Upper Cretaceous (Coniacian) Nova Scotia Group. A regressive period beginning in the Tithonian (~150 Ma), along with decreasing rates of basin subsidence and sediment accumulation, allowed the Berriasian - Barremian Missisauga Formation to dominate sedimentation and bury the Jurassic carbonate reef. The heterolithic, siliciclastic Missisauga Formation likely represents a nonmarine, predominantly fluvial/delta front, depositional environment (CNSOPB, 2009). The fissile, carbonaceous Naskapi Shale overlies the Missisauga Formation and represents the initiation of a major marine transgression in the early Aptian (~125 Ma). Evidence of this transition is supported by the observable change in lithology from heterolithic Missisauga delta front deposits to the thick, blocky, deltaic sands of the Logan Canyon Formation deposited during the Albian to early Cenomanian (113-94 My) (Post et al., 2016). The Dawson Canyon Formation comprised of a thick, calcareous mudstone caps the Logan Canyon Formation below (Post et al., 2012). Deposition of the Dawson Canyon was in the late Cenomanian to Turonian, coinciding with a major margin-wide transgression, with highest global sea levels of the Cretaceous during this period (Miller et al., 2005), and subsequent transition from delatic to marine (prodelta/slope) deposition.

CCS Potential

In order for an offshore reservoir to be a potentially successful target for carbon storage, the reservoir must exhibit a checklist of critical features: sufficient porosity (> ~20%) and permeability (> ~1000 mD), correct depth/thickness of injection zone (below depth of supercritical fluid storage), and an adequate caprock (i.e., shales) (Litynski et al., 2011; Kopp et al., 2009). For buried CO_2 to remain in a supercritical state (in which it behaves like a gas but has a “liquid” density), burial temperatures must remain greater

than 31.1° C with burial pressures above 7.38 MPa (Bachu, 2003). Assuming a common geothermal gradient of 25° C/km, 12° C surface temperatures and a lithostatic gradient of 27 MPa/km, Miller et al. (2018) calculated a minimum injection depth of ~800 m for safe and efficient regional supercritical CO_2 storage. A data compilation of geophysical logs, core observations, well-cuttings, and sidewall core from the COST G1 and G2 wells indicate that strata below 3050 m (10,000 ft) have less than < 20% porosity and <100 millidarcys (mD) (Graham, 2018; Scholle and Wenkam, 1982) and therefore poor targets for carbon sequestration. Above this depth, the Missisauga Formation and Logan Canyon Formation exhibit porosities greater than 25% and permeabilities greater than 100 mD. Thick sandstone units are ideal for injection due to high porosity and permeability measurements necessary for successful CO_2 storage and injectivity (Scholle and Wenkam, 1982; Bachu, 2003; Cummings et al., 2017). With no well data in the western GBB, unit porosity and permeability values are unknown and can only be estimated from eastern well measurements.

I evaluate the western GBB's potential for offshore carbon storage and sequestration by integrating the "back to basics" techniques of seismic sequence stratigraphy with available MCS reflection profiles on the depositional sequences of the Missisauga and Logan Canyon Fms. (Miller et al., 2018; Post et al., 2012, Poag, 1982; McIver, 1972; Graham, 2018).

METHODS

Overview

Initial interpretations of MCS profiles were guided from integrated well log-seismic stratigraphy in the eastern GBB (Graham, 2018). Gamma ray logs from available

wells were tied to corresponding MCS profiles using Petrel to interpret the eastern sequence stratigraphy. Petrel is an advanced multi-channel seismic and well log analysis software package produced by Schlumberger. Additional data, including other geophysical logs (Spontaneous Potential [SP], Neutron Porosity [NP], velocity logs), biostratigraphy, and lithostratigraphic core descriptions assisted in the development of a sequence stratigraphic framework. These interpretations were traced along seismic data into the WGBB in this study.

Seismic Reflection Data

Between 1973 and 1978, the United States Geological Survey (USGS) collected 6400 km of 48-channel common depth point (CDP) MCS reflection data over 32 tracklines across the offshore Massachusetts to offshore Maryland region (Schlee & Fritsch, 1983; Schlee et al., 1985). A second survey of 4000 km six-channel reflection profiles collected by WHOI supplemented the USGS data (Schlee and Klitgord, 1988). USGS reconnaissance seismic data were reprocessed in 2016 by the Canadian-based Absolute Imaging (AI) company. Imaging was greatly improved by velocity modeling, data migration, noise and spike suppression, among other modern reprocessing steps (Fortin et al., 2017). Four lines from the reprocessed USGS survey lie within the boundaries of the western GBB. Of those four potential lines (totaling 1321 km), three (totaling 431 km) were investigated (Table 2). Lines 5, 12, and 21 show adequate seismic resolution, while line 8 exhibits poor seismic quality.

Seismic data collected between 1976 and 1982 on the U.S. Outer Continental Shelf (OCS) for exploratory purposes were recently released by BOEM/USGS (Treizenberg et al., 2016) as a part of the National Archive of Marine Seismic Surveys

(NAMSS). MCS reflection profiles from six seismic surveys in the NAMSS database were used in this study. The six surveys recorded a total of 45,000 km of data over 759 tracklines along the entire United States margin. This study investigated ~13,300 km, over 177 tracklines, of that data spanning an area of ~25000 km^2 of the margin (Table 2). Data were acquired by 2D airgun and streamer system, provided in SEG-Y format, and imported into a workstation running Petrel v. 2017. Processing steps applied (stacking, migrations) varied slightly from survey to survey, explaining potential differences between profiles.

In 1976, the U.S. petroleum industry initiated hydrocarbon exploration of the GBB's OCS with the drilling of two deep wells (COST G-1 and COST G-2). Over the next six years, drilling of eight more exploratory offshore wells followed. Well data, along with interpretations of seismic, geomagnetic, and gravity data have since been made public (Poag, 1982).

Mapping seismic surfaces

The field of sequence stratigraphy was originally developed using seismic reflection profiles in accordance with the first widely-accepted definition of a depositional sequence: "a stratigraphic unit composed of a relatively conformable succession of genetically related strata and bounded at its top and base by unconformities or correlative conformities" (Mitchum et al., 1977). Seismic sequence stratigraphy is the study of stratigraphy and depositional facies as interpreted from seismic reflection data (Vail et al., 1977; Mitchum et al., 1977) (Figs. 10A, 11A, 12A). Sequence stratigraphy integrates seismic profiles with outcrop and core observations, well data, and downhole wireline logs (Van Wagoner et al., 1987; Vail, 1987).

By following a set of objective mapping procedures (first outlined by Mitchum and Vail, 1977 and Mitchum et al., 1977), seismic profiles can be subdivided into depositional sequences (Figs. 10B, 11B, 12B). These methods highlight the importance between continuous and discontinuous stratal relationships within a stratigraphic framework. Seismically reflected bedding surfaces with discontinuous geometric features often result in termination reflections - characterized as onlap, downlap, toplap, erosional truncations, or apparent truncations (Mitchum et al., 1977) (Figs. 10B, 11B, 12B). Reflections of bedding surfaces may also exhibit concordance, meaning no terminations are observable.

Sequence stratigraphy is based on significant seismic surfaces – characterized by sequence boundaries (SB), transgressive surfaces (TS), and maximum flooding surfaces (MFS). Surfaces are identified by recognizing where bedding surface reflections terminate in a geometrically consistent way (Mitchum et al., 1977; Vail et al., 1977; Neal and Abreu, 2009). Seismically, sequence boundaries are regional surfaces of erosion that are defined by downward shifts in onlap, erosional truncation, toplap, and downlap. Maximum flooding surfaces are commonly characterized as regional downlap surfaces (Vail, 1987). Using the clinoform rollover model (e.g., Neal and Abreu, 2009; Miller et al., 2018), strata can be interpreted to exhibit either progradational, retrogradational, or aggradational vertical stacking patterns. Stratigraphically significant bounding surfaces (SB, TS, MFS) can be identified in well logs by changes in vertical stacking patterns (Neal and Abreu, 2009) and on seismic profiles by trends in reflection terminations. Once bounding surfaces are identified, stratigraphic sequences can be mapped based on regional lateral continuity, as well as stratal geometry thickness, and orientation. Systems

tracts are depositional systems identified and connected by vertical stacking patterns and separated by bounding surfaces (Posamentier and Vail, 1988). Depositional sequences are subdivided into three system tracts: lowstand systems tract (LST: the lower regressive systems tract), transgressive systems tract (TST), and high-stand systems tract (HST: upper regressive systems tract) (Posamentier and Vail, 1988). A falling stage systems tract (FSST) is sometimes recognized by downstepping seismic reflectors below the sequence boundary (Posamentier et al., 1992; Plint and Nummendal, 2000).

Analyzing seismic facies evaluates the depositional environmental setting and ultimately lithofacies characteristics from seismic data. Seismic facies are groups of mappable reflectors with recognizable, definable limits with differing characteristics (amplitude, continuity, frequency, configuration, interval velocity) from neighboring facies sets (Mitchum et al., 1977). Internal reflection terminations have implications for predicting both depositional processes and environments and potential lithology of a sequence. Stratal configurations are characterized by parallel, subparallel, divergent, prograding (e.g., sigmoid, oblique, shingled, hummocky), chaotic reflections, or reflection-free. Age estimates are assigned based on available biostratigraphic picks using core data.

Reflection configuration patterns (layered, chaotic, and reflection-free) provide constraints on depositional and erosional processes. Lateral continuity of bedding is characterized by discontinuous or continuous reflections. Amplitude and frequency of reflections have implications for impedance contrasts and bed spacing (Sangree and Widmier, 1979).

RESULTS

Petrel

The study area contains profiles from six of the BOEM surveys (B-03-75-AT, B-06-76, B-13-76, B-04-80, B-01-81, and B-04-83) and the reprocessed USGS survey (lines 5, 8, 12, 21) (Table 2); local chronological control is poor due to the lack of well data. Quality of the BOEM data also varied: B-01-81, B-04-80, and B-04-83 contain resolvable data, quality fluctuates between lines in surveys B-03-75, B-06-76, and B-13-76. Surveys B-04-82 and B-10-81 contain either poorly resolved or missing seismic data.

The boundary lines of the western GBB (Fig. 1) for this study are defined by the location of much of the available seismic data, as well as the location of the southwest border of the eastern GBB originally defined by Graham (2018). Basin boundaries were created in a new 'map' project on a workstation running Petrel. Boundaries were arbitrarily established based primarily on the criteria of incorporating the majority of available surveys. The resulting 2D geometry is an E-W trending oblong oval that covers ~233 km in the E-W direction and ~110 km N-S, resulting in an area totaling ~25000 km^2.

Using Petrel, well-seismic ties to USGS Line 12 (Fig. 5) were made at Block-133 and Block 975 explorations wells by using geophysical well log data and previously published biostratigraphic interpretations (Graham, 2018). With the guidance of the seismic profiles, stratigraphic horizons were traced within the EGBB seismic grid. Horizons were then projected to the western region, along strike Line 12 (Fig. 5), the primary profile that connects the two baisns. Lines from the BOEM data that intersected Line 12 built the framework for the western GBB's seismic grid (Figs. 6A, 6B).

Interpretation of the seismic sections used sequence stratigraphy principles. Stratal reflector terminations were first identified first to recognize significant seismic surfaces. The sequence stratigraphic framework was defined after basin-wide mapping of seismic horizons. Reasons for potentially incorrect matchups of seismic horizon intersections across the basin are due to differences in data acquisition and processing techniques, availability to strictly 2D data, large fluctuations of quality on individual lines, shot lines with missing data, and possible incorrect manual tracings of reflections. A Petrel feature termed 'ghost mode' is used to correct for seismic horizon mis-matchups. Polarity reversal was used on some seismic lines in order to assure all lines exhibit similar seismic impedance patterns.

Mapping Seismic Horizons

In all, seven distinct seismic reflectors (oldest to youngest: UJ1, LK2, LK1, MK3, MK2, MK1, UK2GB [upper bounding surface] – Figs. 7B, 8B, Table 1) were identified and looped correlated. These reflectors are associated with six depositional seismic sequences (JU1, Miss/MS1, LC3, LC2, LC1, DCx, respectively) identified in well logs (Fig. 3) (Graham, 2018), were mapped across the western GBB. Individual sequence continuity and occurrence differ throughout the basin due to varying seismic resolution. It was difficult to identify internal stratal reflection terminations in areas with poor seismic resolution. Seismic profile resolution decreases with increasing profile depth, resulting in less-confident correlations of older sedimentary intervals (e.g., UJ1, LK2). Regardless, multiple distinct reflections (LK2, LK1, MK3, MK1) were mappable basin-wide. Horizons UJ1, MK2, and UK2GB were not mapped across the entirety of the western

GBB due to consistently poor resolution, leading to the inability to correctly loop correlate across the seismic grid, as well as inaccurate interpolations by Petrel.

Seismic profiles within the southeastern subregion of the WGBB proved to be extremely useful, showing numerous reflection terminations. Eleven dip (NW-SE) and eight strike lines (SW-NE) (Fig. 5, Table 3) from this subregion within survey grids B-04-80-AT and B-01-81-AT were thoroughly examined. Dip line, TP80-300 (CLF – Figs. 11A-D), is the westernmost line within the subregion; ten more dip lines, CLG (PP81-182) through CLN (TP80-298) run parallel to TP80-300 (CLF) and are spaced progressively more eastward. Here, all seismic horizons could be traced and interpreted for seismic sequence stratigraphy. Three dip lines: CLF, CLE, CLD (Figs. 10-12) and one strike line: SLA (Fig. 13) are interpreted in-depth to support the development of a sequence stratigraphic framework. It is important to note that the identification of significant seismic surfaces was based strictly on the observable internal stratal geometry and subsequent reflection terminations. Ages assigned to the reflections are based generally on the well log-seismic stratigraphic ties integrated with available biostratigraphy in Graham (2018) (Fig. 3). The Upper Jurassic to early Late Cretaceous depositional sequences are described below.

Seismic Sequences

The JU1 sequence (~Oxfordian-Tithonian)

The Mic-Mac and Mohawk Formations (Oxfordian-Tithonian), are heterolithic siliciclastic units (Post et al., 2012; CNSOPB, 2009) that correspond to an Upper Jurassic depositional megasequence (JU1). This sedimentary interval is bounded by horizon LK2 (bottom Missisauga) at the top and horizon UJ1 at the bottom. Mapping the basal UJ1

surface was difficult in much of the basin. The combination of the heterolithic sedimentary nature of the unit (mixed sandstones and shales) and low vertical resolution of the data contributed to the chaotic, discontinuous reflections observed on the profiles (Fig. 7B). However, the UJ1 seismic reflection is slightly more continuous along the present-day shelf edge, permitting somewhat confident tracings. Here, the UJ1 seismic boundary lies below ~2300 ms and between 2600 and 2800 ms (Figs. 10D, 11D, 12D, 13A).

The MS1 sequence (Berriasian-Barremian)

Seismic reflections LK1 and LK2 bound the Missisauga depositional sequences (Fig. 8B). The uppermost bounding surface, LK1, is the basal LC3 depositional surface. The lower, less prominent surface, LK2, corresponds with the top of the Jurassic strata. This interval contains the Berriasian-Barremian Missisauga Formation: a heterolithic, siliciclastic, shallow-water (tidal/fluvial environment) deposit (CNSOPB, 2009). On average, the top of LK1 lies below 1820 ms TWTT and the top of LK2 generally lies around 2200 ms, with both reflections shallower in the northwest (Fig. 9A). Despite well-log stratigraphy showing three higher order depositional sequences (Graham, 2018), the low resolution of the seismic data makes correlating seismic surfaces to higher-order depositional sequences difficult. Hints of internal reflections are present in the LK2/MS1 sequence that may indicate high-order sequences (e.g., onlap at CDPs 180-201 [Fig. 7B]), but no consistent tracing was possible due to suboptimal data resolution. Where the LK2 reflection is prominent, it is somewhat continuous, flat-lying, and subparallel with moderate amplitudes (Figs. 6B, 7B).

The LC3 (Aptian)

The Aptian LC3 depositional sequence is the oldest of the three depositional sequences regionally identified within the Logan Canyon Formation. The LC3 sequence boundary is placed at the change from the Barremian LK2/Missisauga sediment package to the Naskapi Shale Formation and correlates to seismic surface LK1 (Graham, 2018). The Naskapi Shale Member of the Logan Canyon Formation is a carbonaceous, fissile shale unit (McIver, 1972) (Fig. 4) associated with an Aptian initiation of the transition from a fluvial-alluvial environment to a deltaic one (Miller et al., 2018). This package is bounded at the top by the MK3 horizon and the LK1 horizon at the base. The LC3 depositional sediment package is thickest in the south-central region of the GBB (~250 ms) and thins to the outer margins of the basin (~100 ms) (Fig. 14B).

The LK1 reflector can be loop-correlated throughout the entirety of the western GBB. In the southwest, the horizon is continuous, flat-lying, and high amplitude (Fig. 8B); farther north, LK1 becomes harder to trace due to a change to a wavy, discontinuous internal reflector (Fig. 7B). There are some observable internal reflections within the LK1 seismic sequence in the southeast. Identifiable reflections are slightly wavy and discontinuous; terminations either appear to slightly onlap onto the surface (Fig. 12D: CDPs 178-267), are associated with downlap onto the LK1 horizon (Fig. 10D: CDP 1414; Fig. 11D: CDPs 1422-1509) or truncate below (Fig. 12D: CDPs 267, 444). The LC3 sequence is the thinnest sequence in the study area, which may contribute to the poor seismic resolution and ultimately difficulty in determining higher order sequences (Fig. 10D, Fig. 11D. Fig. 12D, Fig. 13B).

The LC2 sequence (Albian)

The Albian LC2 sequence is composed of thick, blocky sands that were likely deposited during a time of prodeltaic sedimentation based on well logs from the EGBB (Graham, 2018; Miller et al., 2018). This sequence is correlative to the upper Logan Canyon Formation of Libby-French (1984; Table 1). The MK3 seismic reflector correlates to the bottom of the LC2 depositional sequence (Table 1; Fig. 3). The MK2 horizon caps the LC2 sequence. Due to variable seismic resolution, the MK2 horizon was only mapped continuously in the basin's southeast region, where the surface is high amplitude and continuous (Fig. 11C). Elsewhere, internal reflections are wavy and discontinuous (Fig. 7B) thus proving difficult in mapping MK2 across the entire basin. Thus, depositional sequences LC1 and LC2, the sedimentary package between the basal MK3 and upper MK1 surfaces, are combined for isopach map construction (Fig. 14C).

The MK3 seismic reflector is high-amplitude, flat-lying, and continuous in the western WGBB, as well in the north-central areas (Fig. 6B, 7B, 8B). Reflection terminations are observed in the LC2 sequence in the southern region of the basin. When observed on dip lines (Table 3), the MK3 surface is associated with downlapping reflections that terminate onto the surface (Fig. 10D: CDPs 1503-1769; Fig. 12D: CDPs 223-444) and erosional truncation of underlying reflections (Fig. 11D: CDP 1509).

The LC1 sequence (Lower Cenomanian)

The LC1 depositional sequence is the youngest of the three Logan Canyon sequences. The MK2 reflector is the basal surface of the LC1 sequence, and MK1 lies atop the sequence. This package is the thickest of the LC sequences, averaging 320 ms, and thins slightly to the west (<100 ms) (Fig. 14C). In the north and central regions, the

MK1 surface generally lies below 1100-1300 ms of TWTT, with the MK3 surface generally around 1350-1650 ms (Figs. 9C, 9D). If unaffected by periods of erosion or nondeposition, the MK2 seismic surface lies between 1100 and 1650 ms in the northern and central regions. Where MK2 is confidently traced in the south, it lies at ~1800 ms (Figs. 10D, 11D, 12D, 13B). The upper bounding MK1 horizon is mapped continuously throughout the basin, exhibiting high amplitude, continuous reflections in almost all areas (Figs. 6B, 7B, 13B).

Within areas of the basin where the MK2 horizon is confidently traced, internal reflections can be observed in thicker sections of the LC1 sequence. Reflections observed on dip lines (Table 3) near the present shelf break generally downlap onto MK2 (e.g., Fig. 10D: CDPs 1414-1681; Fig. 11D: CDPs 1289-1554; Fig. 12D: CDPs 134-178, 400-444). The MK2 sedimentary interval consists of high relief prograding clinoforms towards the ocean-continent boundary (Figs. 10D, 11D). The internal geometry of the clinoforms assist in identification of the upper bounding surface MK1. Reflections observed on strike lines (Table 3) are conformable and flat-lying, continuous, with rare instances of termination (Figs. 8B, 13B).

The DCx sequence (Upper Cenomanian-Turonian)

Capping the LC1 sequence in the GBB is a mud-rich, shaley unit termed the Dawson Canyon Formation (Libby-French, 1984; Fig. 3), deposited in Cenomanian – Turonian deep shelf environments, coinciding with long-term sea-level rise (Miller et al., 2005; Kennedy et al., 2005). The Dawson Canyon Formation correlates to the DCx (where x = unnamed number until additional data permits subdivision of this composite sequence) depositional sequence (Graham, 2018; Schmelz et al., 2019; Fig. 3).

Determining higher-order sequences within the DCx depositional sequence using the data available proved difficult in most of the basin, excluding numerous profiles in the southeast subarea (Table 3). The prominent MK1 surface is the upper surface of the high-angled prograding clinoforms seen in the MK2 seismic sequence/LC1 depositional sequence (Figs. 10D, 11D) and correlates to basal surface of depositional sequence DCx (Table 1; Fig. 3). Upper bounding surface UK2GB loosely correlates to the UK2 horizon previously interpreted in the southern Baltimore Canyon Trough (Schmelz et al., 2019; Baldwin et al., in review). UK2GB lies atop the relatively low-angled, flat-lying reflections that make up DCx sequence observed in the southeastern GBB (Fig. 10D, 13B). The UK2GB surface was not mapped elsewhere in the basin.

Near the modern shelf/slope break, the DCx sequence generally thickens downdip (Figs. 11C, 12C) and characterized by relatively flatter, continuous reflections up-dip (Fig. 10D). UK2GB onlaps onto the MK1 reflector, subsequently capping the top of the DCx depositional sequence (Fig. 10D: CDP 1281; Fig. 11D: CDP 1200, CDP 1475; Fig. 12D: CDP 355). UK2GB is also associated with downlap (Fig. 10D: CDP 1414; Fig. 11D: CDP 1422, 1509) from the above depositional sequence (unnamed in this study).

Structural Contours and Isopachs

Basin-wide structural contour maps of depth to the most prominent and continuous surfaces, LK2, LK1, MK3, MK1 (Figs. 9A-9D), and isochron – isopach (time thickness) maps of the Lower Cretaceous (MS1; Fig. 14A), middle Cretaceous (LC3; Fig. 14B), and lowermost Upper Cretaceous (LC2, LC1; Fig. 14C) depositional sequences were constructed. These maps are critical in assessing basin-wide changes in the location of sedimentary depocenters during the latest Jurassic to earliest Late Cretaceous.

Structural contours are set at sea floor, spaced at 100 ms TWT with a contour smoothing filter width of 10.

Initial observations indicate areas of shallower travel times in the north-northwest subareas of the western GBB throughout the entirety of the Cretaceous. Greatest travel times are in the southeast portion of the basin (Figs. 9A-9D). No prominent topographic highs or lows are observed. Isochron – isopach maps for all depositional sequences indicate sediment is thickest in the southeast portion of the basin, mimicking the geography of the modern shelf-slope break (Figs. 14A-C). However, when cross referenced with MCS profiles, it appears Petrel incorrectly interpolated the tracings near the modern shelf break on several profiles for all surface. The general southeast thickening trend observed is likely correct, however the details of the contours are likely data artifacts. Thus, the abnormally thick packages observed in the area are falsely represented and subsequently ignored for both interpretation and consideration for carbon storage (Figs. 14 A-C). A bullseye observed in the contours north-central subarea of the basin (Figs. 14A-C) is also likely a data artifact created by Petrel. Nevertheless, loop correlations can be closed elsewhere in the basin, ultimately allowing for confident seismic horizon interpretations.

Lower Cretaceous sequence – Missisauga

Lower Cretaceous elevations in the northwest subregion are roughly -1400 ms TWT (Figs. 9A, 9B). LK2 surface contours are consistently spaced through most of the basin and become much closer together around the -2600 ms contour at the modern shelf break (Fig. 9A). LK1 contours are similarly spaced, also becoming closer at the shelf break around the -2300 ms contour (Fig. 9A). Similar depths of the two surfaces imply

low relief of Lower Cretaceous strata within the western subregion, with a steep shelf-slope break at similar positions (beginning of shelf break: Fig. 11D – CDP: 1597). The average thickness of Lower Cretaceous sediments is about 300 ms (Fig. 14A). A consistent gradational southeastward thickening of sediments from the northwest margin (50 ms) to directly northwest of the present-day continental shelf-slope break (~500 ms) is observed (Fig. 11D: CDP 1597). The gradational thickening implies a continental sediment source from the northwest, likely outside of the boundaries of the western GBB. This thickening correlates with decreasing depths in the southeast direction. LK2 SB depths (top Jurassic sediments; Fig. 9A) support a similar increase in two-way travel time seaward trend throughout the Early Cretaceous.

Middle Cretaceous sequence – LC3

The sedimentary interval between the top of the Missisauga Formation (LK1) and reflector MK3 is generally 150 ms thick (Fig. 14B). Sediments deposited in the middle Cretaceous (LC3 sequence) exhibit the most uniform pattern of deposition across the basin at any time interval. Sediment is relatively thin on the northwest margin and thicken slightly to the southeast (Fig. 14B). The sediments in the south-central portion thicken (by ~100 ms) with decreasing elevation (~ -2600 ms) (Figs. 9B, 14B) and represent middle Cretaceous sedimentary depocenters near the outer shelf lobes. The sediment source is difficult to observe, as sediment thickness was relatively uniform throughout the basin. Potential sediments sources may be from either the north or northwest (Fig. 14B), likely outside of the limits of the western GBB, towards the continent. Contour lines within the main basin are more regular spaced than older Cretaceous sediments (Fig. 9B, 9C), supporting a gradual sedimentary fill in areas of

slightly higher relief. Therefore, the majority of the GBB was likely an area of relatively low relief during the middle Cretaceous. Like the LK2 lower Cretaceous sequences, contours become closer together at the modern shelf-slope break, around the -2200 ms contour (Fig. 9C).

Late Cretaceous sequences – LC2, LC1, DCx

The average thickness of Upper Cretaceous sediments is about 320 ms (Fig. 14C). Sediment is relatively the thickest (~500 ms) in the center of the basin (Fig. 14C). Similar thicknesses are observed on the basin's central-eastern margin as well. Northwest areas of relatively higher elevation (-900 ms) correspond with thinner packages of sediment (~100 ms) and thicken towards the east (Figs. 9D, 14C). The large difference in travel times of the MK2 surface contour (~1300 ms in the north and central regions, 1800 ms in the south (Fig. 9D)) may indicate a significant deepening southwards towards the present-day shelf break during the Cenomanian. A prominent area of thin sediment packages (25-200 ms) is observed due north of the modern shelf-slope break (Fig. 14C). This significant thinning is likely due to prograding clinoforms within the depositional sequence LC1 and associated downlapping of reflections onto the MK2 surface (Fig. 10D: CDPs 1414-1814; Fig. 11D: CDPs 1289, 1465-1597). Progradation occurs within the individual sequences, however the trend of the Late Cretaceous sequences displays an overall retrogradational stacking pattern. The main sedimentary depocenter is centrally located, suggesting northern Late Cretaceous sediment sources (Fig. 14C).

DISCUSSION

Basin Sedimentation and Sources

Accommodation is the vertical space available for sediment accumulation created by many factors including changes in global sea-level, tectonic seafloor subsidence, basin geometry, faulting, folding, sediment loading, and sediment compaction. Accommodation balanced with sediment flux essentially controls basin deposition and together they are responsible for the progradational and retrogradational movements of a shoreline. The quantity of sediment transported into a basin is highly dependent on its distance from a sediment source and what type of source is supplying the basin. The relationship between tectonics and climate and depositional paleoenvironment is also significant on sedimentation. A seismic sequence stratigraphic framework was established using MCS profiles to evaluate Cretaceous sedimentation, and ultimately the CCS potential of these sediments, within the western GBB. Sedimentary package sequence thicknesses, location of sediment sources and depocenters, as well as paths of sediment movement, were assessed in order to interpret the primary means of Cretaceous sediment deposition in the western GBB.

The Early Cretaceous Missisauga sequence is a non-marine, likely fluvial, deposit, supported by the observation of interbedded heterolithic sandstones and shales and chaotic, irregular, wavy-like seismic reflections, varying in amplitude (Figs. 6B, 13D) throughout the basin. In the western GBB, sediment depocenters are in various areas along the present-day OCS and slope. The thickest depocenter is along the southeastern margin of the basin, indicating possible northern sources of sediment that are likely outside of the boundaries of the western GBB (Fig. 14A).

During the Aptian, sediment deposition regionally transitioned from fluvial to mostly deltaic environments. This is supported by HSTs within the Aptian-Cenomanian sequences becoming blockier and sand-prone while thickening and coarsening upsection, observed in multiple industry wells drilled in the eastern GBB interpreted by Graham (2018). The Aptian (LC3) sequence is thin (~100-150 ms) on interpretations of MCS profiles (Figs. 7B, 10C, 12C) but easily distinguishable, and shows high amplitude, more continuous seismic reflections, and distinct reflection terminations (Fig. 6B) at depths that coincide with the transition in depositional environment observed on well log data (Fig. 3). The sequence's thin nature may imply a sediment source outside the limits of the western GBB. The LK1 reflector is associated with downlap onto it, as well as erosional truncation (Fig. 11D). There is also a slight landward shift in sediment depocenters (Fig. 14B) in the Aptian, also supporting the initiation of a transgressive event.

The Albian LC2 sequence is associated with downlapping reflection terminations onto the MK3 reflector (Figs. 10D, 12D) as well as evidence of erosional truncations onto it (Fig. 11D). The sequence thins slightly downdip towards the modern OCS (Fig. 10C). The Albian-Cenomanian sequences (LC2 and LC1) are the thickest of the sequences, averaging 320 ms (Fig. 14C). Well log stratigraphy indicates the thickest, blockiest sands in the basin are in these sequences (Graham 2018; Fig. 3). There is also a landward, northern shift in sediment depocenters (Fig. 14C), located in the center of the basin near the inner continental shelf. Depositional environments transitioned from terrestrial/deltaic to mostly marine, supporting a significant rise in relative sea level from the Early (~Barriemian) to earliest Late Cretaceous (Miller et al., 2018).

The thickness the of DCx sequence is difficult to determine basin-wide but in the southeast subarea, it is thinner than the underlying LC sequence packages and dips significantly to the southeast near the modern OCS boundary (Figs. 10D, 11D, 12D). Distinct prograding clinoforms appear to be absent in the DCx sequence within the subarea. The UK2GB surface onlaps onto the surface of the MK1 reflector and is associated with erosional truncation (Figs. 10C, 11C). Erosional truncation or toplap occurs around 1550 ms (TWT) on multiple dip lines, CLE and CLF (Figs. 10C, 11C, 12C). This significant truncation or toplap on the MK1 surface indicates either the occurrence of erosion or a period of non-deposition. The absence of prograding clinoforms in the DCx sequence could be explained by a time of erosion. The MK1 seismic sequence boundary may represent the transition from lower Cenomanian shelf deposits to outer shelf depocenters. The capping UK2GB surface is likely upper Turonian based on regional correlations from southern basins to well logs and cycle charts (Schmelz et al., 2019; Miller et al., 2005). This surface may be associated with a major flooding event globally, (Miller et al., 2005; Haq, 2014) potentially coinciding with Ocean Anoxic Event (OAE) 2 (Kennedy et al., 2005; Miller et al., 2018).

Carbon Sequestration Potential in the Western GBB

Storing supercritical CO_2 in offshore reservoirs requires both a porous (>20%) and permeable (> 1000 mD) reservoir with a suitable cap layer, as well as burial depths greater than 800 m (Bachu, 2000; Miller et al., 2018). The Cretaceous sands (Logan Canyon Fm. and Mississauga Fm.) of the GBB are both porous (~ 30%) and permeable (>100 mD) (Amato and Bebout, 1980; Amato and Simonis, 1980) and are overlain by thick shale units (Dawson Canyon Fm. and Naskapi Fm., respectively). Graham (2018)

concluded that the Logan Canyon sands were too shallow for suitable injection (< 800 m) in the eastern region of the GBB but the Missisauga remains a viable target.

However, closer seismic stratigraphic examination of the extensive amount of seismic data previously collected in the GBB, seismic sequences of both the Logan Canyon and Missisauga sands can be traced in the western GBB. Implementing the techniques of seismic stratigraphy in the western GBB allows observations of sequence thicknesses and depths where wells are unavailable.

The LC depositional sequences in the southeastern subregion of the western GBB are suitably deep and safe for CO_2 injection (Figs. 9C, 9D) (all sequences >800 mbsl). The overlying thick (>100 m), shaley DCx depositional sequence provides an excellent cap rock and seal for LC sand reservoirs. If LC sands here have similar porosity and permeability measurements as the eastern GBB and southern BCT LC sands, potential for carbon storage is also good. To assure that the LC sands are an adequate reservoir for storage, it is necessary for wells to be drilled in the southeastern portion of the western GBB. Wells would probably be accompanied by neutron/density porosity log data and permeability data, as well as biostratigraphy and core collection, allowing chronostratigraphic integration with the seismic sequence stratigraphic interpretations in this study. If porosity and permeability measurements and lithology-seismic integration allow, the LC sands in southeastern margin of the western GBB are a sufficient storage location for supercritical CO_2 with potential to be a viable target for sequestration.

Like the eastern GBB (Graham, 2018), the western GBB Missisauga Fm. sands (MS1, MS2, MS3 sequences), also have potential for successful carbon storage and sequestration. The Missisauga sands are mapped below 800 mbsl, but above 3280 mbsl

(Figs. 9A, 9B), throughout the basin. This implies targets deep enough for suitable storage pressure, but shallow enough for adequate porosity and permeability values (Edson et al., 2000). The overlying basin-wide Naskapi Shale deposit is a good cap rock and seal for the Missisauga sands. Like the LC sequences, drilling of the LK2/Miss sequence is necessary for accurate porosity and permeability measurements and chronostratigraphic/lithologic control. The Mississauga/LK2 sequence is potentially a viable target here; however, the heterolithic nature of these fluvial-deposited sands offer a less favorable reservoir than the thicker, deltaic LC depositional sequences.

Data and Interpretation Uncertainties

A number of reasons contribute to the uncertainty of sequence stratigraphic interpretations in the western GBB. Sources of skepticism range from the overall vertical resolution of seismic data, lack of well data, and accuracy in seismic grid projection from well-log stratigraphy in the eastern subregion (Graham, 2018). Seismic stratigraphic interpretation is most affected by the vertical resolution of data. Any seismic artifact (side-swipes [i.e., synclines, anticlines, faults], water multiples, diffractions, pullups/pushdowns) has the potential to modify the 'true' thickness and continuity of stratal packages. The fluctuation in quality among the numerous seismic surveys alters sequence stratigraphic interpretation as well. The seafloor is offset at the intersection of some profiles, forcing even the highest of amplitude horizons to necessarily not appear continuous along a composite line. Internal reflections were sometimes difficult to observe due to varying seismic resolution. Seismic surfaces sometimes appeared discontinuous, or stratal packages thinned to a level within the vertical resolution. Loop

correlating high amplitude, continuous reflections across the seismic grid assisted in resolving some resolution uncertainties.

The lack of wells drilled in this subregion also creates huge uncertainties. Without biostratigraphic ground truth available, assigning accurate (even just estimated) ages to the strata extremely difficult. The accuracy of velocity surveys directly affects projection of lithologic and biostratigraphic data from wells onto seismic profiles. Therefore, a precise time-depth model was unable to be constructed for this subregion.

CONCLUSIONS

By developing a sequence stratigraphic framework for the sedimentary units in the Georges Bank Basin, the history of past sea level and basin sedimentation patterns can be reconstructed. To assist in these reconstructions, six depositional sequences (JU1, MS1, LC3, LC2, LC1, DCx) within Upper Jurassic and Cretaceous strata were first identified in well log stratigraphy (Graham 2018, Fig. 3) in the eastern GBB. These well log sequences boundaries correlate to seven reflectors (UJ1, LK2, LK1, MK3, MK2, MK1, UK2GB) traced from the eastern GBB to the western GBB on recently released multichannel seismic data (Triezenberg et al., 2016).

Integrating seismic surface seismic stratigraphy with eastern subarea well log stratigraphy and converting time to metric depth using a time-velocity function (Schmelz et al., 2019), ultimately resulted in the regional structural contour maps and isochron – isopachs for the western GBB. These maps, combined with previous sedimentary evaluations of the basin, assisted in understanding of basin sedimentation throughout the Cretaceous. The deepening of water depths and the landward shift of the paleoshoreline, combined with an increase in observable clinoform geometries in the seismic data

support an overall transgression from the Early to Late Cretaceous and a likely transition from a fluvial environment to deltaic deposition. Mid-Cretaceous sediments were deposited gradually filling in areas of earlier moderately low relief, resulting in relatively uniform sediment thicknesses basinwide. Increased sedimentation rates as well as a shift to marine deposition in the Late Cretaceous (Turonian), support a relative sea-level rise across the margin.

The Upper Cretaceous Logan Canyon sands (depositional sequences LC2 and LC1) in the southeast subarea of the western Georges Bank Basin have potential to be a suitable target for carbon storage because of adequate unit thickness, porosity, and permeability measurements, are below the burial depth of supercritical storage, and are capped by the thick Dawson Canyon shales (MK1). However, without well data and cores, it is impossible to know the units' true thickness and lithology, as well as the actual porosity and permeability measurements. Therefore, drilling must first be done in the western GBB before this southeastern subregion can be truly considered as an excellent target for carbon storage and sequestration.

REFERENCES

Amato, R.V., and Bebout, J.W., 1980, Geologic and Operational Summary, COST NO. G-1 Well, Georges Bank Area, North Atlantic OCS: Open File Report 80-269, United States Department of the Interior, Geological Survey. Atlantic OCS Region.

Amato, R.V., and Simonis, E.K., 1980, Geologic and Operational Summary, COST NO. G-2 Well, Georges Bank Area, North Atlantic OCS: Open File Report 80-269, United States Department of the Interior, Geological Survey. Atlantic OCS Region.

Bachu, S., 2000, Sequestration of CO_2 in geological media: criteria and approach for site selection in response to climate change: Energy Conversion and Management, v. 41, no. 9, p. 953-970, doi:10.1016/S0196-8904(99)00149-1.

Bachu, S., 2003, Screening and ranking of sedimentary basins for sequestration of CO_2 in geological media in response to climate change: Environment Geology, v. 44, no. 3, p. 277-289, doi:10.1007/S00254-003-0762-9.

Baldwin, K.E., Miller, K.G., Schmelz, W.J., Mountain, G.S., Jordan, L.M., and Browning, J.V., 2019, Cretaceous sequence stratigraphy of the northern Baltimore Canyon Trough: Implications for tectonic, paleogeographic, and sea-level evolution of the basins: Geosphere, (in press).

Benson, S.M., and Surles, T., 2006, Carbon dioxide capture and storage: an overview with emphasis on capture and storage in Deep Geological Formations: Proceedings of the IEEE, v. 94, no. 10, p. 1795-1805, doi:10.1109/JPROC.2006.883718.

Carswell, A.B., Koning, T., and Hibbs, D.C., 1990, Structural and stratigraphic evolution of the East Georges Bank Basin, offshore Nova Scotia, Canada: American Association of Petroleum Geologists Bulletin, v. 75, no. 5, p. 625-626.

CNSOPB (Canada-Nova Scotia Offshore Petroleum Board), 2009, Call for Bids 2009-2010 Regional Geoscience Overview: http://callforbids.cnsopb.ns.ca/2009/01/regional_geoscience.html (accessed 10-Oct-2018).

Cummings, L., Gupta N., Miller, K., Lombardi, C., Goldberg, D., Ten Brink, U., Schrag, D., Andreasen, D., and Carter, K., 2017, Mid-Atlantic Offshore Carbon Storage Resource Assessment: Energy Procedia, v. 114, p. 4629-4636.

Edson, G.M., Olson, D.L., and Petty, A.J., 2000, Exxon Lyndonia Canyon Block 133 No. 1 Well - Geological and Operational Summary: U.S. Department of the Interior, Minerals Management Service. New Orleans: Gulf of Mexico OCS Region, Office of Resource Evaluation.

Emery, K.O., and Uchupi, E., 1965, Structure of Georges Bank. Marine Geology, v. 3, no.5, p. 349-358, doi:10.1016/0025-3227(65)90023-X.

Fortin W., Goldberg, D., Hutchinson, D.R., and Slagle, A.L., 2017, Carbon Sequestration Potential in Mesozoic Rift Basins Offshore the US East Coast: Teaching Old Seismic Data New Tricks: Abstract T51D-0512, presented at 2017 Fall Meeting, AGU, New Orleans, Louisiana, 11-15 December.

Graham, S.J., 2018, Georges Bank Basin Stratigraphy: Cretaceous Gamma Log Sequences correlated with Seismic Data [M.S. thesis]: Rutgers University, 100 p.

Grow, J.A., and Sheridan, R.E., 1988, US Atlantic continental margin; a typical Atlantic-type or passive margin, *in* Sheridan, R.E., and Grow, J.A., eds., The Atlantic Continental Margin: U.S.: Boulder, Colorado, Geological Society of America, Geology of North America, v. I-2, p. 1-8.

Gunter, W.D., Bachu, S., and Benson, S., 2004, The role of hydrogeological and geochemical trapping in sedimentary basins for secure geological storage of carbon dioxide, *in* Baines, S.J., and Worden, R.H., eds., Geological Storage of Carbon Dioxide: Geological Society, London. Special Publications 233, p. 129-145.

Haq, B.U., 2014, Cretaceous eustasy revisited: Global and Planetary Change, v. 112, p. 44-58, doi:10.1016/j.gloplacha.2013.12.007.

Hathaway, J.C., Poag, W.C., Page, V.C., Miller, R.E., Schultz, D.M., Manheim, F.T., Kohout, F.A., Bothner, M.H., and Sangrey, D.A., 1979, U.S. Geological Survey Core Drilling on the Atlantic Shelf: Science, v. 206, n. 4418, p. 515-527, doi:10.1126/science.206.4418.515.

Hitchon, B., ed., 1996, Aquifer Disposal of Carbon Dioxide: Hydrodynamic and Mineral Trapping - Proof of concept: Geoscience Publishing Ltd., 165 p.

Hutchinson, D.R., Klitgord, K.D., and Detrick, R.S., 1986, Rift basins of the Long Island platform: GSA Bulletin, v. 97, no. 6, p. 688-702, doi:10.1130/0016-7606(1986)97<688:RBOTLI>2.0.CO;2

Kennedy, W., Walaszczyk, I., and Cobban, W., 2005, The global boundary stratotype section and point for the base of the Turonian stage of the Cretaceous: Pueblo, Colorado, U.S.A.: Episodes–Newsmagazine of the International Union of Geological Science, v. 28, no. 2, p 93-104.

Kidston, A.G., Brown, D.E., Smith, B.M., and Altheim, B., 2005, The Upper Jurassic Abenaki Formation Offshore Nova Scotia: A Seismic and Geologic Perspective: Canada-Nova Scotia Offshore Petroleum Board, Halifax, Nova Scotia, 169.

Klitgord, K.D., and Behrendt, J.C., 1979, Basin Structure of the U.S. Atlantic Margin: Rifted Margins, in Watkins, J.S., Montadert, L., Dickerson, P.W., eds., Geological and geophysical investigations of continental margins: American Association Petroleum Geologists, Memoir 29, p. 85-112.

Klitgord, K. D., Hutchinson, D.R., and Schouten, H., 1988, U.S. Atlantic continental margin; Structural and tectonic framework, *in* Sheridan, R.E., and Grow, J.A., eds., The Atlantic Continental Margin: U.S.: Boulder, Colorado, Geological Society of America, Geology of North America, v. I-2, p. 19-56.

Knight, K.B., Nomade, S., Renne, P.R., Marzolie, A., Bertrand, H., and Youbi, N., 2004, The Central Atlantic Magmatic Province at the Triassic-Jurassic boundary: paleomagnetic and 40Ar/39Ar evidence from Morocco for brief, episodic volcanism:

Earth and Planetary Sciences Letters, v. 228, no. 1-2, p. 143-160, doi:10.1016/j.epsl.2004.09.022.

Koning, T., 2011, The East Georges Bank Basin, Offshore Nova Scotia: An Undrilled Basin with Significant Oil and Gas Potential: AAPG Annual Convention and Exhibition, New Orleans, Louisiana, 11-14 April 2010.

Kopp, A., Class, H., and Helmig, R., 2009, Investigations on CO_2 Storage Capacity in Saline Aquifers: Part 1. Dimensional analysis of flow processes and reservoir characteristics: International Journal of Greenhouse Gas Control, v. 3, no. 3, p. 263-276, doi:10.1016/j.ijggc.2008.10.002.

Krause, R., Carley, S., Warren, D., Rupp, J., and Graham, J., 2014, "Not in (or Under) My Backyard": Geographic Proximity and Public Acceptance of Carbon Capture and Storage Facilities: Risk Analysis, v. 34, no. 3, p. 529-540, doi:10.1111/risa.12119.

Libby-French, J., 1984, Stratigraphic Framework and Petroleum Potential of Northeastern Baltimore Canyon Trough, Mid-Atlantic Outer Continental Shelf: AAPG Bulletin 68, no. 1, p. 50-73.

Litynski, J.T., and Vikara, D.M., 2011, Carbon capture and sequestration: The U.S. Department of Energy's R&D efforts to characterize opportunities for deep geologic storage of carbon dioxide in offshore resources: Offshore Technology Conference, Houston, Texas, USA, 2-5 May 2011.

Manspeizer, W., and Cousminer, H.L., 1988, Late Triassic-Early Jurassic synrift basins of the US Atlantic Margin, *in* Sheridan, R.E., and Grow, J.A., eds., The Atlantic Continental Margin: U.S.: Boulder, Colorado, Geological Society of America, Geology of North America, v. I-2, p. 197-216.

May, P.R, 1971, Pattern of Triassic-Jurassic Diabase Dikes around the North Atlantic in the Context of Predrift Position of the Continents: Geological Society of America Bulletin, v. 82, no. 5, p. 1285-1292, doi:10.1130/0016-7606(1971)82[1285:POTDDA]2.0.CO;2.

MacIver, N.L. 1972, Cenozoic and Mesozoic Stratigraphy of the Nova Scotia Shelf: Canadian Journal of Earth Sciences, v. 9, no. 1, p. 54-70, doi:10.1139/e72-005.

Miller, K.G., Kominz, M.A., Browning, J.V., Wright, J.D., Mountain, G.S., Katz, M.E., Sugarman, P.J., Cramer, B.S., Christie-Blick, N., and Pekar, S.F., 2005, The Phanerozoic record of global sea-level change: Science, v. 310, no. 5752, p. 1293-1298, doi:10.1126/science.1116412.

Miller, K.G., Lombardi, C.J., Browning, J.V., Schmelz, W.J., Gallegos, G., Mountaun, G.S., and Baldwin, K.E., 2018, Back to Basics of Sequence Stratigraphy: Early Miocene and Mid-Cretaceous examples from the New Jersey paleoshelf: Journal of Sedimentary Research, v. 88, no. 1, p. 148-176, doi:10.2110/jsr.2017.73.

Mitchum, R.M., Jr., 1977, Seismic Stratigraphy and Global Changes of Sea Level: Part 11. Glossary of Terms used in Seismic Stratigraphy: Section 2. Application of Seismic Reflection Configuration to Stratigraphic Interpretation, *in* Payton, C.E., ed., Seismic

Stratigraphy: Applications to Hydrocarbon Exploration: American Association of Petroleum Geologists, Memoir 26, p. 205-212.

Mitchum, R.M., Jr., and Vail, P.R., 1977, Seismic Stratigraphy and Global Changes of Sea Level: Part 7. Seismic Stratigraphic Interpretation Procedure, *in* Payton, C.E., ed., Seismic Stratigraphy: Applications to Hydrocarbon Exploration: American Association of Petroleum Geologists, Memoir 26, p. 135-143.

Mitchum, R.M., Jr., Vail, P.R., and Thompson, S., III, 1977, Seismic Stratigraphy and Global Changes of Sea Level: Part 2. The Depositional Sequence as a Basic Unit for Stratigraphic Analysis, *in* Payton, C.E., ed., Seismic Stratigraphy: Applications to Hydrocarbon Exploration: American Association of Petroleum Geologists, Memoir 26, p. 53-62.

Neal, J., and Abreu, V., 2009, Sequence stratigraphy hierarchy and the accommodation succession method: Geology, v. 37, no. 9, p. 779-782, doi:10.1130/G25722A.1.

Olsen, P.E., 1999, Giant Lava Flows, Mass Extinctions, and Mantle Plumes. Science, v. 284, no. 5414, p. 604-605, doi:10.1126/science.284.5414.604.

Olsen, P.E., Kent, D.V., Et-Touhami, M., and Puffer, J., 2003, Cyclo-, Magneto, and Bio-Stratigraphic Constraints on the Duration of the CAMP Event and its Relationship to the Triassic-Jurassic Boundary: Geophysical Monograph - American Geophysical Union, v. 136, p. 7-32, doi:10.7916/D8KW5RC6.

Plint, A.G, and Nummedal, D., 2000, The falling stage systems tract: recognition and importance in sequence stratigraphic analysis: Geological Society, London, Special Publications 172, no. 1, p. 1-17, doi:10.1144/GSL.SP.2000.172.01.01.

Poag, W.C., 1982, Stratigraphic Reference Section for Georges Bank Basin – Depositional Model for New England Passive Margin: The American Association of Petroleum Geologists Bulletin, v. 66, no. 8, p. 1021-1041.

Posamentier, H.W., and Vail, P.R., 1988, Eustatic Control on Clastic Deposition II – Sequence and System Tract Models, *in* Wilgus, C.K., et al., eds., Sea-level changes: An integrated approach: Society of Economic Paleontologists and Mineralogists Special Publication 42, p. 47-69.

Posamentier, H.W., Allen, G.P., James, D.P., Tesson, M., 1992, Forced regressions in a sequence stratigraphic framework: Concepts, examples, and exploration significance: AAPG Bulletin, v. 76, p. 1687-1709.

Post, P.J., Elliott, E.T., Klazynski, R.J., Klocek, E.S., Decort, T.M., Jr., Riches, T.J., and Li, K., 2012, US central Atlantic: new plays and petroleum prospectivity, *in* Mohriak, W.U., Danforth, A., Post, P.J., Brown, D.E., Tari, G.C., Nemcok, M., and Sinha, S.T., eds., Conjugate Divergent Margins: Geological Society, London, Special Publications 369, p. 323-336, doi:10.1144/SP369.2.

Post, P.J., Klazynski, R.J., Klocek, E.S., Riches, T.J., and Li, K., 2016, Inventory of Technically and Economically Recoverable Hydrocarbon Resources of the Atlantic Outer Continental Shelf as of January 1 2014: Bureau of Ocean Energy Management.

Rast, N., 1988, Variscan-Alleghanian orogen, *in* Manspeizer, W., ed., Triassic-Jurassic Rifting, Developments in Geotectonics: Elsevier, v. 22, p. 1-27, doi:10.1016/B978-0-444-42903-2.50006-3.

Sangree, J.B., and Widmeir, J.M., 1979, Interpretation of depositional facies from seismic data: Geophysics, v. 44, no. 2, p. 131-160, doi:10.1190/1.1440957.

Savva, D., Chrest, T., Saint-Ange, F., MacDonald, A., Luheshi, M., and Cuilhe, L., 2016, Structural Impact of the Yarmouth Arch in the Central Atlantic Opening and on the SW Nova Scotian Margin Architecture: AAPG Annual Convention and Exhibition. Calgary, Alberta, Canada.

Schlee, J.S., and Fritsch, J., 1983, Seismic stratigraphy of the Georges Bank Basin complex offshore New England: American Association of Petroleum Geologists Memoir, v. 43, p. 223-251.

Schlee, J., Poags, C., and Hinz, K., 1985, Seismic Stratigraphy of the Continental Slope and Rise Seaward of Georges Bank, *in* Poag, C.W., ed., Geologic Evolution of the United States Atlantic Margin, p. 265-292.

Schlee, J.S., and Klitgord, K.D., 1988, Georges Bank Basin: A regional synthesis, *in* Sheridan, R.E., and Grow, J.A., eds., The Atlantic Continental Margin: U.S.: Boulder, Colorado, Geological Society of America, Geology of North America, v. I-2, p. 243-268.

Schlische, R.W., Withjack, M.O., and Olsen, P.E., 2003, Relative Timing of CAMP, Riftings, Continental Breakup, and Basin Inversion: Tectonic Significance, *in* Hames, W.E., McHone, J.G., Renne, P.R., Ruppel, C., eds., The Central Atlantic Magmatic Province: Insights From Fragments of Pangea: American Geophysical Union Monograph 136, p. 33-60.

Schmelz, W.J., Miller, K.G., Mountain, G.S., Browning, J.V., and Baldwin, K., 2019, Onshore-offshore correlations of fluvial-deltaic sequences from the mid-Cretaceous of the southern Baltimore Canyon Trough, *accepted*.

Scholle, P.A., and Wenkam, C.R., 1982, Geological Studies of COST Nos. G-1 and G-2 Wells, United States North Atlantic Outer Continental Shelf: US Geological Survey, no. 861, doi:10.3133/cir861.

Steckler, M.S., and Watts, A.B., 1978, Subsidence of the Atlantic-type continental margin off New York: Earth and Planetary Science Letters, v. 41, no. 1, p. 1-13, doi:10.1016/0012-821X(78)90036-5

Thomas, W.A., 2006, Tectonic inheritance at a continental margin: GSA Today, v. 16, no. 2, p. 4-11, doi:10.1130/1052-5173(2006)0162.0.CO;2.

Triezenberg, P.J., Hart, P.E., Childs, J.E., 2016, The National Archive of Marine Seismic Surveys: USGS, doi:10.5066/F7930R7P.

Vail, P.R., Mitchum R.M., Jr., Thompson S. III, 1977, Seismic Stratigraphy and Global Changes of Sea Level: Part 4. Global cycles of relative changes of sea level, *in* Payton, C.E., ed., Seismic Stratigraphy: Applications to Hydrocarbon Exploration: American Association of Petroleum Geologists, Memoir 26, p. 83-97.

Vail, P.R., 1987, Seismic Stratigraphy Interpretation using Sequence Stratigraphy: Part 1: Seismic Stratigraphy Interpretation Procedure, *in* Bally, A.W., ed., Atlas of Seismic Stratigraphy: American Association of Petroleum Geologists, Studies in Geology #27, v. 1, p. 1-10.

Van Wagoner, J.C., Mitchum, R.M., Jr., Posamentier, H.W., and Vail, P.R., 1987, Seismic Stratigraphy Interpretation using Sequence Stratigraphy: Part 2: Key Definitions of Sequence Stratigraphy *in* Bally, A.W., ed., Atlas of Seismic Stratigraphy: American Association of Petroleum Geologists, Studies in Geology #27, v. 1, p. 11-14.

Wade, J.A., and Maclean, B., 1990, The geology of the southeastern margin of Canada. In: Keen, M.J., and Williams, G.L., eds., Geology of the continental margin of eastern Canada: Geological Survey of Canada, Geology of Canada 2, p. 167-238.

Withjack, M.O., Schlische, R.W., and Olsen, P.E., 1998, Diachronous Rifting, Drifting, and Inversion on the Passive Margin of Central Eastern North America: An Analog for Other Passive Margins: AAPG Bulletin, v. 82, no. 5A, p. 817-835.

Withjack, M.O., Schlische, R.W., and Olsen, P.E., 2005, Development of the Passive Margin of Eastern North America: Mesozoic rifting, igneous activity, and breakup, *in* Roberts, D.G., and Bally, A.W., eds., Principles of Phanerozoic Regional Geology: Elsevier, v. 1, 300-335.

FIGURE CAPTIONS

Figure 1: Location map of the available 2D MCS data within the western Georges Bank Basin (GBB), offshore Cape Cod, Massachusetts, United States. Seismic lines are displayed in different colors according to survey. Well locations in the eastern GBB are shown in red diamonds. Map scale is 1:1582272 m. Map boundaries and seismic lines were exported from Petrel and overlain onto a topographic map of the sea floor from GeoMapApp. Entirety of the western GBB lies within the white oval surface, bounded by dark gray lines.

Figure 2: Map of geographic features identified along the margin near the western GBB. Map was created using GeoMapApp. GeoMappApp's default setting is in Mercator projection where geographic North is pointing straight up and where 1° of longitude is about 111 km so a compass rose and scale bar is redundant in this case. Dotted black line represents the border between the United States and Canada. Grey outlined basins show the borders and proximity between the WGBB and EGBB.

Figure 3A: Gamma Log cross section of the western four wells in the eastern GBB, constructed by Graham (2018), with seven depositional sequences identified; from northwest to southeast (left to right): COST-G1, Exxon 133, Mobile 312, and Shell 357. Both measured depth (ft) and two-way time (TWT) in milliseconds, are shown for each log. Well logs are hung from the youngest LC sequence (LC1). Sequences boundaries are denoted in red, Yellow-shaded hues (low gamma values) correlate to sand lithology, brown-shaded hues (high values) correlate with muds or shales. Exxon 133 and Exxon 975 wells were integrated with seismic line USGS 12 to create well-seismic ties and allow loop correlation closure between the EGBB & WGBB seismic grids.

Figure 3B: Gamma Log cross section of the eastern six wells in the eastern GBB, constructed by Graham (2018), with seven depositional sequences identified; from northeast to southwest (left to right): Exxon 975, COST-G2, Mobile 273, Tenneco 187, Conoco 145, and Shell 410. Other display elements are as described in 3A above.

Figure 4: Generalized stratigraphic column adapted from Post et al. (2012) showing geologic time scale for the North American central Atlantic margin. Red rectangle shows time periods and lithologic units examined in this study.

Figure 5: Zoomed in shot of the mini seismic grid constructed in the southeastern western GBB with locations of 2D seismic survey lines, adjusted from Figure 1. Scale is 1:907044 m. The black box represents the subarea of the basin where 19 lines (along both strike and dip) from surveys B-04-80-AT and B-01-81-AT were interpreted using the techniques of seismic sequence stratigraphy for high-order sequence identification. Westernmost dip line CLF and easternmost dip line CLN are indicated by turquoise arrows and lines. Southernmost strike line SLD and northernmost strike line SLH are indicated by yellow-orange arrows and lines.

Figure 6A: Uninterpreted 2-D along-strike multi-channel seismic profile PP81-291 from survey B-01-81-AT. Cross section is in SW to NE direction. XY scale is 1:78,125 m and vertical exaggeration is 5. CDP numbers are above seismic line on the X-axis, vertical axis is in TWT (500 - 2250 ms). This line is in the northeastern portion of the western

GBB. This seismic profile shows the connecting point between the western GBB and the eastern GBB.

Figure 6B: Same 2-D multi-channel seismic profile as Fig. 6A (same scale and axes). Interpreted seismic reflectors are mapped on the line (oldest to youngest): LK2 (orange) seismic horizon represents basal surface of Mississauga depositional sequence (MS1); LK1 (purple) seismic horizon represents basal surface of LC3 depositional sequence/top Miss; MK3 (green) seismic horizon represents basal surface of LC2 depositional sequence/top LC3; MK1 (pink) seismic horizon represents basal surface of DCx depositional sequence/top LC1. Surfaces UJ1, MK2, and UK2GB are not mapped at this location. The red vertical line at ~CDP 1601 represents the point of intersection between the western GBB and the eastern GBB.

Figure 7A: Uninterpreted 2-D dip multi-channel seismic profile MMG-05 from survey B-06-76-AT. Cross section is in NW to SE direction (along downdip: shoreward to seaward). XY scale is 1:62,000 m and vertical exaggeration is 5. CDP numbers are above seismic line on the X-axis, vertical axis is in TWT (500 - 2250 ms). This line is in the northeastern subregion of the western GBB.

Figure 7B: Same 2-D multi-channel seismic profile as Fig. 7B (same scale and axes). Interpreted seismic reflectors are mapped on the line (oldest to youngest): UJ1 (in blue) seismic horizon represents the basal surface of the JU1 depositional sequence (Mic-Mac); LK2 (orange) seismic horizon represents basal surface of Mississauga depositional sequence (MS1); LK1 (purple) seismic horizon represents basal surface of LC3 depositional sequence/top Miss; MK3 (green) seismic horizon represents basal surface of LC2 depositional sequence/top LC3; MK2 (yellow) seismic horizon represents basal surface of LC1 depositional sequence/top LC2; MK1 (pink) seismic horizon represents basal surface of DCx depositional sequence/top LC1. Surface UK2GB is not mapped at this location. The red horizontal line at ~800 ms (TWT) represents the estimated depth for the supercritical fluid state injection for carbon storage.

Figure 8A: Uninterpreted 2-D multi-channel seismic profile D-169 from survey B-03-75-AT. Cross section is in West-East direction (shoreward to seaward). XY scale is 1:50000 and vertical exaggeration is 5. CDP numbers are above seismic line on the X-axis, vertical axis is in TWT (1300 - 2650 ms). This line is located the south-central subregion of the western GBB.

Figure 8B: Same 2-D multi-channel seismic profile as Fig. 8A (same scale and axes). Interpreted seismic reflectors are mapped on the line (oldest to youngest): UJ1 (in blue) seismic horizon represents the basal surface of the JU1 depositional sequence (Mic-Mac); LK2 (orange) seismic horizon represents basal surface of Mississauga depositional sequence (MS1); LK1 (purple) seismic horizon represents basal surface of LC3 depositional sequence/top Miss; MK3 (green) seismic horizon represents basal surface of LC2 depositional sequence/top LC3; MK2 (yellow) seismic horizon represents basal surface of LC1 depositional sequence/top LC2; MK1 (pink) seismic horizon represents basal surface of DCx depositional sequence/top LC1. Surface UK2GB is not mapped at this location.

Figure 9A: Surface contour map showing the depth to LK2 sequence boundary. Scale is 1:705,044 m. Depths range from 1017 to 3959 milliseconds (ms). Average top depth is 2200 ms. Red colors indicate shallow depths while blue colors indicate deeper depths. The contour interval is 100 ms. The black line indicates the modern shelf-slope break.

Figure 9B: Surface contour map showing the depth to LK1 sequence boundary. Scale is 1:705,044 m. Depths range from 974 to 3311 milliseconds (ms). Average top depth is 1825 ms. Red colors indicate shallow depths while blue colors indicate deeper depths. The contour interval is 100 ms. The black line indicates the modern shelf-slope break.

Figure 9C: Surface contour map showing the depth to MK3 sequence boundary. Scale is 1:705,044 m. Depths range from 903 to 3056 milliseconds (ms). Average top depth is 1550 ms. Red colors indicate shallow depths while blue colors indicate deeper depths. The contour interval is 100 ms. The black line indicates the modern shelf-slope break.

Figure 9D: Surface contour map showing the depth to MK1 sequence boundary. Scale is 1:705,044 m. Depths range from 713 to 2323 milliseconds (ms). Average top depth is 1350 ms. Red colors indicate shallow depths while blue colors indicate deeper depths. Structural contours interval is 100 ms. The black line indicates the modern shelf-slope break.

Figure 10A: Uninterpreted 2-D along-dip multi-channel seismic profile CLE (TP80-299) from survey B-04-80. Cross section is in NW to SE direction. XY scale is 1:62500 and vertical exaggeration is 5. CDP numbers are above seismic line on the X-axis, vertical axis is in TWT (1250-3000 ms). This is a primary dip line in recognizing higher order sequences in the southeastern subarea of the western GBB.

Figure 10B: Same 2-D multi-channel seismic profile as Fig. 10A (same scale and axes). Interpreted for reflection terminations, including onlap surfaces, downlap surfaces, toplaps, and truncations, indicated by red arrows.

Figure 10C: Same 2-D multi-channel seismic profile as Fig. 10A (same scale and axes). Interpreted seismic reflectors are mapped on the line (oldest to youngest) without sequence reflection terminations: UJ1 (in blue) seismic horizon represents the basal surface of the JU1 depositional sequence (Mic-Mac); LK2 (orange) seismic horizon represents basal surface of Mississauga depositional sequence (MS1); LK1 (purple) seismic horizon represents basal surface of LC3 depositional sequence/top Miss; MK3 (green) seismic horizon represents basal surface of LC2 depositional sequence/top LC3; MK2 (yellow) seismic horizon represents basal surface of LC1 depositional sequence/top LC2; MK1 (pink) seismic horizon represents basal surface of DCx depositional sequence/top LC1. Capping surface UK2GB is in teal.

Figure 10D: Same 2-D multi-channel seismic profile as Fig. 10A (same scale and axes). Reflection termination interpretations from figure 10B overlain onto seismic reflector interpretations of 10C.

Figure 11A: Uninterpreted 2-D along-dip profile CLF (TP80-300) from survey B-04-80. Cross section is in NW to SE direction. XY scale is 1:62500 and vertical exaggeration is 5. CDP numbers are above seismic line on the X-axis, vertical axis is in TWT (1250-

3000 ms). This is a primary dip line in recognizing higher order sequences in the southeastern subarea of the western GBB.

Figure 11B: Same 2-D multi-channel seismic profile as Fig. 11A (same scale and axes). Interpreted for reflection terminations, including onlap surfaces, downlap surfaces, toplaps, and truncations, indicated by red arrows.

Figure 11C: Same 2-D multi-channel seismic profile as Fig. 11A (same scale and axes). Interpreted seismic reflectors are mapped on the line (oldest to youngest) without sequence reflection terminations: UJ1 (in blue) seismic horizon represents the basal surface of the JU1 depositional sequence (Mic-Mac); LK2 (orange) seismic horizon represents basal surface of Missisauga depositional sequence (MS1); LK1 (purple) seismic horizon represents basal surface of LC3 depositional sequence/top Miss; MK3 (green) seismic horizon represents basal surface of LC2 depositional sequence/top LC3; MK2 (yellow) seismic horizon represents basal surface of LC1 depositional sequence/top LC2; MK1 (pink) seismic horizon represents basal surface of DCx depositional sequence/top LC1. Capping surface UK2GB is in teal.

Figure 11D: Same 2-D multi-channel seismic profile as Fig. 11A (same scale and axes). Reflection termination interpretations from figure 11B overlain onto seismic reflector interpretations of 11C.

Figure 12A: Uninterpreted 2-D along-dip profile CLD (PP81-177B) from survey B-01-81-AT. Cross section is in NW to SE direction. XY scale is 1:50000 and vertical exaggeration is 5. CDP numbers are above seismic line on the X-axis, vertical axis is in TWT (1600-3000 ms). This is a primary dip line in recognizing higher order sequences in the southeastern subarea of the western GBB.

Figure 12B: Same 2-D multi-channel seismic profile as Fig. 12A (same scale and axes). Interpreted for reflection terminations, including onlap surfaces, downlap surfaces, toplaps, and truncations, indicated by red arrows.

Figure 12C: Same 2-D multi-channel seismic profile as Fig. 12A (same scale and axes). Interpreted seismic reflectors are mapped on the line (oldest to youngest) without sequence reflection terminations: UJ1 (in blue) seismic horizon represents the basal surface of the JU1 depositional sequence (Mic-Mac); LK2 (orange) seismic horizon represents basal surface of Mississauga depositional sequence (MS1); LK1 (purple) seismic horizon represents basal surface of LC3 depositional sequence/top Miss; MK3 (green) seismic horizon represents basal surface of LC2 depositional sequence/top LC3; MK2 (yellow) seismic horizon represents basal surface of LC1 depositional sequence/top LC2; MK1 (pink) seismic horizon represents basal surface of DCx depositional sequence/top LC1. Capping surface UK2GB is in teal.

Figure 12D: Same 2-D multi-channel seismic profile as Fig. 12A (same scale and axes). Reflection termination interpretations from figure 12B overlain onto seismic reflector interpretations of 12C.

Figure 13A: Uninterpreted 2-D along-strike multi-channel seismic profile SLA (PP81-226A) from survey B-01-81-AT. Cross section is in SW to NE direction. XY scale is 1:97565 and vertical exaggeration is 5. CDP numbers are above seismic line on the X-

axis, vertical axis is in TWT (500-3250 ms). This is a primary strike line in recognizing higher order sequences in the southeastern subarea of the western GBB.

Figure 13B: Same 2-D multi-channel seismic profile as Fig. 13A (with same scale and axes). Interpreted seismic reflectors are mapped on the line (oldest to youngest) without sequence stratigraphic interpretations: UJ1 (in blue) seismic horizon represents the basal surface of the JU1 depositional sequence (Mic-Mac); LK2 (orange) seismic horizon represents basal surface of Mississauga depositional sequence (MS1); LK1 (purple) seismic horizon represents basal surface of LC3 depositional sequence/top Miss; MK3 (green) seismic horizon represents basal surface of LC2 depositional sequence/top LC3; MK2 (yellow) seismic horizon represents basal surface of LC1 depositional sequence/top LC2; MK1 (pink) seismic horizon represents basal surface of DCx depositional sequence/top LC1. Capping surface UK2GB is in teal. The red horizontal line at ~800 ms (TWT) represents the estimated depth of supercritical fluid for carbon storage and injection. Vertical white lines represent where this line intersects with dip lines CLF, CLE, and CLD.

Figure 14A: Isopleth (~isopach) map of the LK2 package. Scale is 1:705044 m. Thickness was calculated in Petrel by using the LK2 surface as the basal surface of the package and LK1 surface as the upper boundary. Contour interval is 100 ms. Minimum thicknesses are represented by red, increasing from yellow to green to blue, with purple as maximum thicknesses. Thicknesses range from 22 ms to 906 ms, averaging ~300 ms. The black line indicates the modern shelf-slope break; all data southeast of the line was potentially inaccurately interpolated by Petrel (details in the contour lines are likely artifacts) and not considered for carbon storage. Pink arrows represent the possible direction of sediment supply sources.

Figure 14B: Isopleth (~isopach) map of the LK1 package. Scale is 1:705044 m. Thickness was calculated in Petrel by using the LK1 as the basal surface of the package and seismic surface MK3 as the upper boundary. Contour interval is 100 ms. Minimum thicknesses are represented by red, increasing from yellow to green to blue, with purple as maximum thicknesses. Thicknesses range from 25 ms to 620 ms, averaging ~150 ms. The black line indicates the modern shelf-slope break; all data southeast of the line was potentially inaccurately interpolated by Petrel (details in the contour lines are likely artifacts) and not considered for carbon storage. Pink arrows represent the possible direction of sediment supply sources.

Figure 14C: Isoplelth (~isopach) map of the MK2/MK3 packages. Scale is 1:705044 m. Thickness was calculated in Petrel by using the top of the LK1 sedimentary interval ("MK3 seismic boundary") as the basal surface of the package and the MK1/DCx horizon as the upper bounding surface. Contour interval is 100 ms. Minimum thicknesses are represented by red, increasing from yellow to green to blue, with purple as maximum thicknesses. Thicknesses range from 56 ms to 897 ms, averaging ~320 ms. The black line indicates the modern shelf-slope break; all data southeast of the line was potentially inaccurately interpolated by Petrel (details in the contour lines are likely artifacts) and not considered for carbon storage. Pink arrows represent the possible direction of sediment supply sources.

Table 1: Geologic timeline of strata within the western GBB from the upper Late Jurassic to lower Late Cretaceous, correlated to depositional sequences (identified in Graham 2018) and corresponding seismic boundary name. Oldest strata are the Mic-Mac/Mohawk Fms., getting progressively younger to the Dawson Canyon Fm. The "Well log sequence" column corresponds to identified depositional sequences. Sequences are named for their bottom sequence boundary. Colored seismic boundary lines correspond to the basal surface of that specific sedimentary interval (e.g. The purple LK1 interval is bound by the LK1 sequence boundary at the bottom and MK3 seismic surface at the top; LK1 sedimentary interval corresponds to the LC sequence boundary and LC3 depositional sequence). Brief descriptions of deposition sequences/seismic sedimentary interval characteristics are in the right-hand column.

Table 2: Seismic surveys investigated within the boundaries of the western GBB in order to map the Cretaceous strata. Amount of total tracklines and distance shot (in km) for each of the BOEM surveys are available online (B-03-75-AT, available at (https://walrus.wr.usgs.gov/namss/survey/b-03-75-at/); B-06-76-AT, available at (https://walrus.wr.usgs.gov/namss/survey/b-06-76-at/); B-13-76-AT, available at (https://walrus.wr.usgs.gov/namss/survey/b-13-76-at/); B-04-80-AT, available at (https://walrus.wr.usgs.gov/namss/survey/b-04-80-at/); B-01-81-AT, available at (https://walrus.wr.usgs.gov/namss/survey/b-01-81-at/); B-04-83-AT, available at (https://walrus.wr.usgs.gov/namss/survey/b-04-83-at/)). The number of tracklines examined per survey was constrained by the boundaries of the basin. Kilometers shot was calculated using Petrel's "Measure Distance" tool on each individual trackline that boundaries lie within the basin. The total distance of the USGS lines were measured in the same way. This data was made publicly available within the National Archive of Marine Seismic Surveys (Triezenberg et al., 2016).

Table 3: Dip lines are organized from west to east orientation. Strike lines are organized from south to north orientation. Petrel name column indicates the name given to the profiles within Petrel. Line name column indicates what the line was named when the survey was shot.

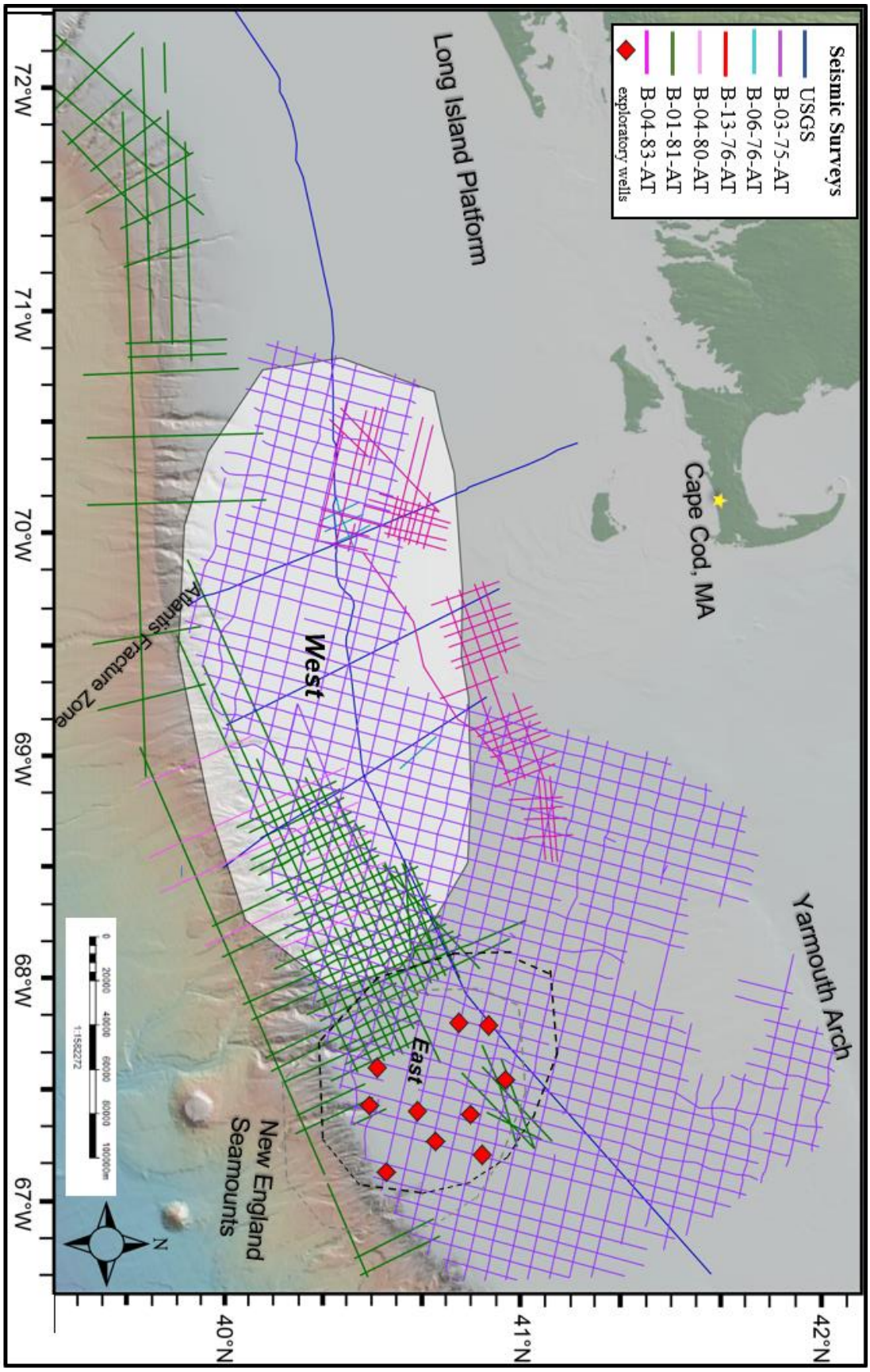

Figure 1: Western GBB Location Map with Available Data

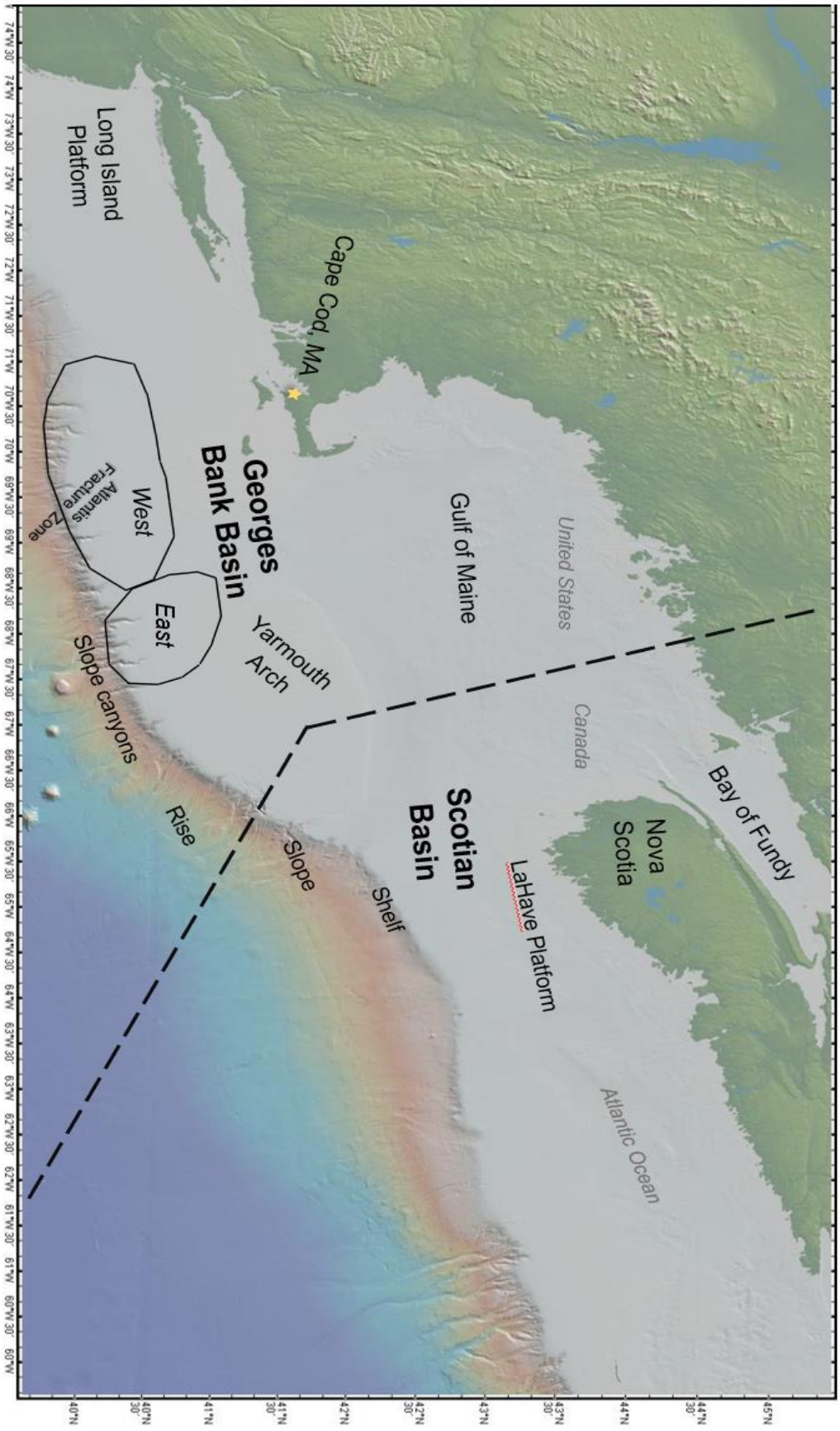

Figure 2: Geographic Features near Western GBB

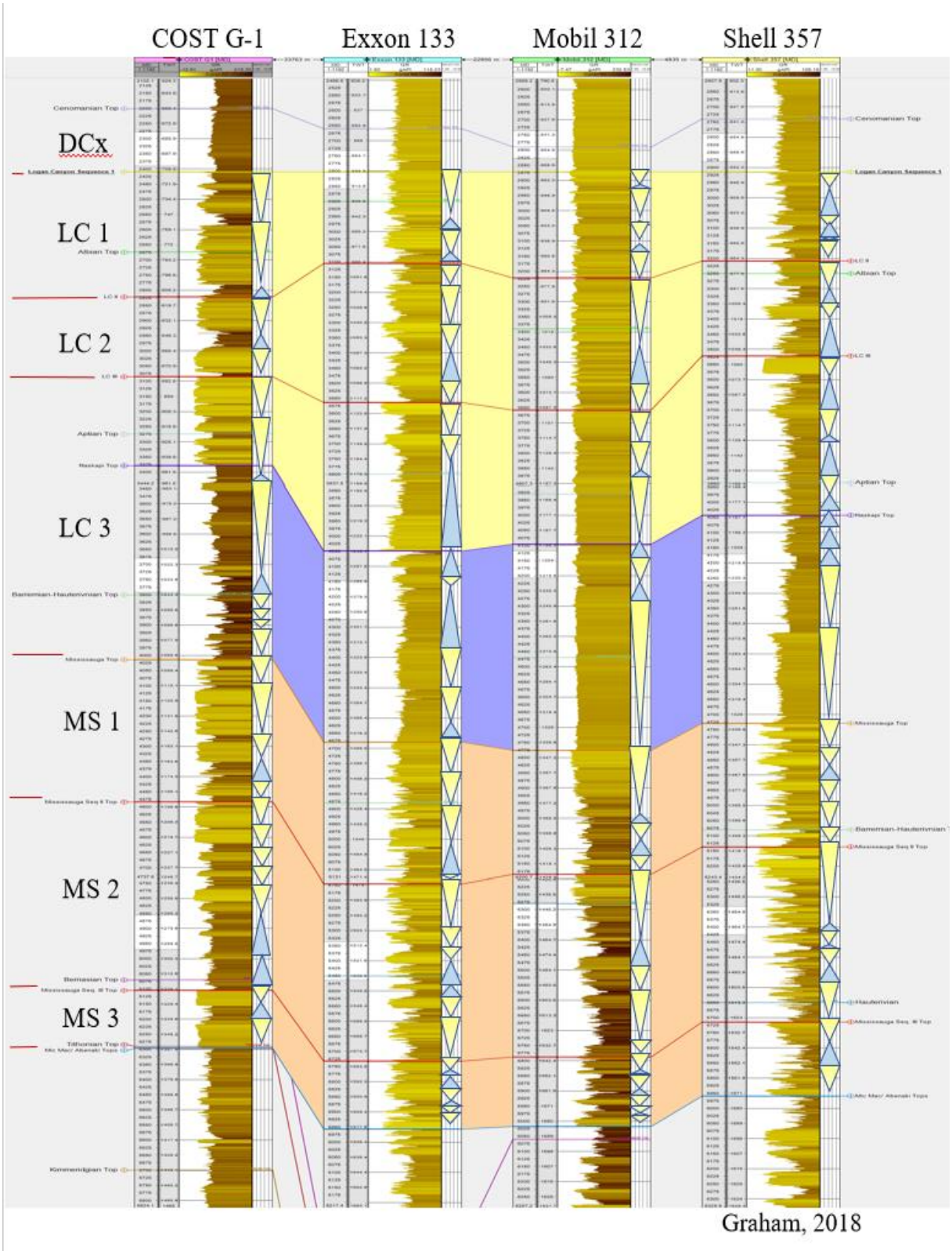

Figure 3A: Western EGBB Gamma Log Cross-Section

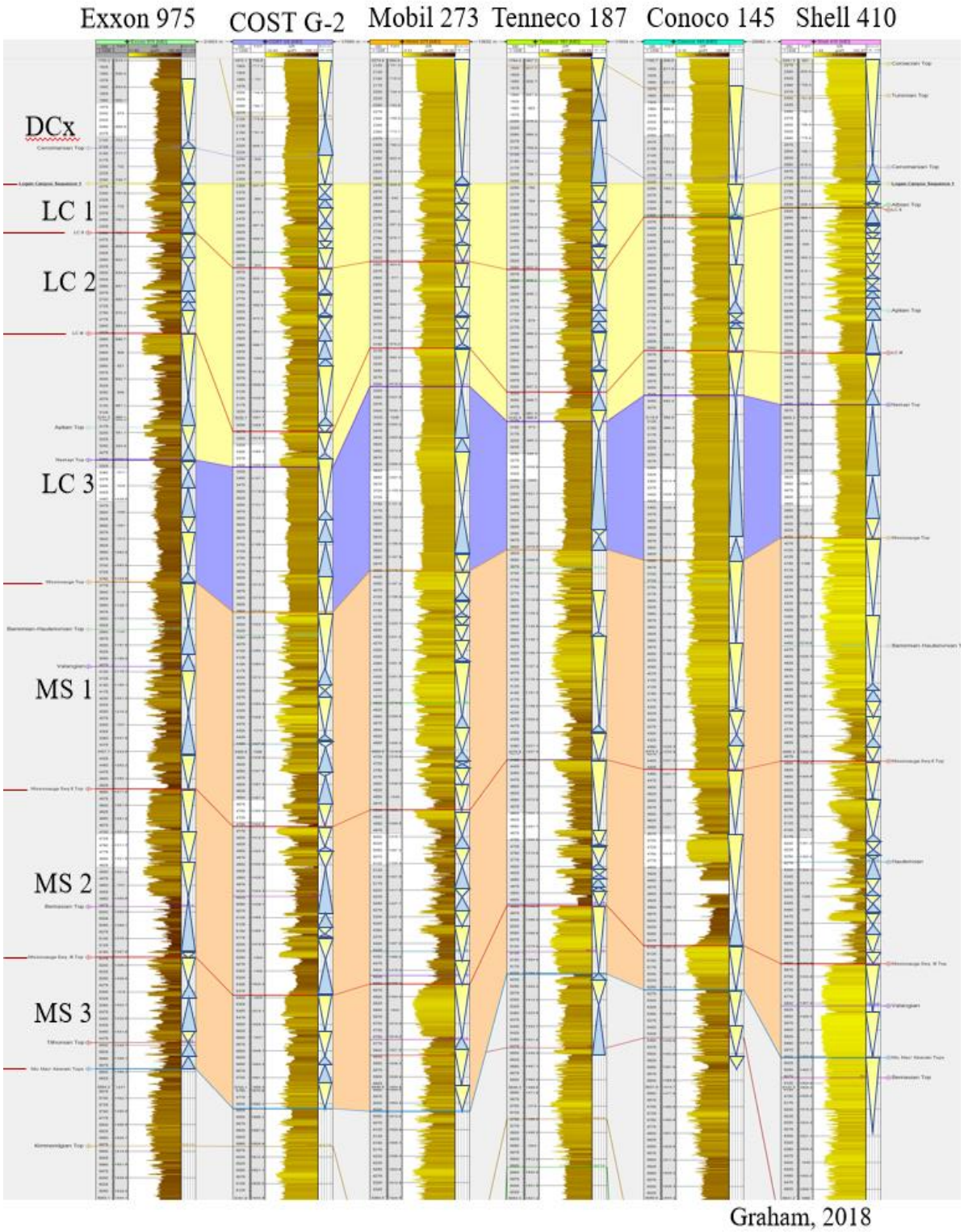

Figure 3B: Eastern EGBB Gamma Log Cross-Section

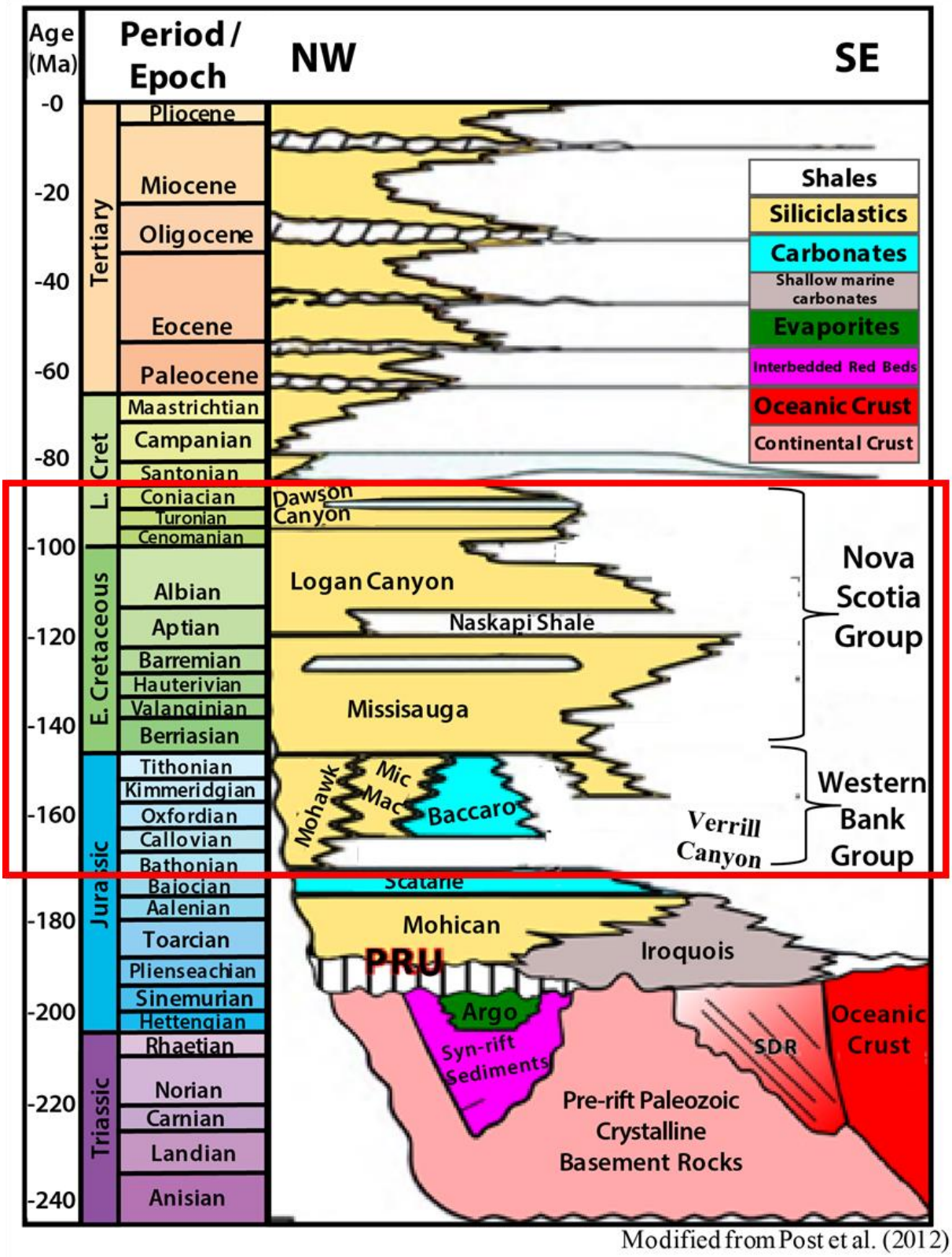

Modified from Post et al. (2012)

Figure 4: Generalized Stratigraphic Column

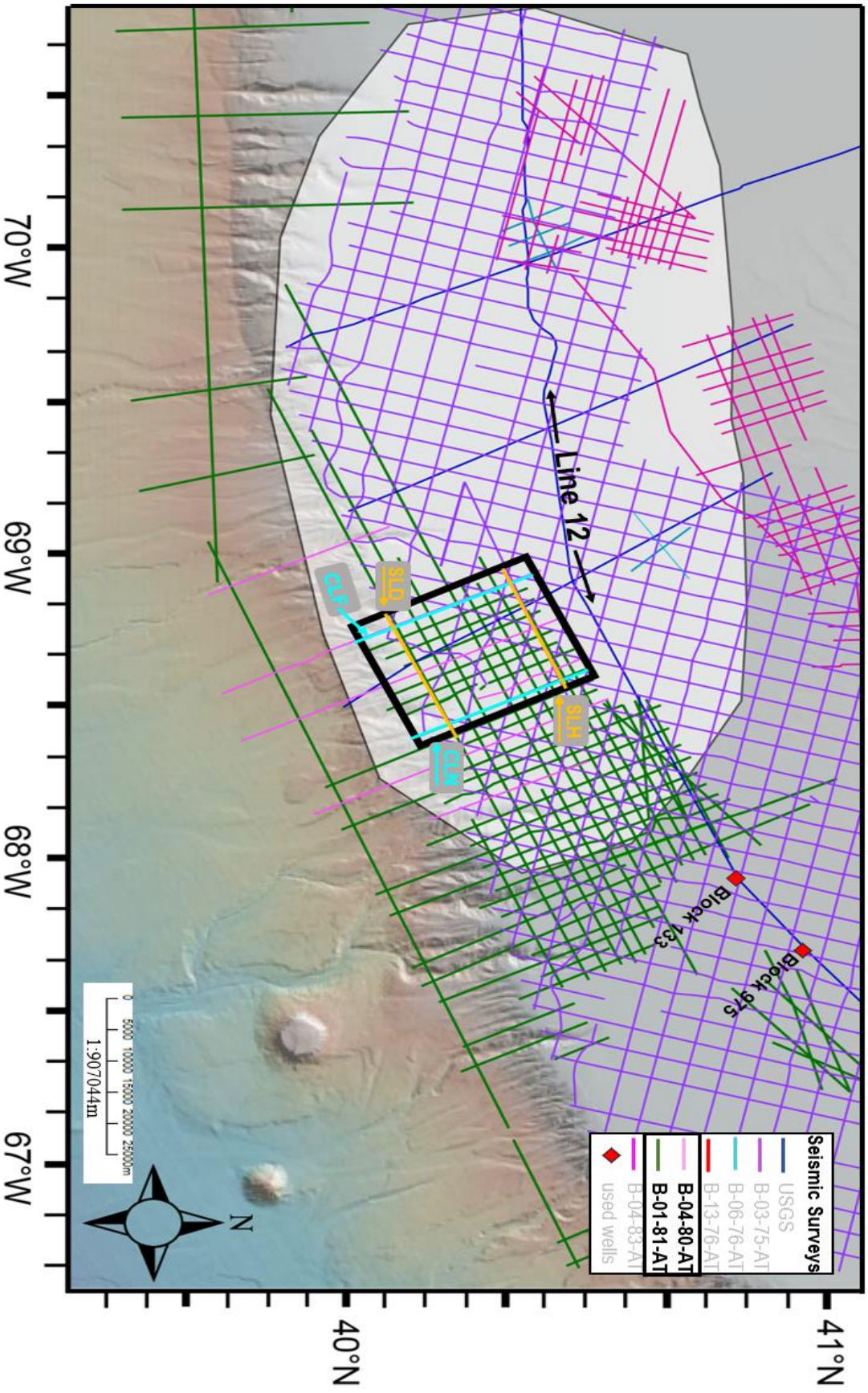

Figure 5: Mini-Grid Seismic Survey Location Map

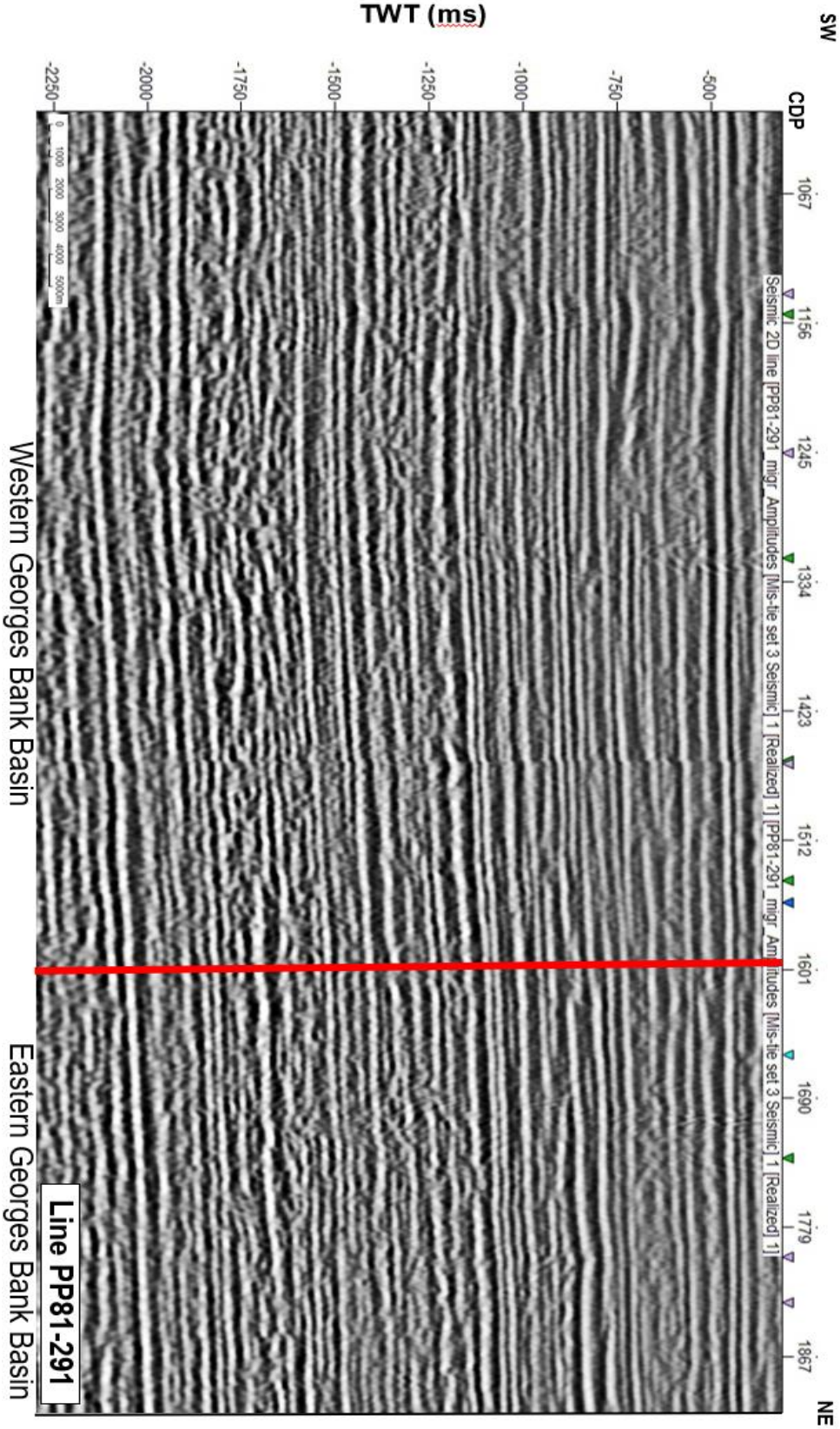

Figure 6A: Uninterpreted Strike Line PP81-291

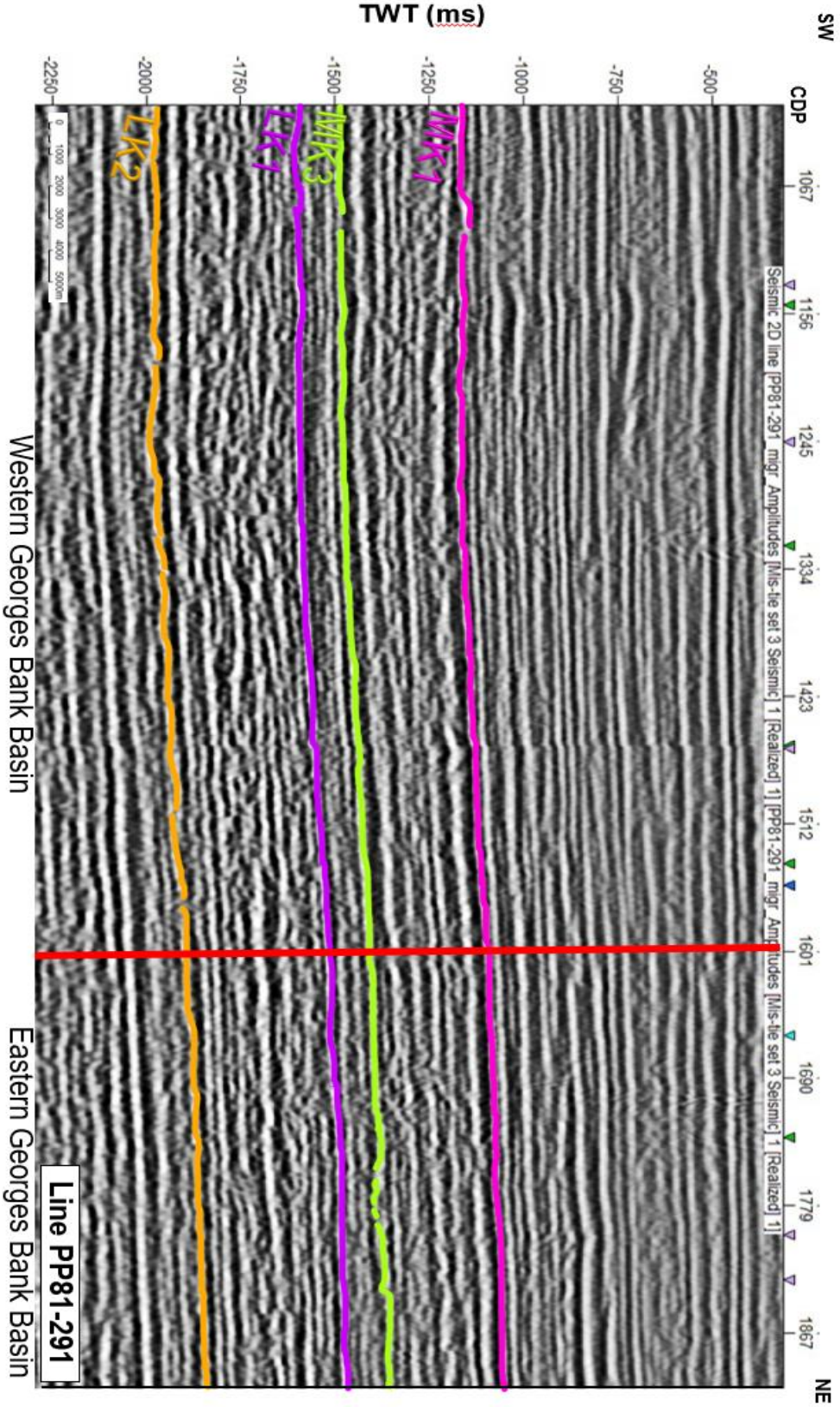

Figure 6B: Seismic Reflector Interpreted Strike Line PP81-291

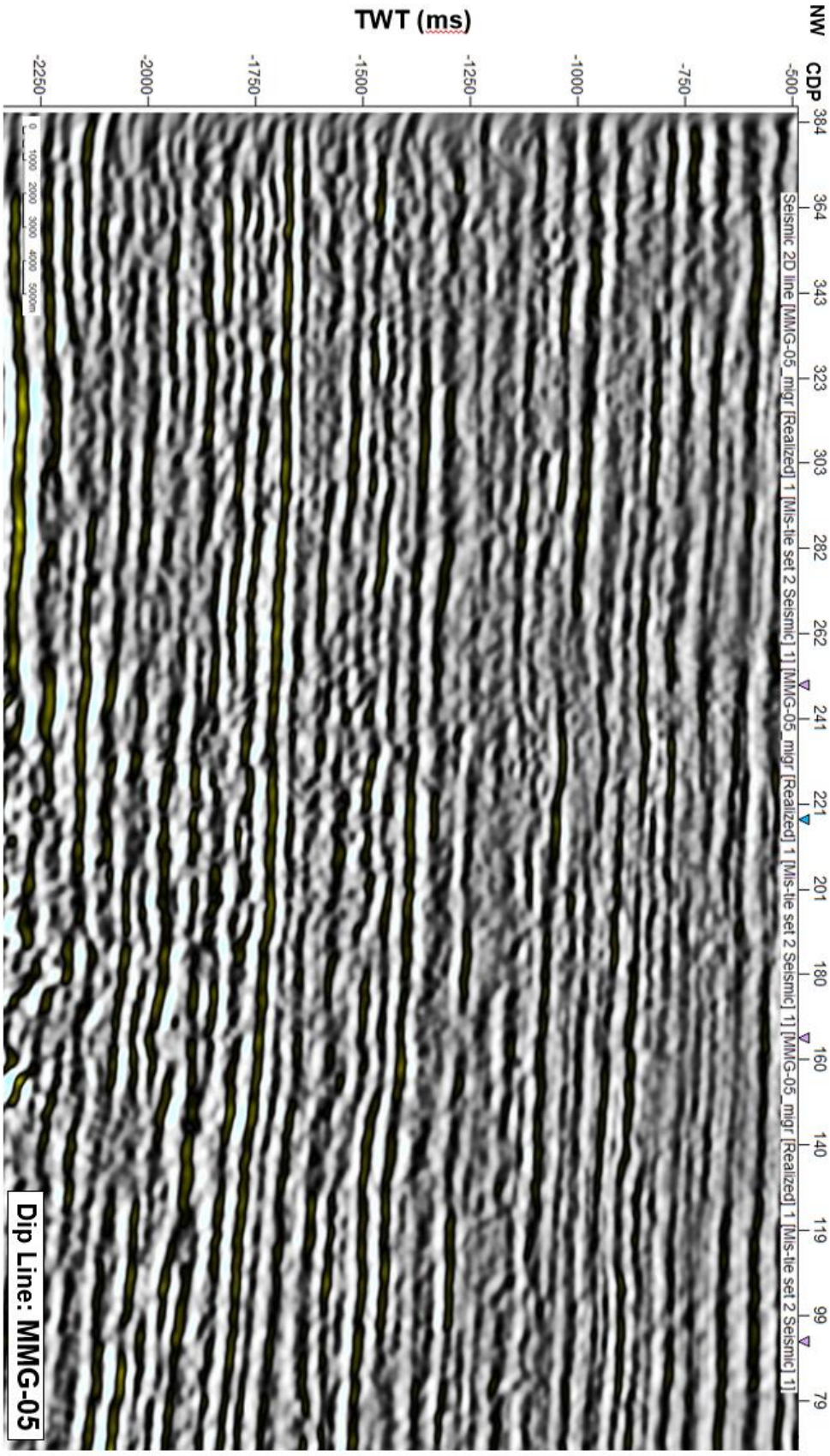

Figure 7A: Uninterpreted Dip Line MMG-5

Figure 7B: Interpreted Dip Line MMG-5

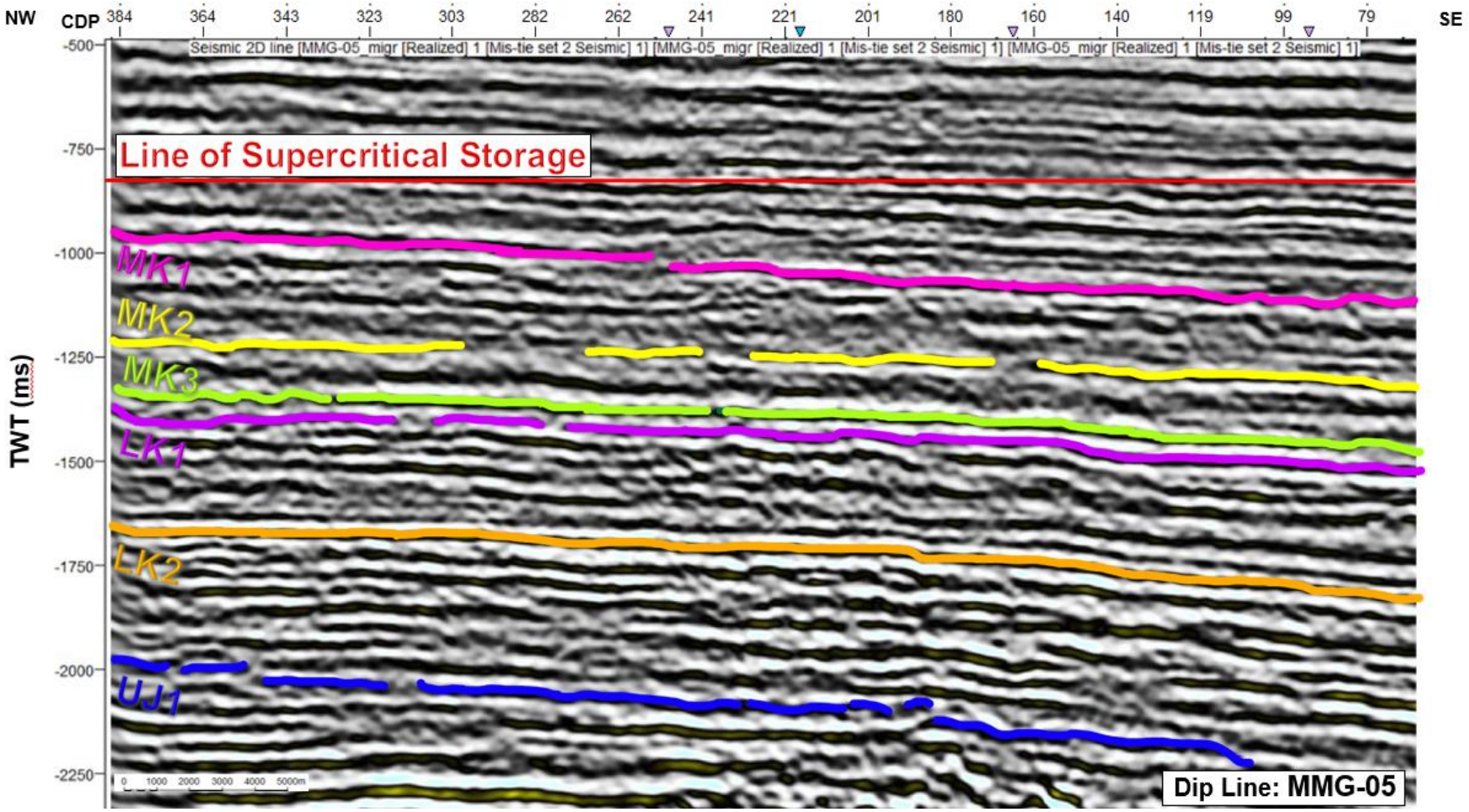

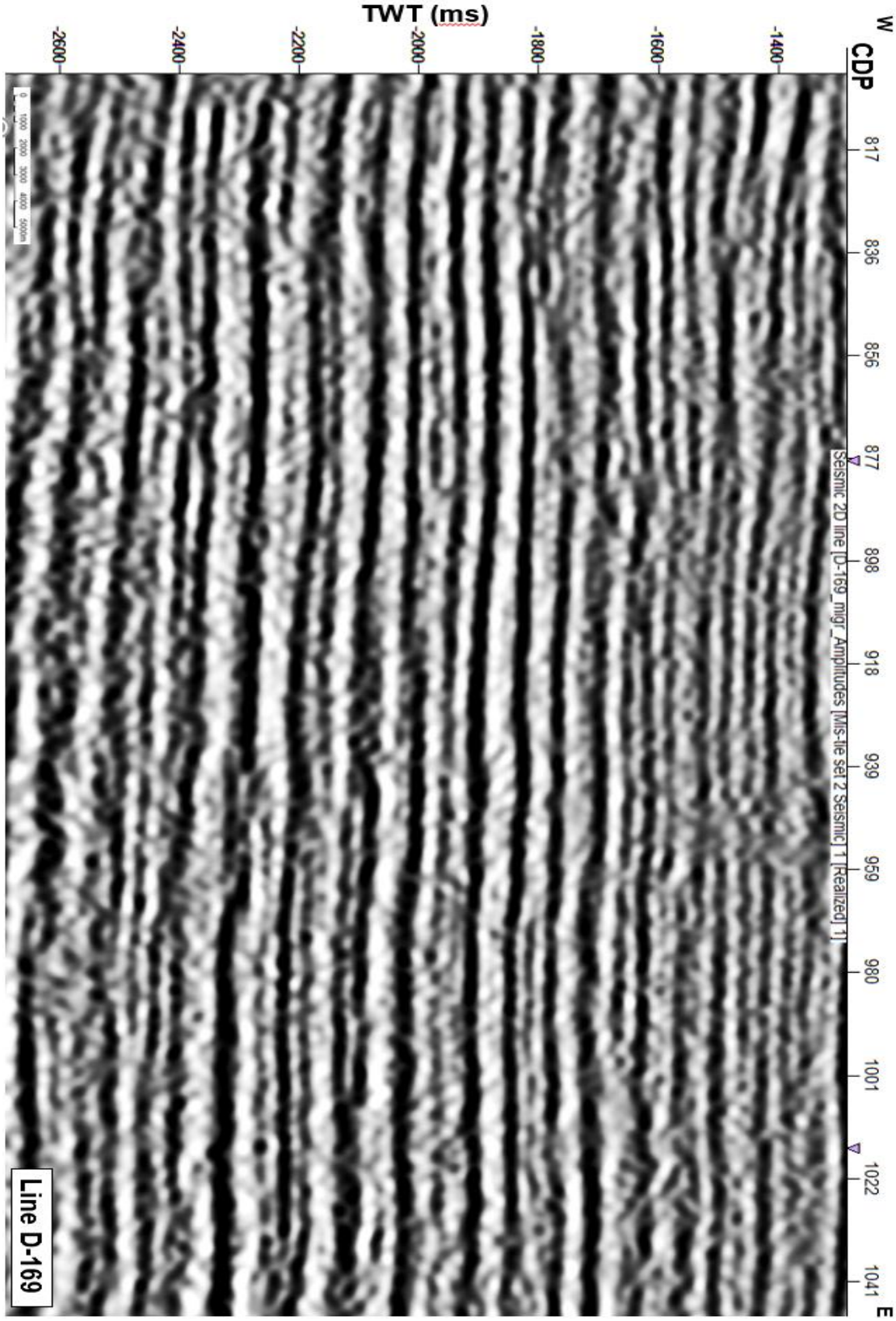

Figure 8A: Uninterpreted Strike Line D-169

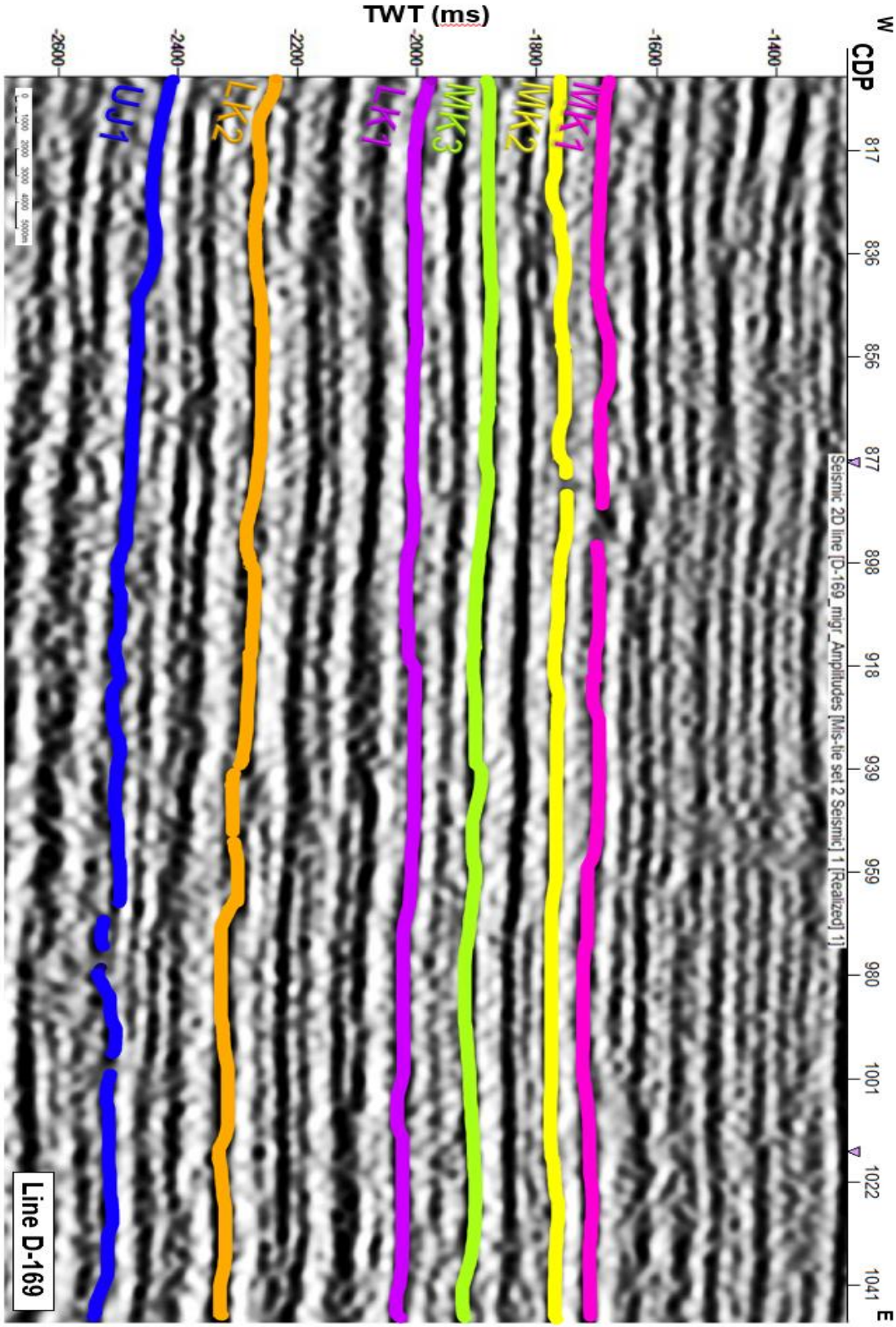

Figure 8B: Interpreted Strike Line D-169

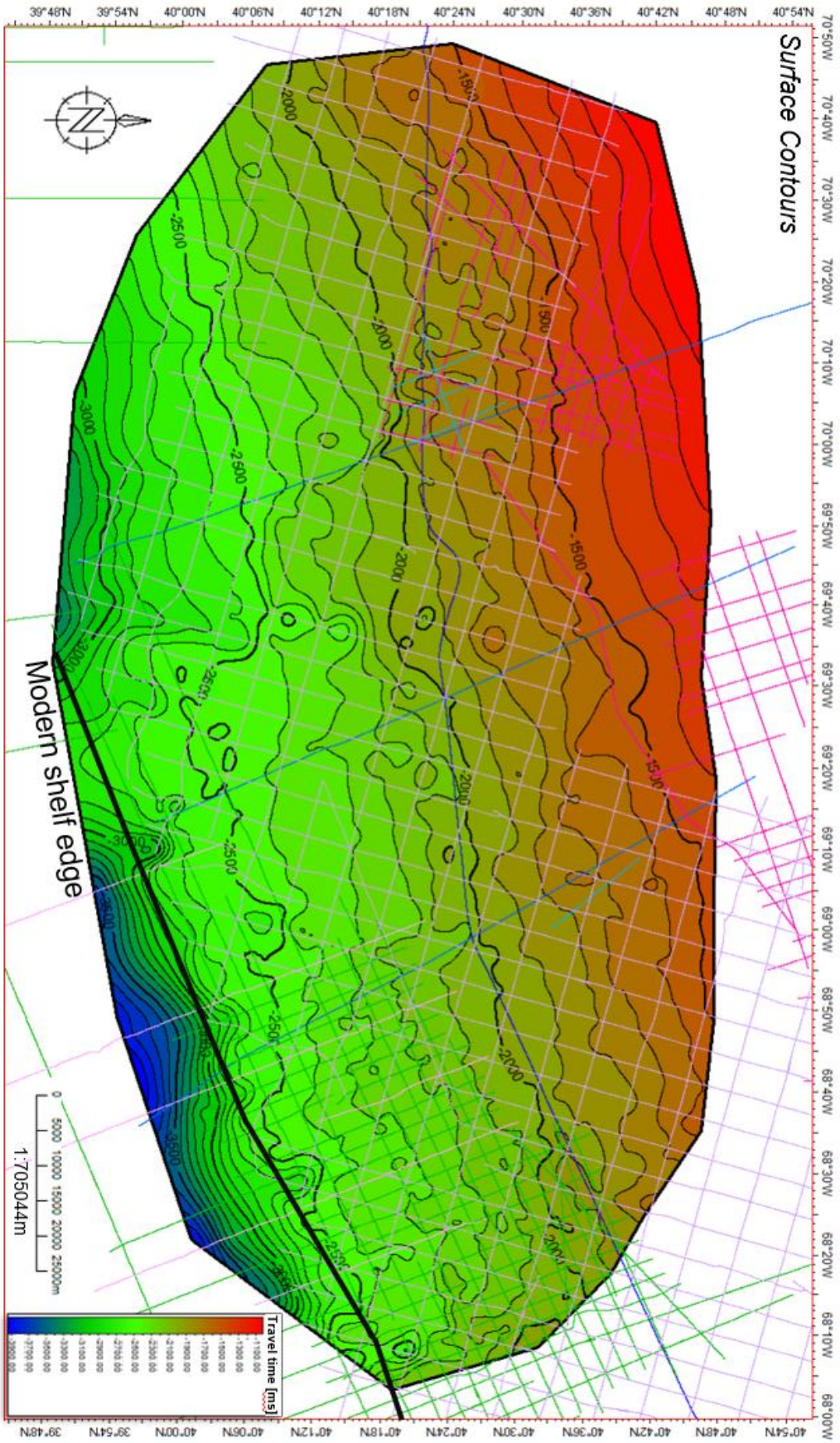

Figure 9A: Surface Contour Map of LK2

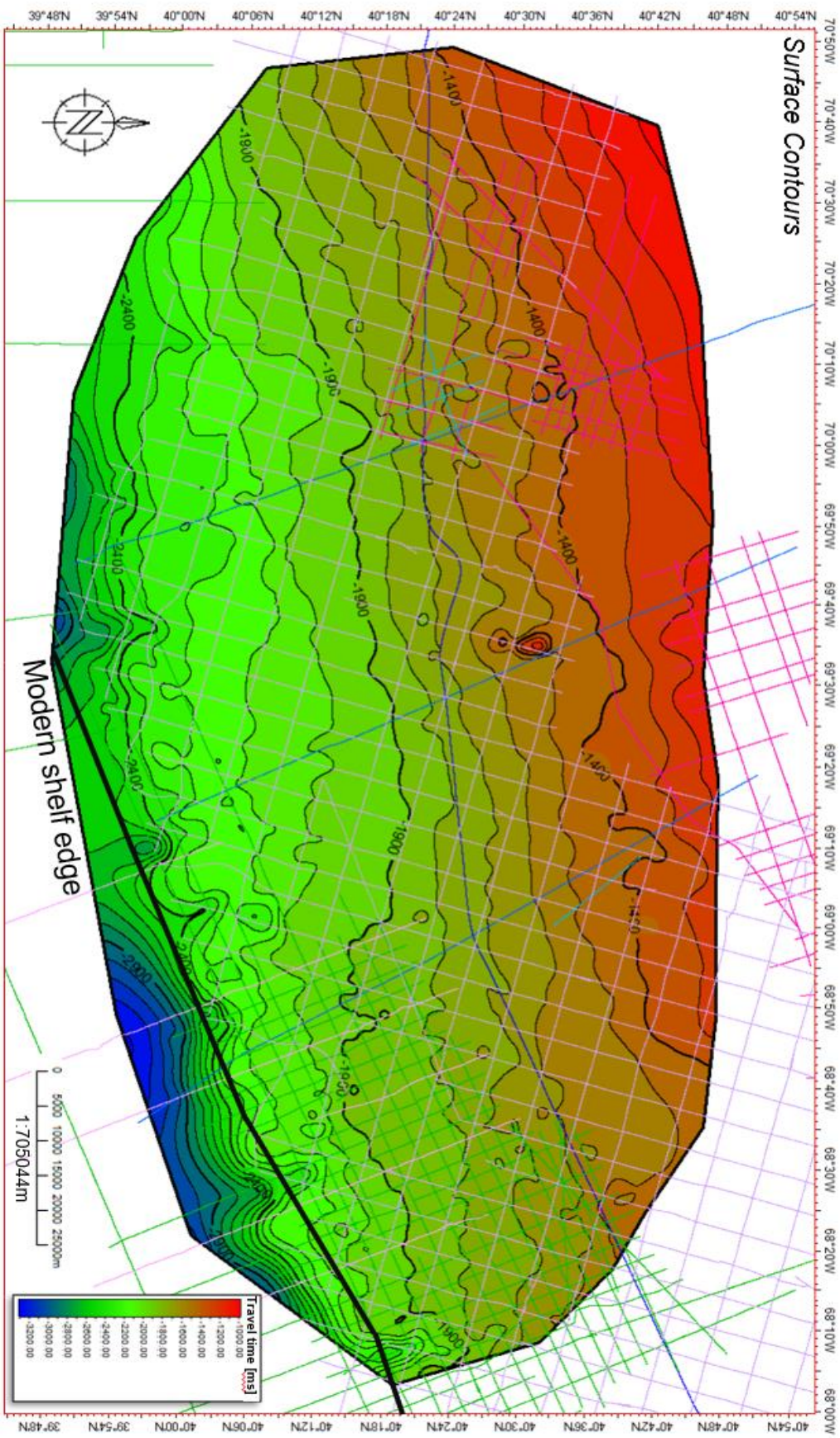

Figure 9B: Surface Contour Map of LK1

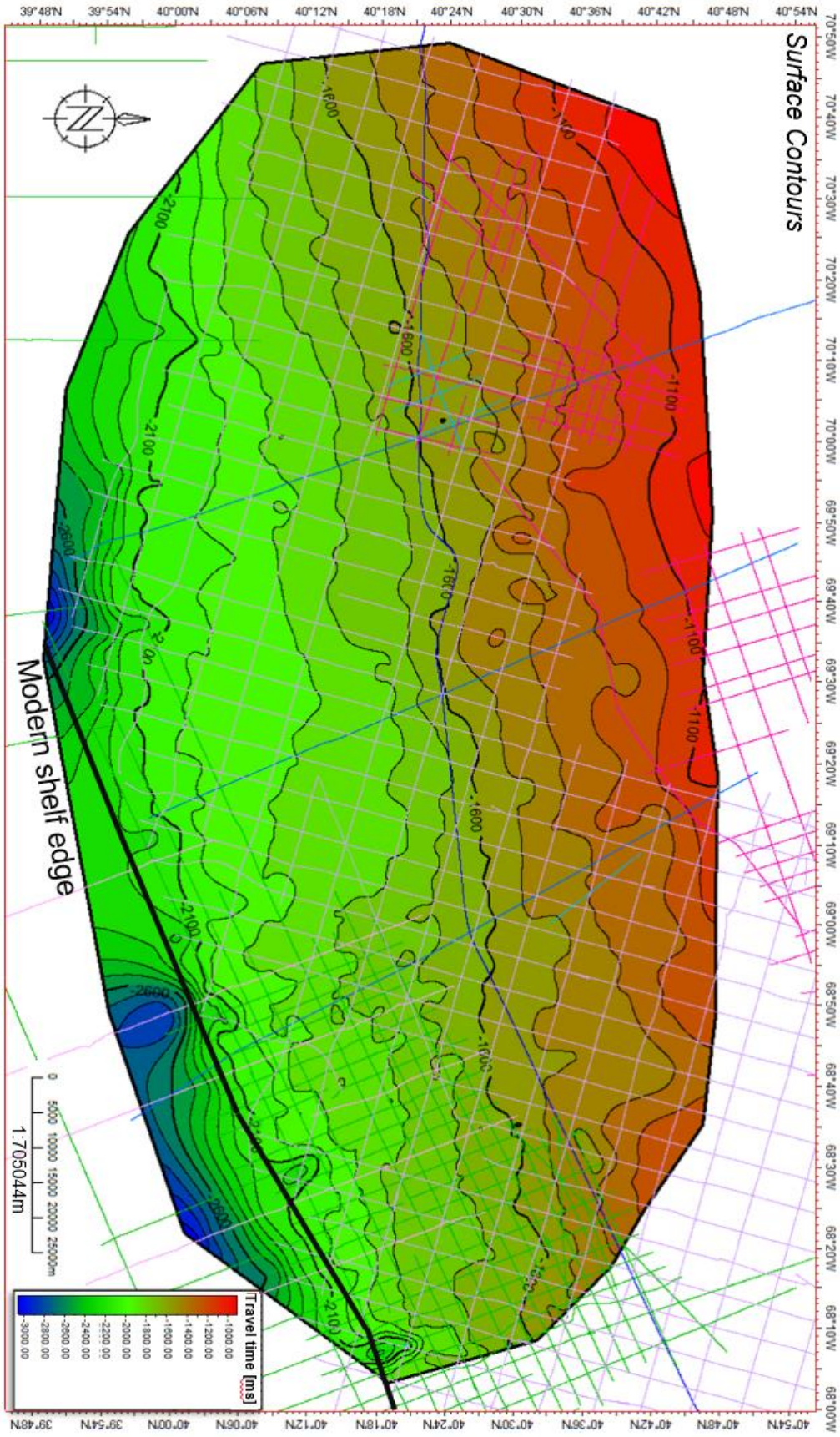

Figure 9C: Surface Contour Map of MK3

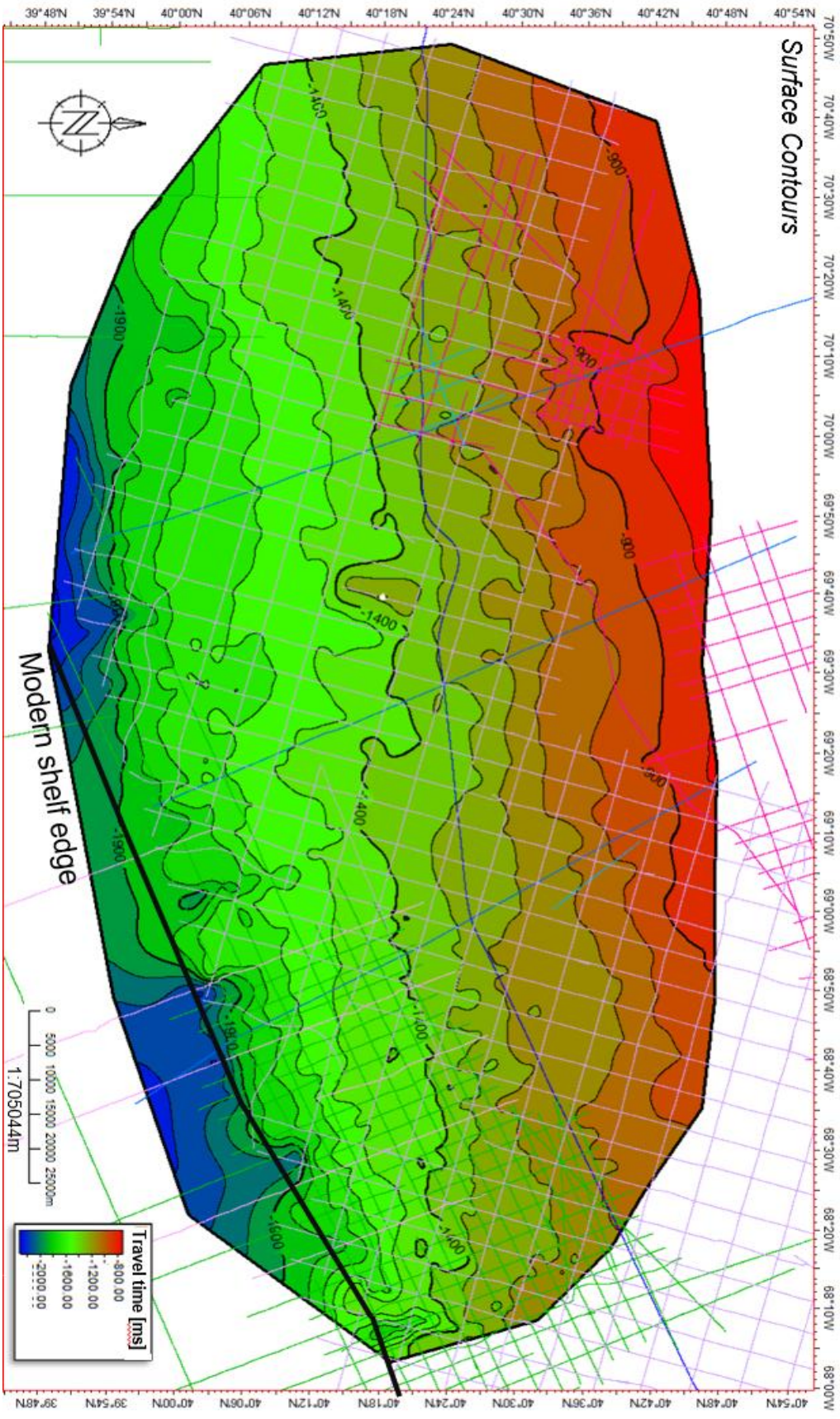

Figure 9D: Surface Contour Map of MK1

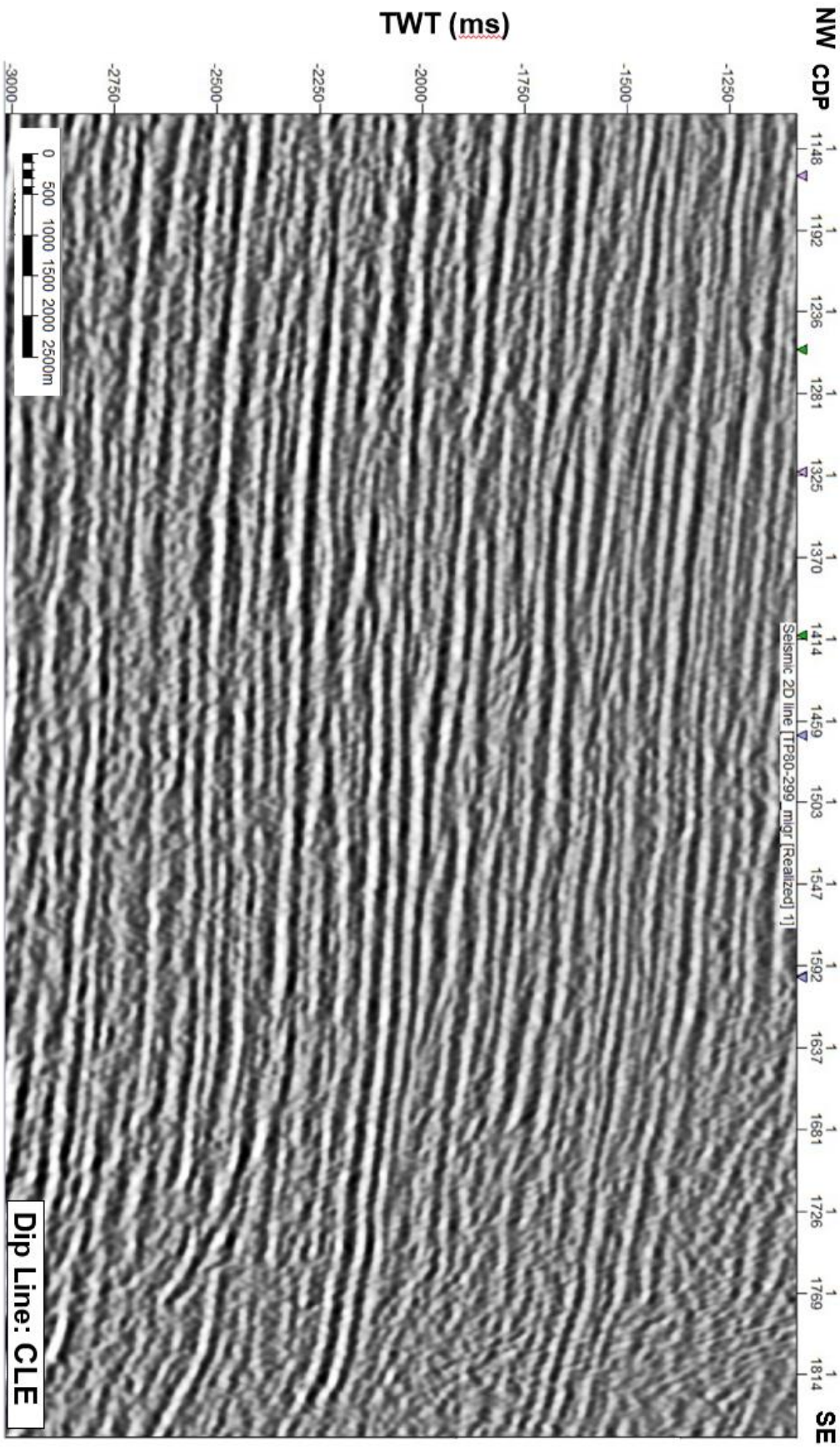

Figure 10A: Uninterpreted Dip Line: CLE

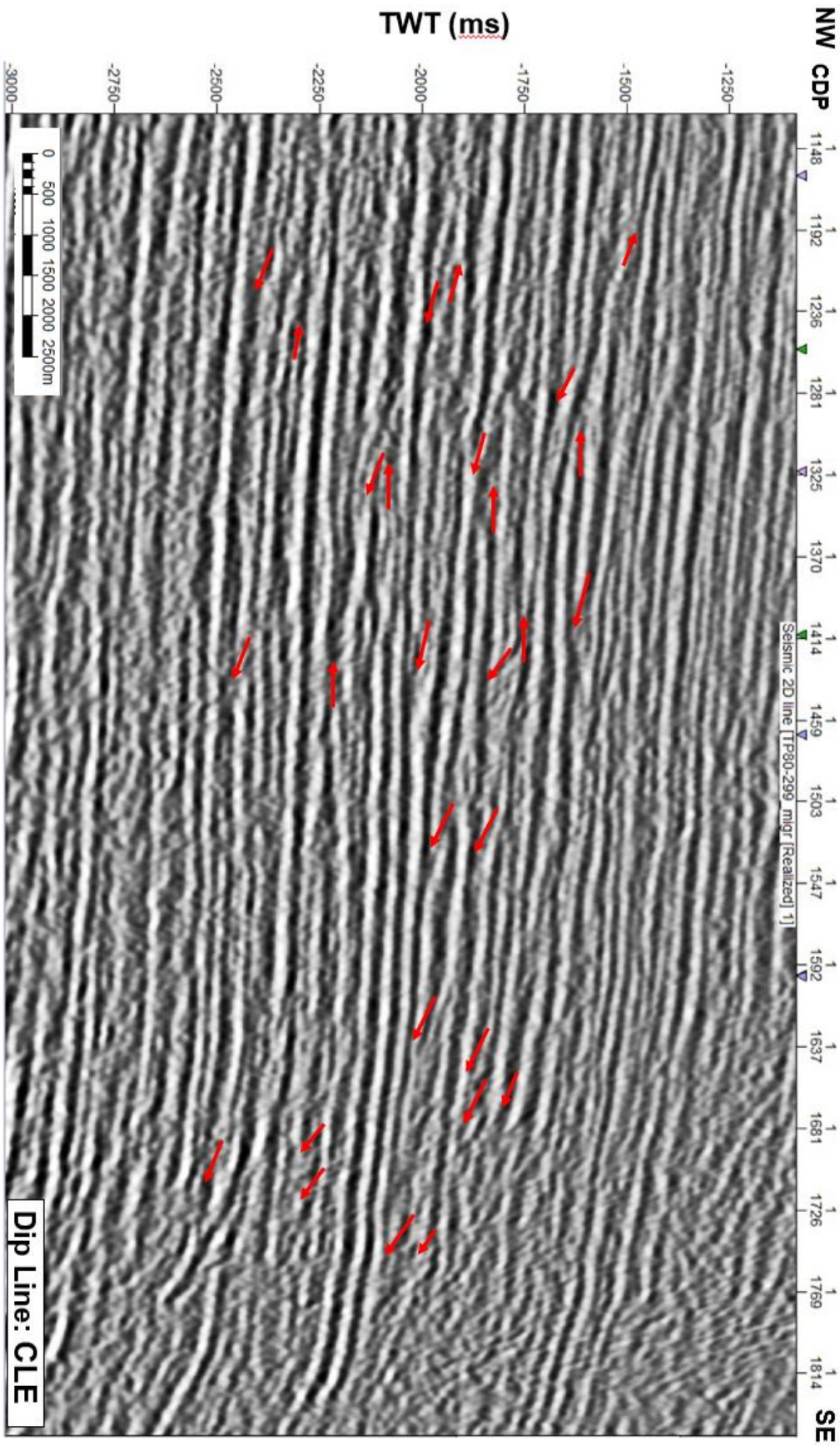

Figure 10B: Reflection Termination Interpreted Dip Line: CLE

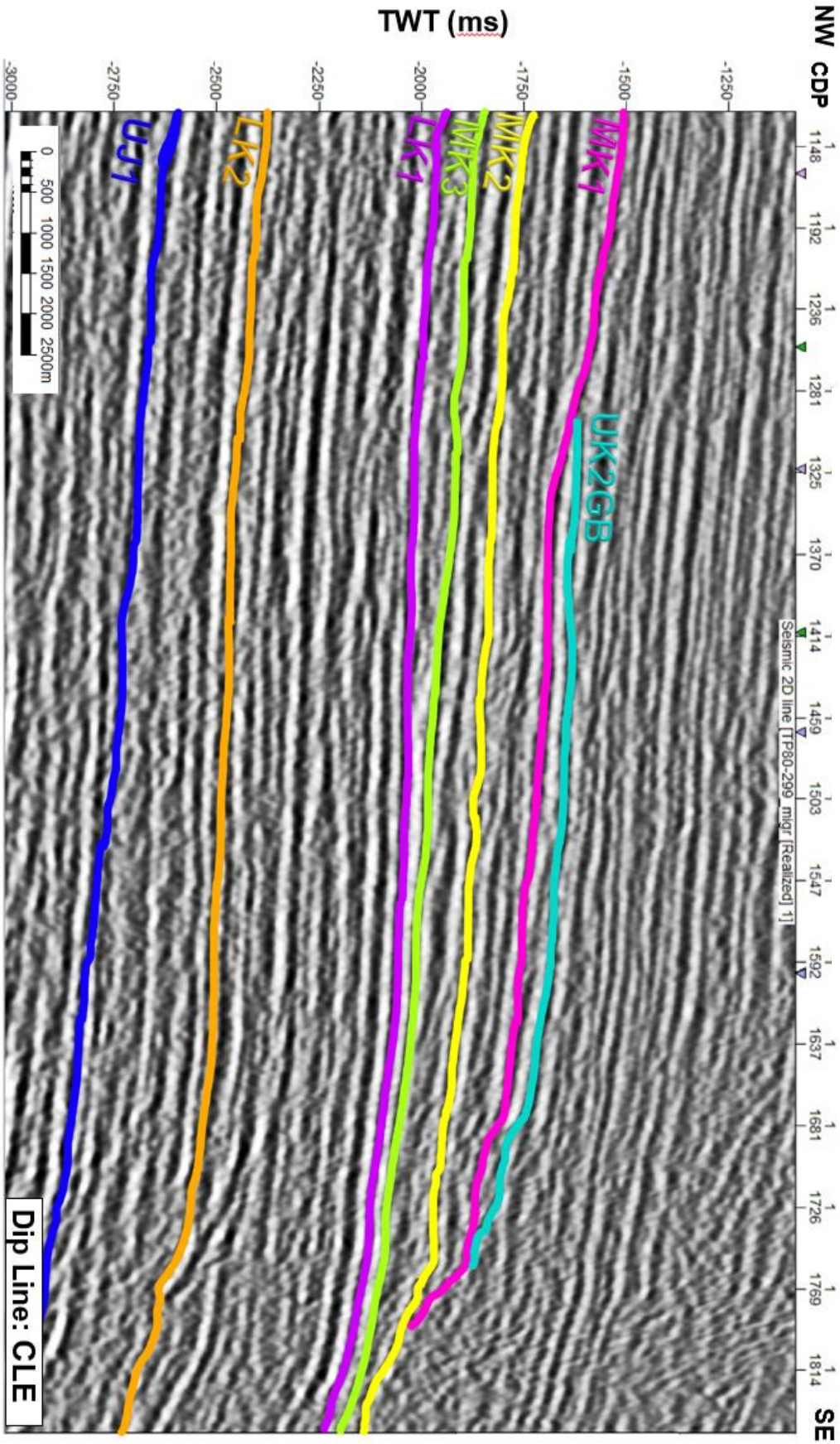

Figure 10C: Seismic Reflector Interpreted Dip Line: CLE

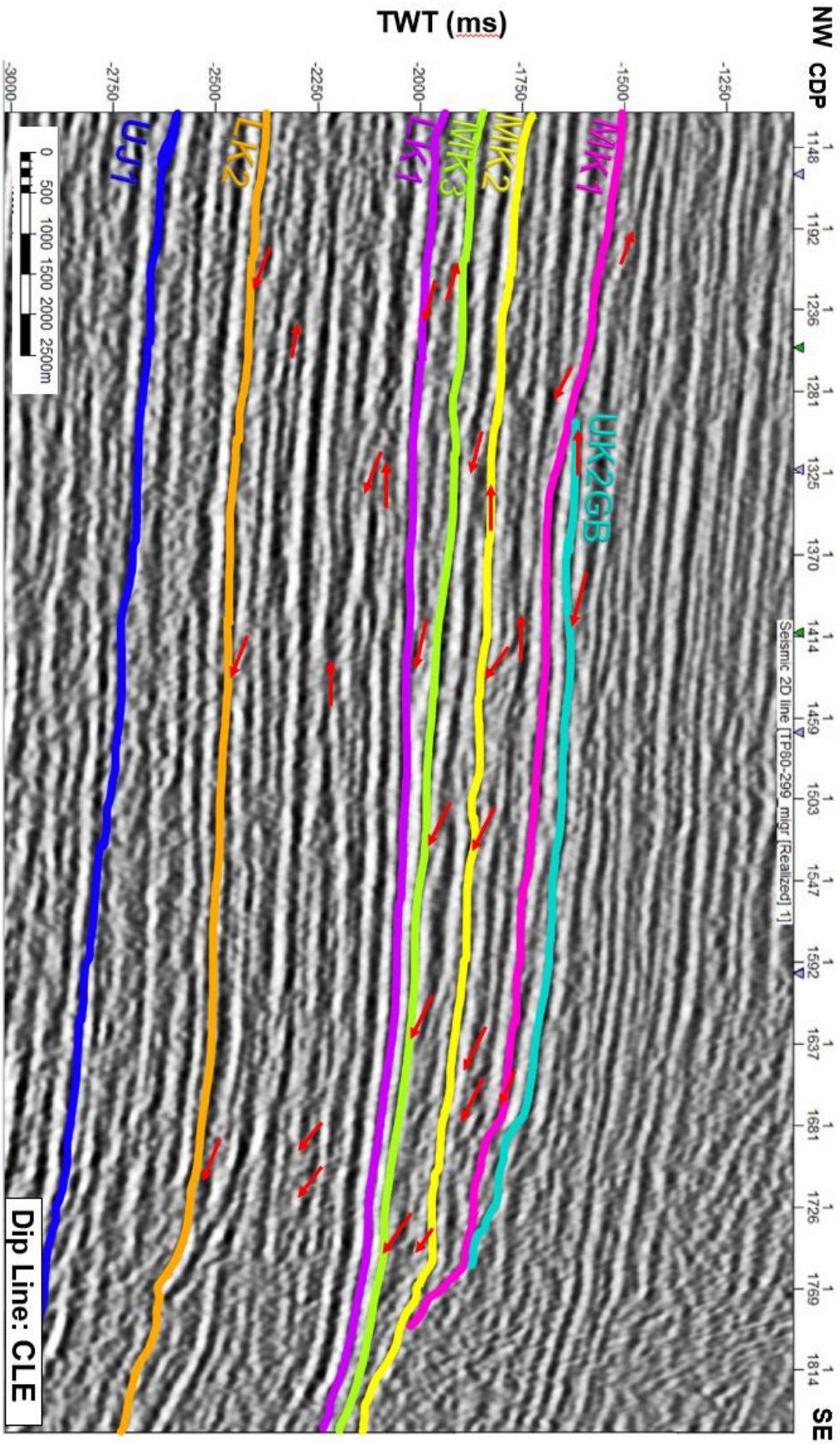

Figure 10D: Termination and Seismic Reflector Interpreted Dip Line: CLE

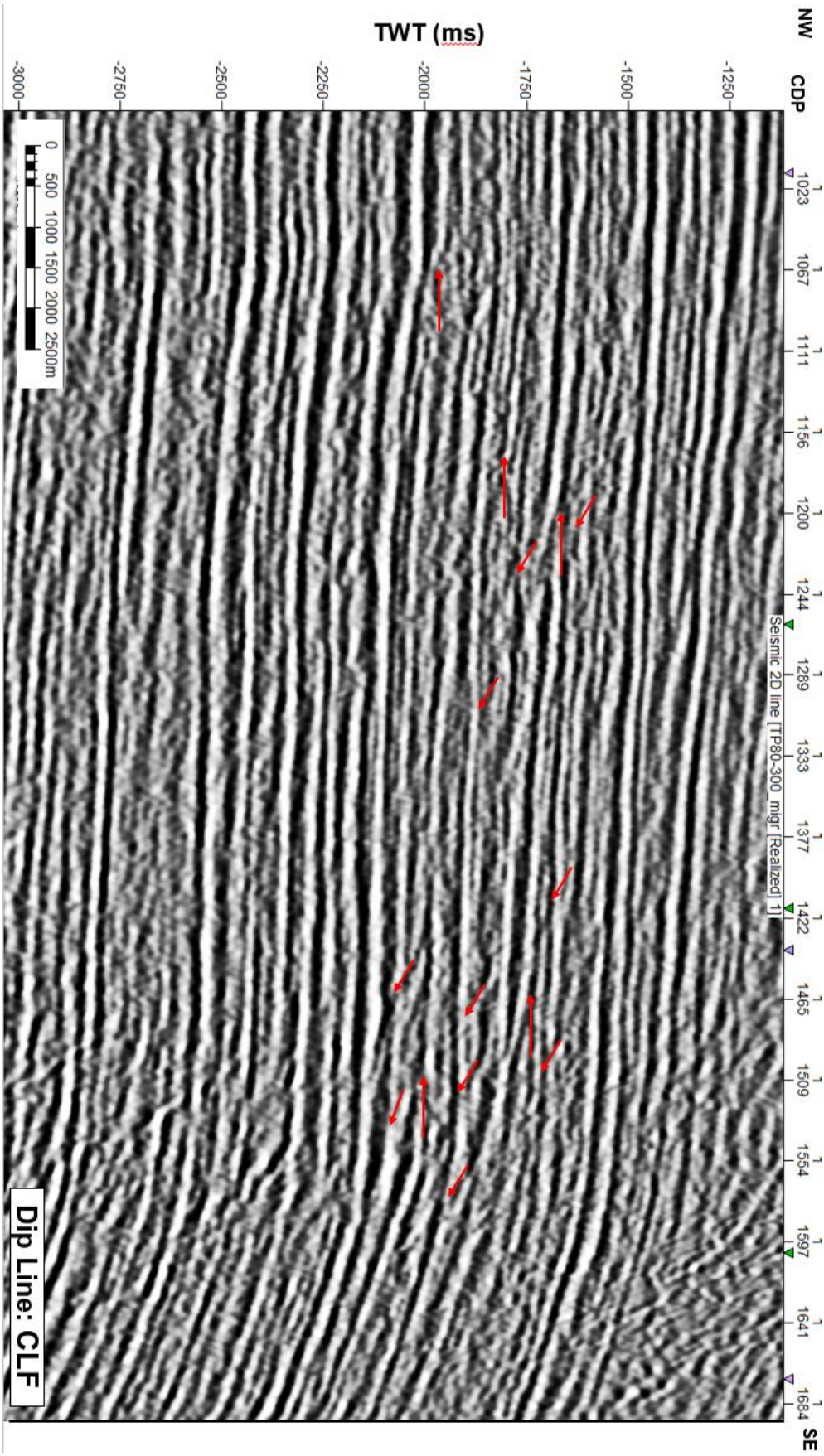

Figure 11A: Uninterpreted Dip Line: CLF

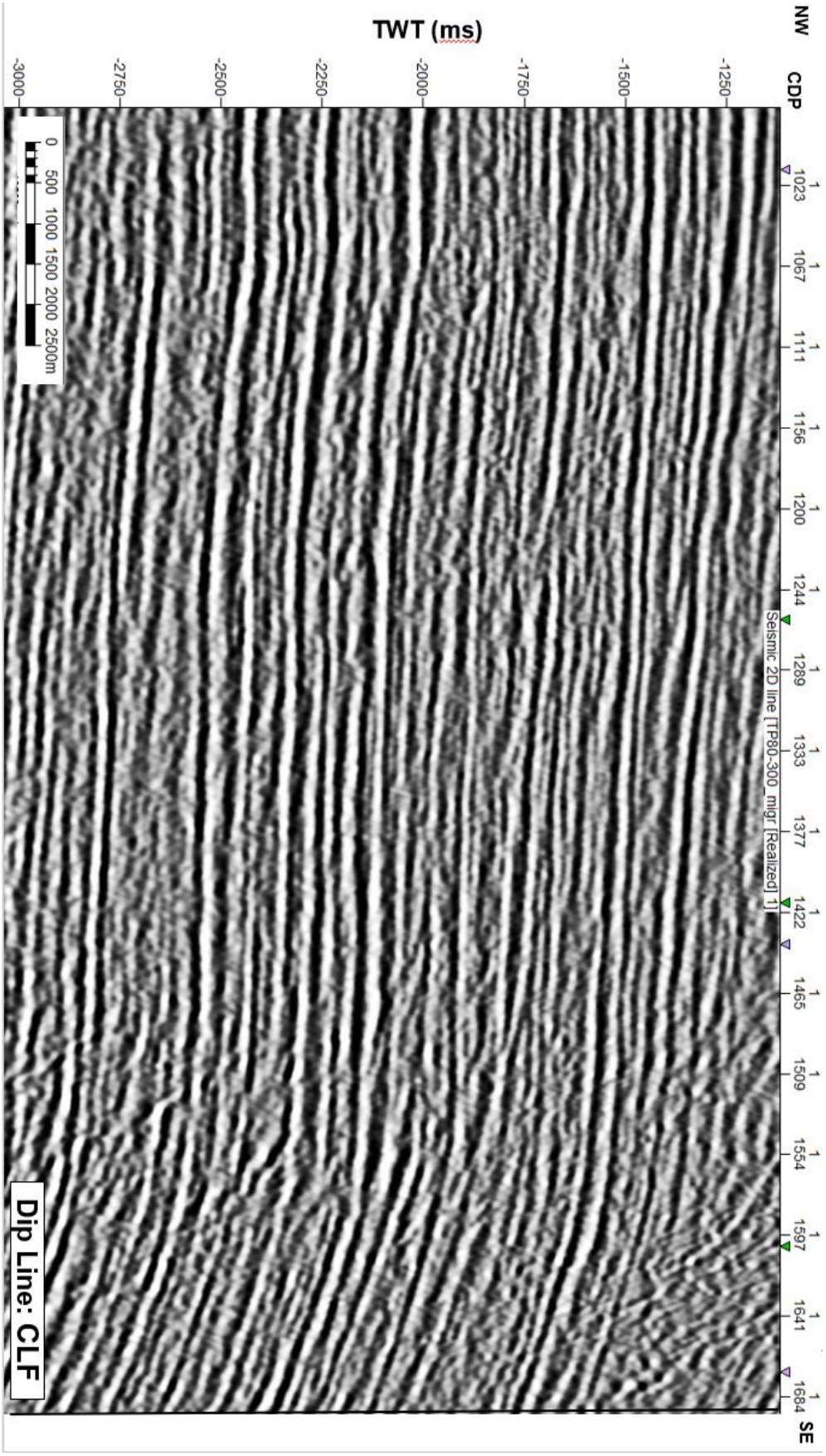

Figure 11B: Reflection Termination Interpreted Dip Line: CLF

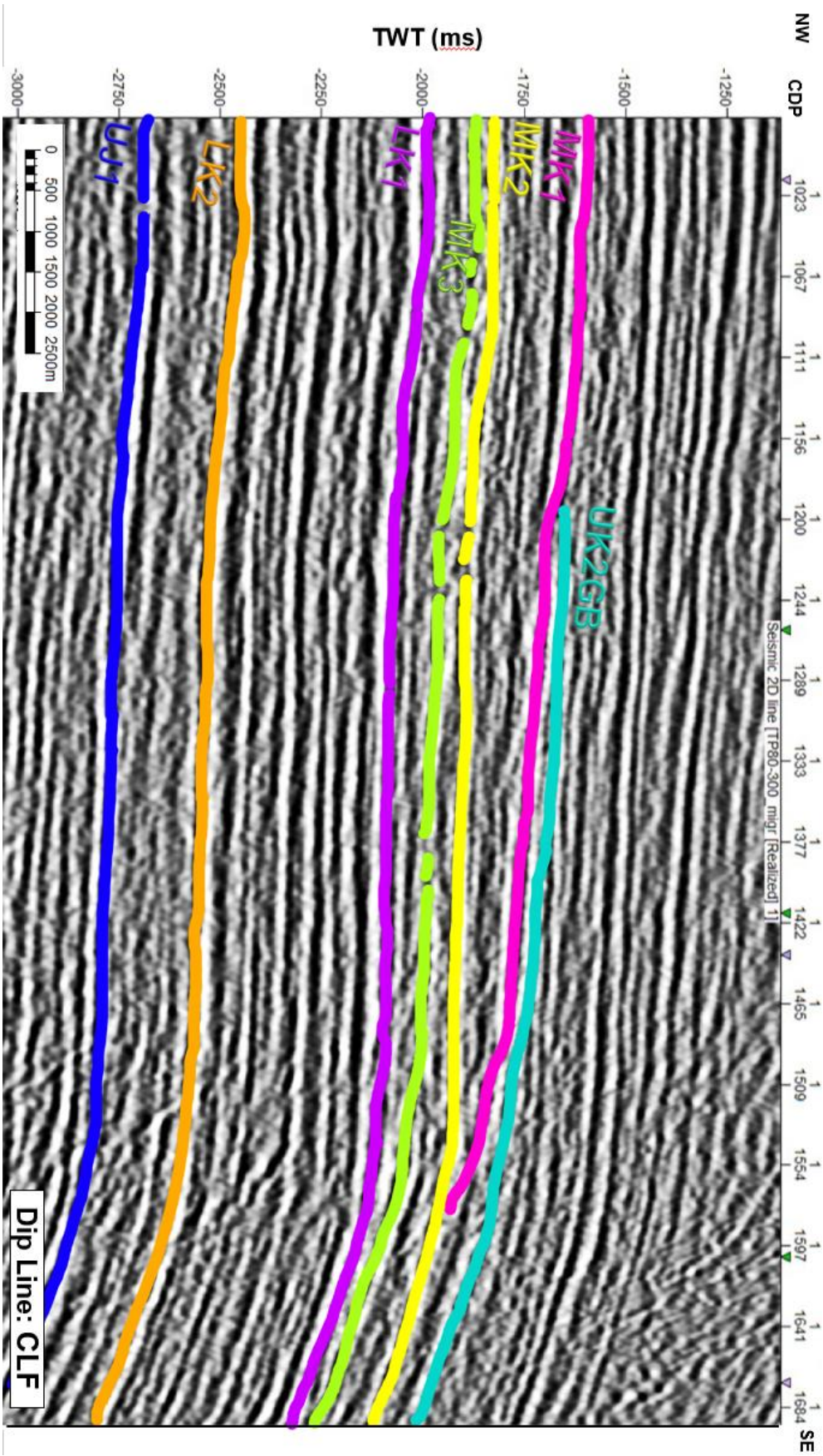

Figure 11C: Seismic Reflector Interpreted Dip Line: CLF

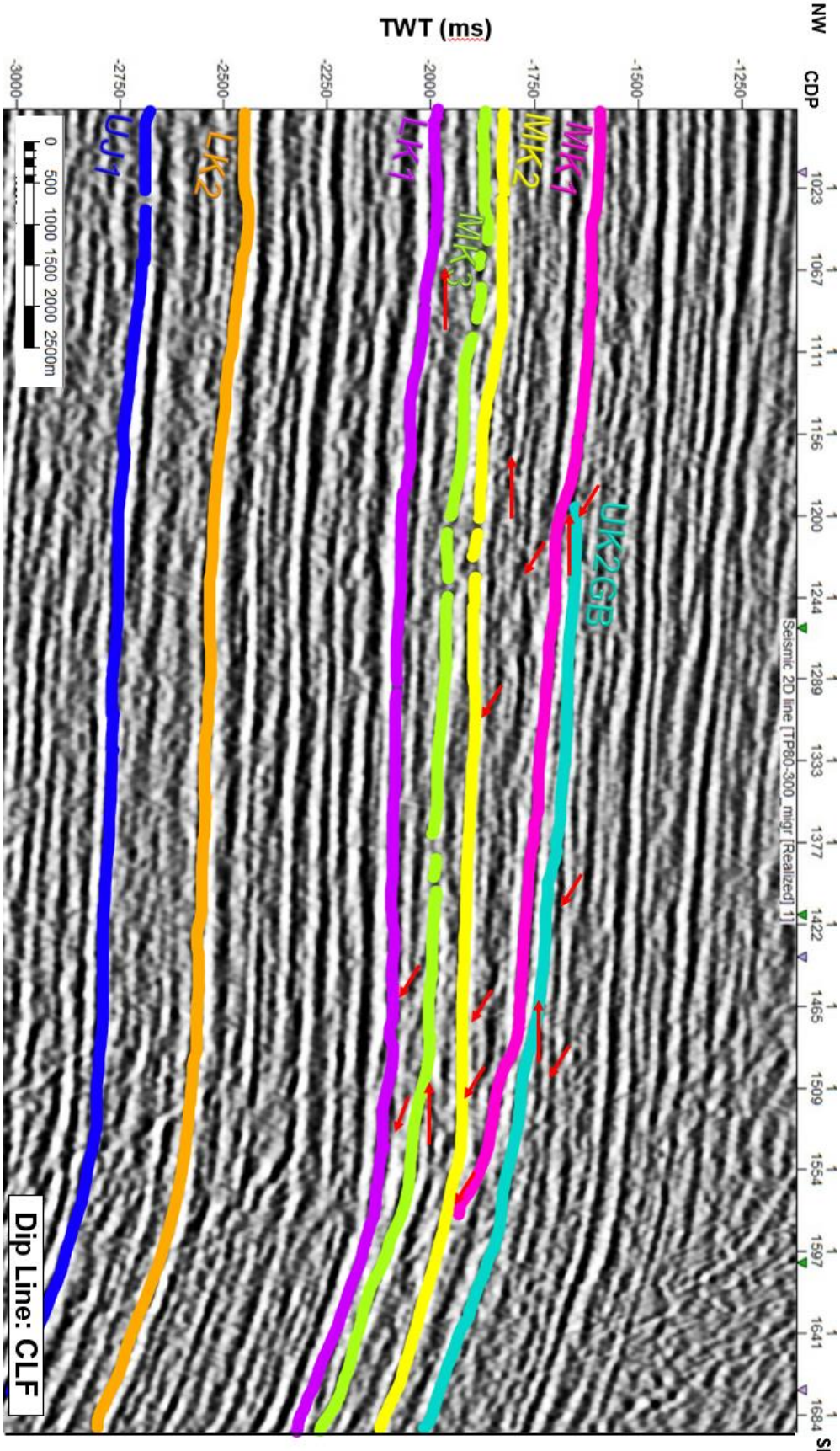

Figure 11D: Termination and Seismic Reflector Interpreted Dip Line: CLF

Figure 12A: Uninterpreted Dip Line: CLD

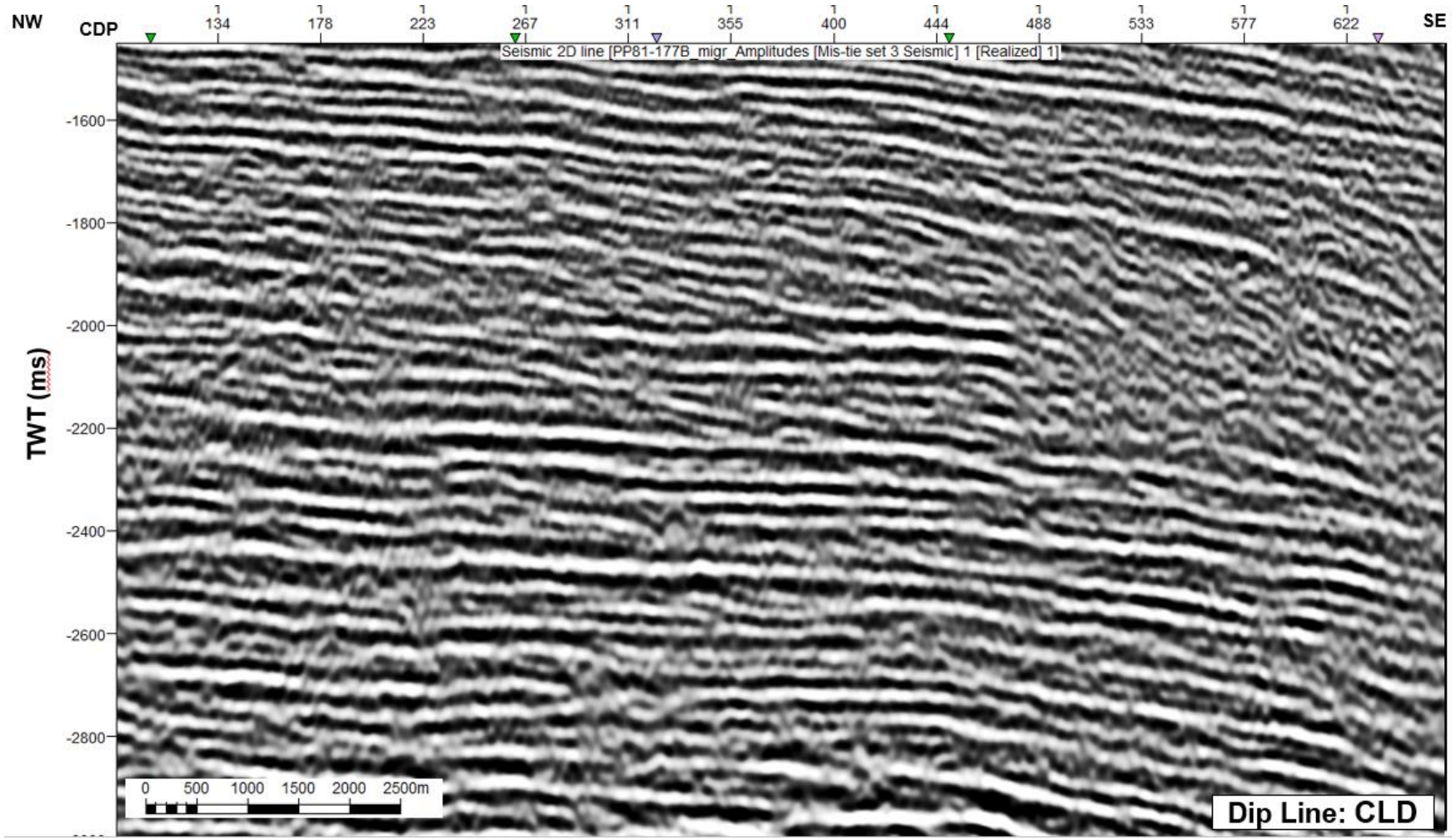

Figure 12B: Reflection Termination Interpreted Dip Line: CLD

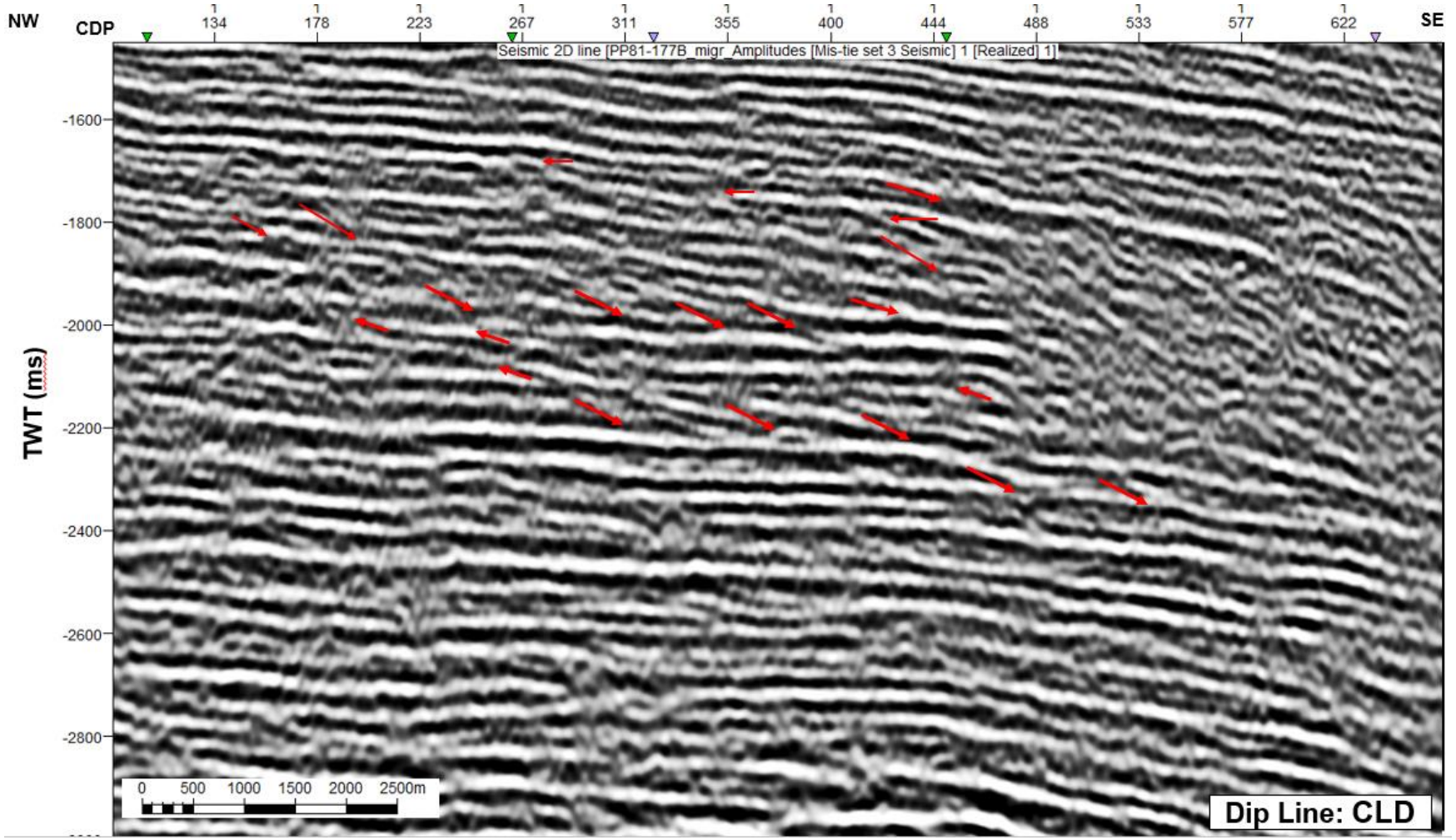

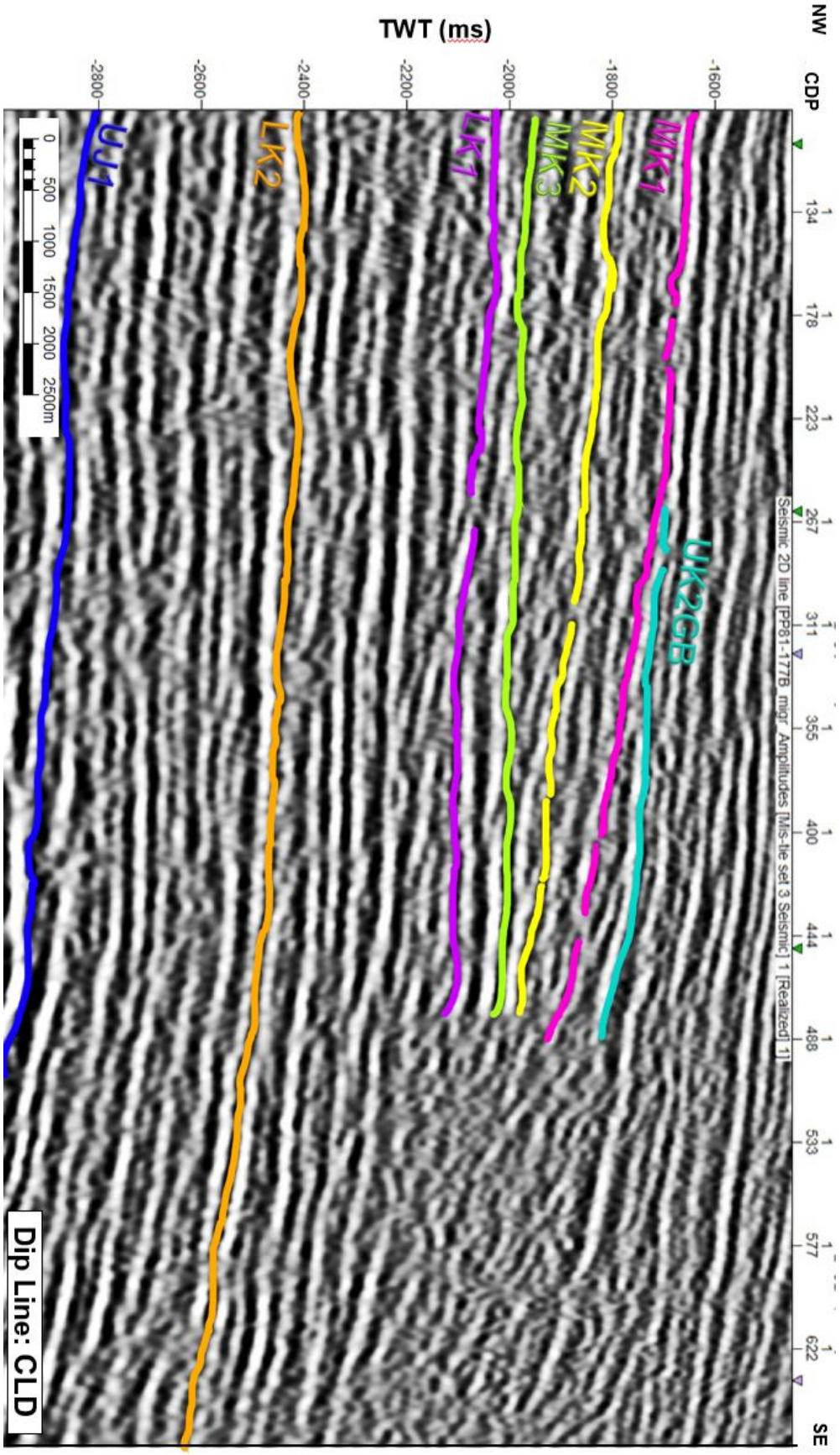

Figure 12C: Seismic Reflector Interpreted Dip Line: CLD

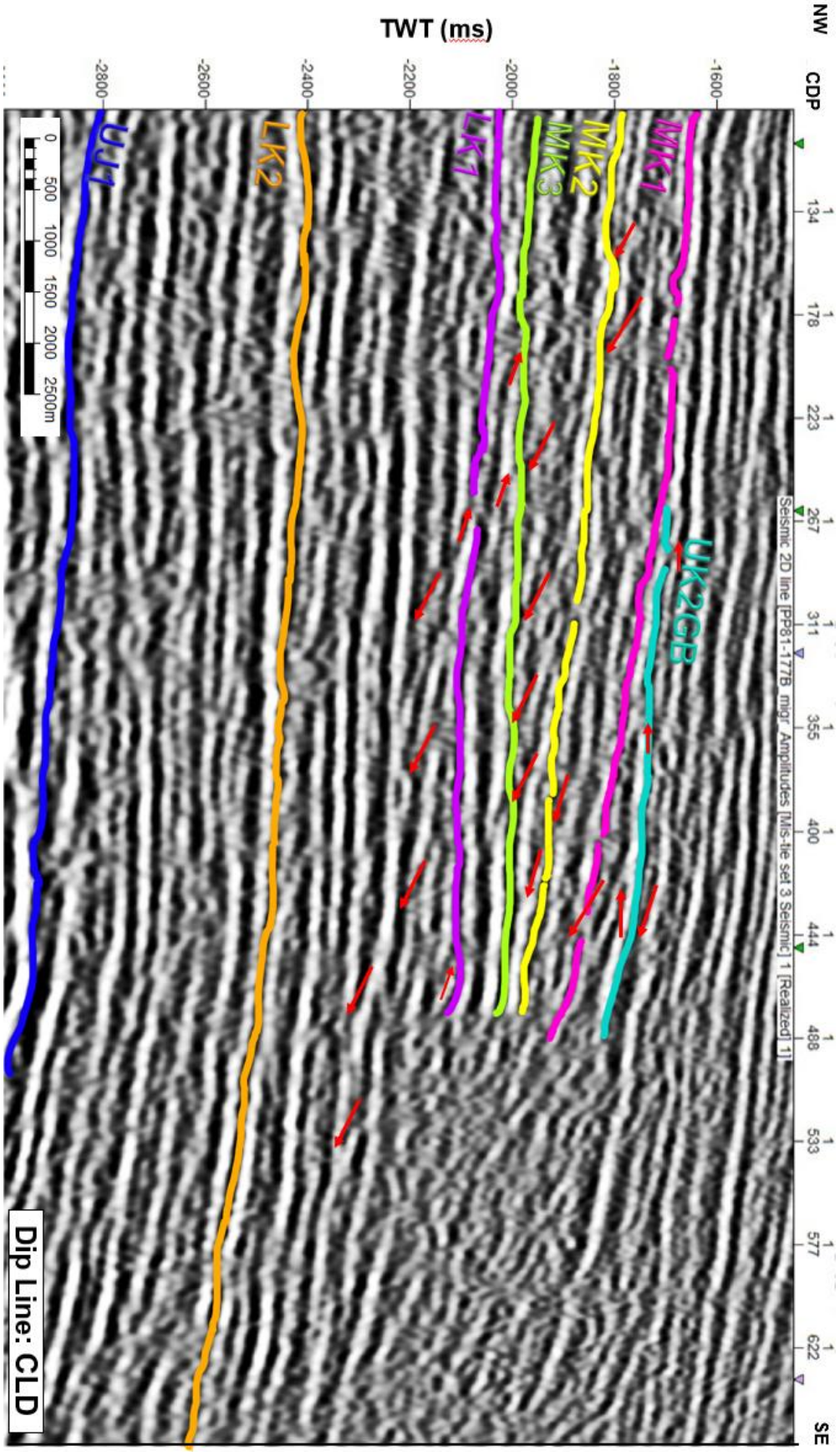

Figure 12D: Termination and Seismic Reflector Interpreted Dip Line: CLD

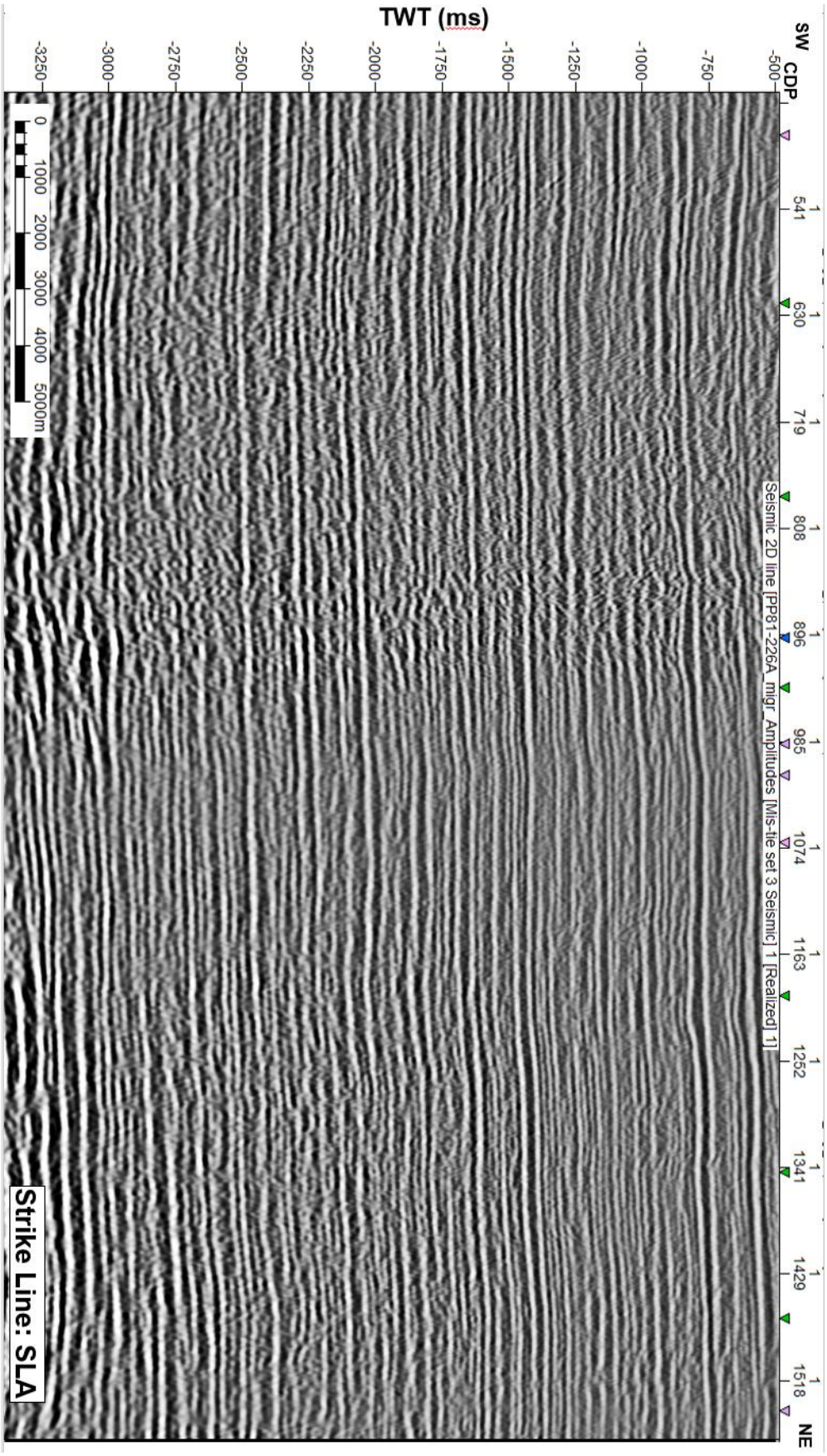

Figure 13A: Uninterpreted Strike Line: SLA

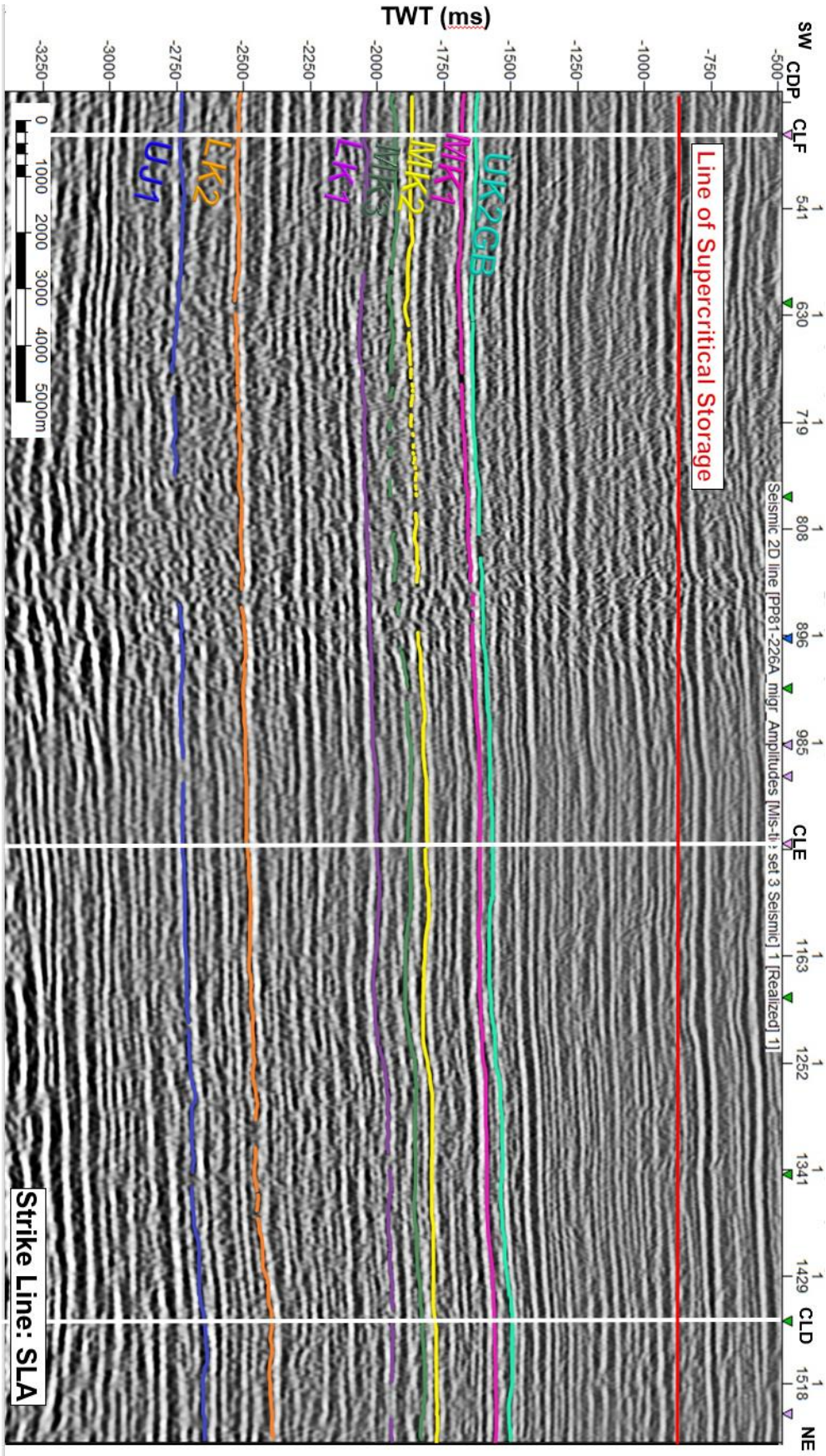

Figure 13B: Seismic Reflector Interpreted Strike Line: SLA

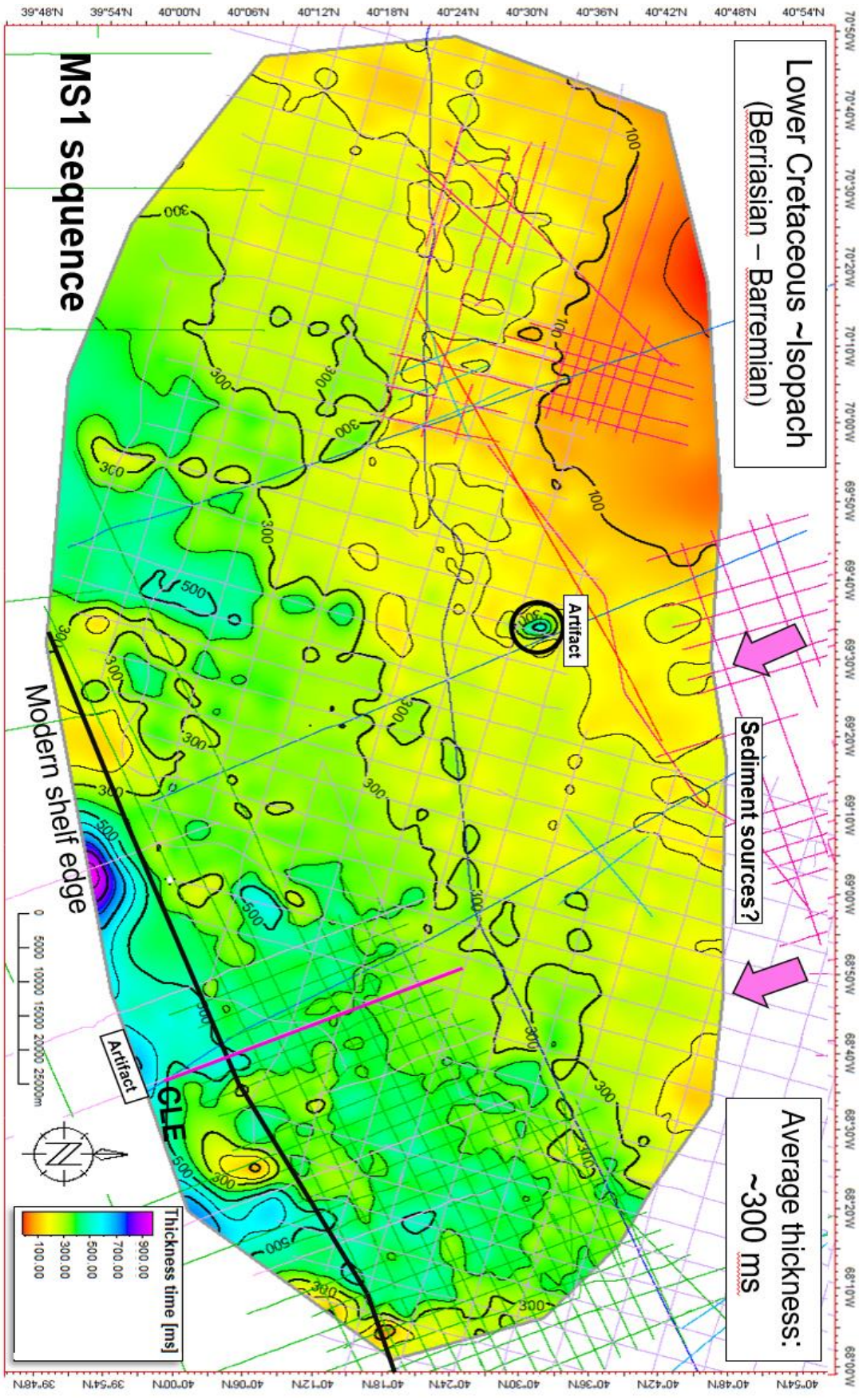

Figure 14A: Isopleth (~Isopach) Map of Lower Cretaceous Sediments

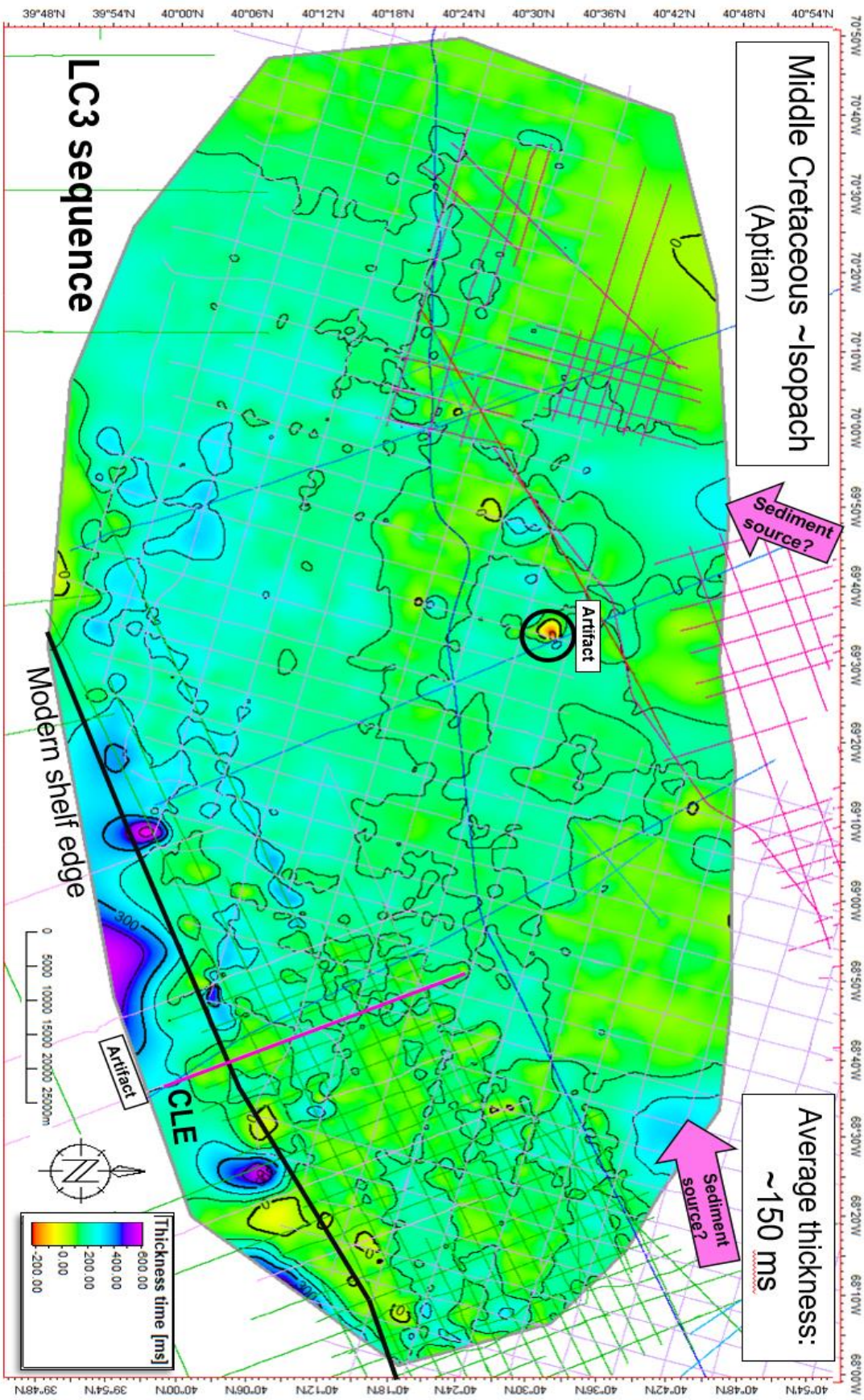

Figure 14B: Isopleth (~Isopach) Map of Middle Cretaceous Sediments

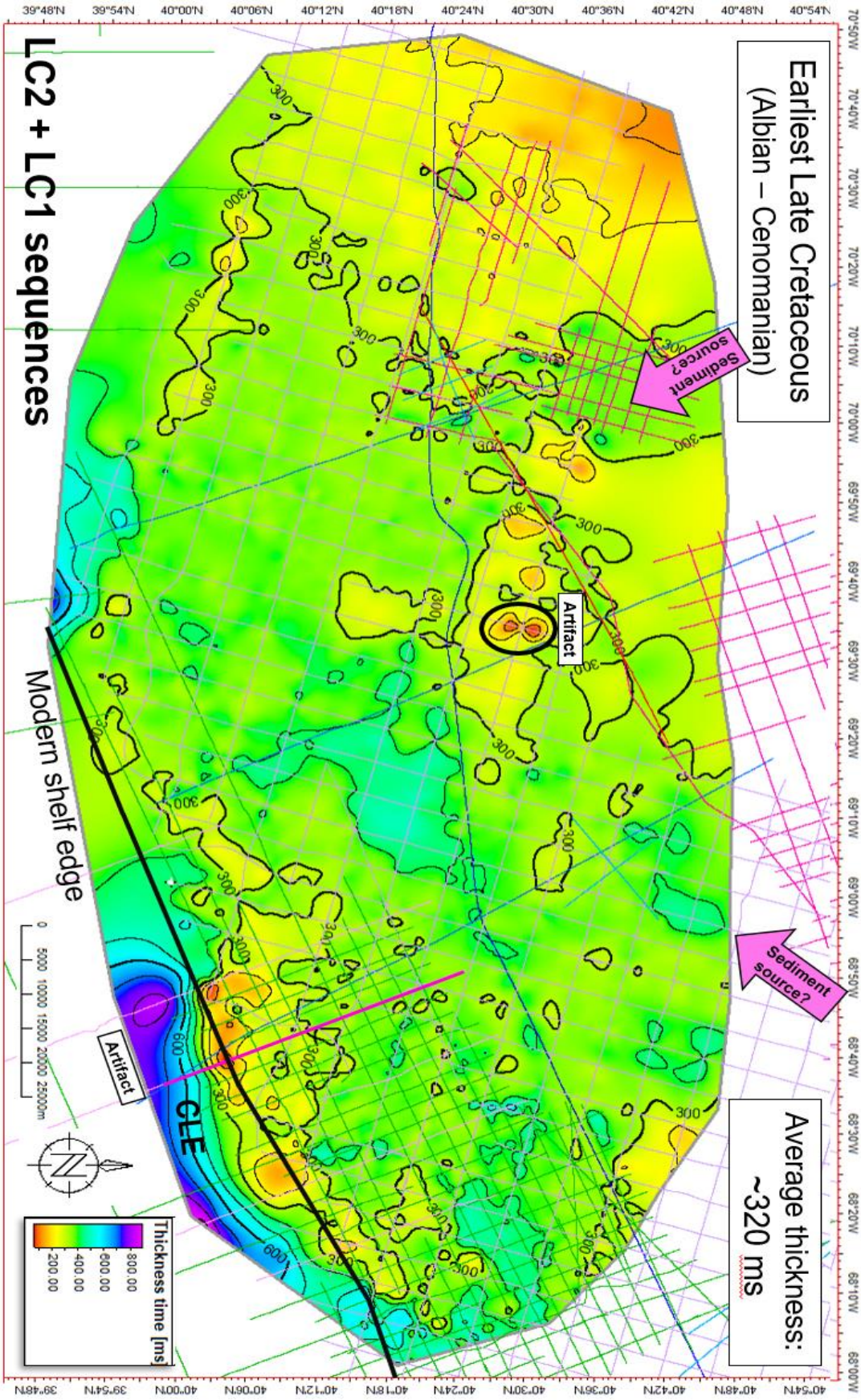

Figure 14C: Isopleth (~Isopach) Map of Late Cretaceous Sediments

Table 1: Geologic Timeline and Descriptions of Cretaceous Strata

Seismic reflector	Well log sequence	Lithologic Units	Age/stage	Unit characteristics
UK2GB	?	Dawson Canyon Shale?	upper Turonian- Coniacian	equivalent of UK2 reflector in BCT
MK1	DCx	Dawson Canyon Shale	upper Cenomanian- Turonian	thick shale caprock
MK2	LC1	Logan Canyon Sandstone	lower Cenomanian	thick, blocky sandstone reservoirs
MK3	LC2	Logan Canyon Sandstone	Albian	thick, blocky sandstone reservoirs
LK1	LC3	Naskapi Shale	Aptian	fissile, carbonaceous shales
LK2	MS1	Mississauga Sandstone	Berriasian- Barremian	heterolithic, sand-prone reservoirs
UJ1	JU1	Mic-Mac/Mohawk Formations	Oxfordian- Tithonian	heterolithic siliciclastics, potential reservoir?

Table 2: Compilation of Seismic Surveys with Distances Shot (km)

Survey Name	Year	Lines (available)	Lines (used)	Distance (total)	Distance (used)
B-03-75-AT	1975	325	66	28511 km	8568 km
B-06-76-AT	1976	45	6	1809 km	135 km
B-13-76-AT	1976	25	1	786 km	109 km
B-04-80-AT	1980	71	8	2549 km	484 km
B-01-81-AT	1981	227	71	9190 km	3171 km
B-04-83-AT	1983	65	25	1993 km	861 km
USGS	1976	4	3	4321 km	1321 km
TOTALS	-	763	180	46159 km	13759 km

Table 3: Mini-Grid Dip and Strike Lines

Dip Lines

Petrel Name (W-E)	Line Name	Survey
CLF	TP80-300	B-04-80
CLG	PP81-182	B-01-81
CLJ	PP81-181	B-01-81
CLI	PP81-180	B-01-81
CLE	TP80-299	B-04-80
CLH	PP81-179	B-01-81
CLL	PP81-178C	B-01-81
CLK	PP81-178B	B-01-81
CLD	PP81-177B	B-01-81
CLM	PP81-177A	B-01-81
CLN	TP80-298	B-04-80

Strike Lines

Petrel Name (S-N)	Line Name	Survey
SLD	PP81-228B	B-01-81
SLE	PP81-228C	B-01-81
SLB	PP81-227A	B-01-81
SLC	PP81-227B	B-01-81
SLA	PP81-226A	B-01-81
SLF	PP81-224B	B-01-81
SLG	PP81-223	B-01-81
SLH	PP81-222	B-01-81